ÇUKUROVA UNIVERSITY
INSTITUTE OF NATURAL AND APPLIED SCIENCES

PhD THESIS

Fırat EKİNCİ

PASSIVE CONTROL OF VORTEX SHEDDING AROUND A CIRCULAR CYLINDER BY DETACHED PLATE

DEPARTMENT OF MECHANICAL ENGINEERING

ADANA-2016

ÇUKUROVA UNIVERSITY
INSTITUTE OF NATURAL AND APPLIED SCIENCES

PASSIVE CONTROL OF VORTEX SHEDDING AROUND A CIRCULAR CYLINDER BY DETACHED PLATE

Fırat EKİNCİ

PHD THESIS

DEPARTMENT OF MECHANICAL ENGINEERING

We certify that the thesis titled above was reviewed and approved for the award of degree of the Doctor of Philosophy by the board of jury on 21/11/2016.

…….....	……	…….....
Prof. Dr. Hüseyin AKILLI	Prof. Dr. Beşir ŞAHİN	Prof. Dr. M. Sami AKÖZ
SUPERVISOR	MEMBER	MEMBER

...…….....	...……..
Asst. Prof. Dr. Ertaç HÜRDOĞAN	Asst. Prof. Dr. Erhan FIRAT
MEMBER	MEMBER

This MSc Thesis is written at the Department of Institute of Natural And Applied Sciences of Çukurova University.

Registration Number:

Prof. Dr. Mustafa GÖK
Director
Institute of Natural and Applied Sciences

Note: The usage of the presented specific declarations, tables, figures, and photographs either in this thesis or in any other reference without citation is subject to "The law of Arts and Intellectual Products" number of 5846 of Turkish Republic

ABSTRACT

PhD THESIS

PASSIVE CONTROL OF VORTEX SHEDDING AROUND A CIRCULAR CYLINDER BY DETACHED PLATE

Fırat EKİNCİ

ÇUKUROVA UNIVERSITY
INSTITUTE OF NATURAL AND APPLIED SCIENCES
DEPARTMENT OF MECHANICAL ENGINEERING

Supervisor :Prof. Dr. Hüseyin AKILLI
Year: 2016, Pages:155
Jury : Prof. Dr. Hüseyin AKILLI
: Prof. Dr. Beşir ŞAHİN
: Prof. Dr. M.Sami AKÖZ
: Asst. Prof. Dr. Ertaç HÜRDOĞAN
: Asst. Prof. Dr. Erhan FIRAT

The aim of present study is to control the vortex shedding around a circular cylinder by use of single and double detached plate arrangements at various plate angles. Experiments were performed in deep water flow using Particle image velocimetry (PIV) and flow visualization techniques. The main parameters of the study are the normalized plate length (*L/D*), the plate angle (α), and the gap ratio between plate and the cylinder (*G/D*). The effects of these parameters were explained by means of the Reynolds Shear Stress (RSS), Turbulent Kinetic Energy contours (*TKE*), and Vorticity contours (ω).

Key Words: Vortex Shedding, Passive Control, Detached plate, PIV

ÖZ

DOKTORA TEZİ

BİR SİLİNDİR ETRAFINDA AYRIK PLAKA İLE GİRDAP KOPMASININ PASİF YÖNTEMLE KONTROLÜ

Fırat EKİNCİ

ÇUKUROVA ÜNİVERSİTESİ
FEN BİLİMLERİ ENSTİTÜSÜ
MAKİNA MÜHENDİSLİĞİ ANABİLİM DALI

Danışman :Prof. Dr. Hüseyin AKILLI
Yıl: 2016, Sayfa: 155
Jüri :Prof. Dr. Beşir ŞAHİN
:Prof. M. Sami AKÖZ
:Yrd. Doç. Dr. Ertaç HÜRDOĞAN
:Yrd. Doç. Dr. Erhan FIRAT

Bu çalışmanın temel amacı, bir silindir arkasında oluşan girdap kopmasının silindir etrafında farklı açılarda ayrık şekilde yerleştirilen tek ve çift plaka düzeni ile kontrolünün sağlanmasıdır. Deneyler derin suda, dijital parçacık görüntülemeli hız ölçüm (DPIV) ve akış görselleştirme teknikleri kullanılarak gerçekleştirilmiştir. Çalışmanın ana parametreleri plaka uzunluğu (*L/D*), plaka açısı (α) ve plaka ve silindir arasındaki mesafedir (*G/D*). Yapılan deneylerde plaka ve silindir arasındaki mesafenin girdap kopmasına etkisi farklı açılarda gösterilmiştir. Deney sonuçları, Reynolds Kayma Gerilmesi (RSS), Türbulans Kinetik Enerji (*TKE*) ve Girdap Konturları (ω) ile açıklanmıştır.

Anahtar Kelimeler: Girdap kopması, pasif kontrol, ayrık plaka, PIV

GENİŞLETİLMİŞ ÖZET

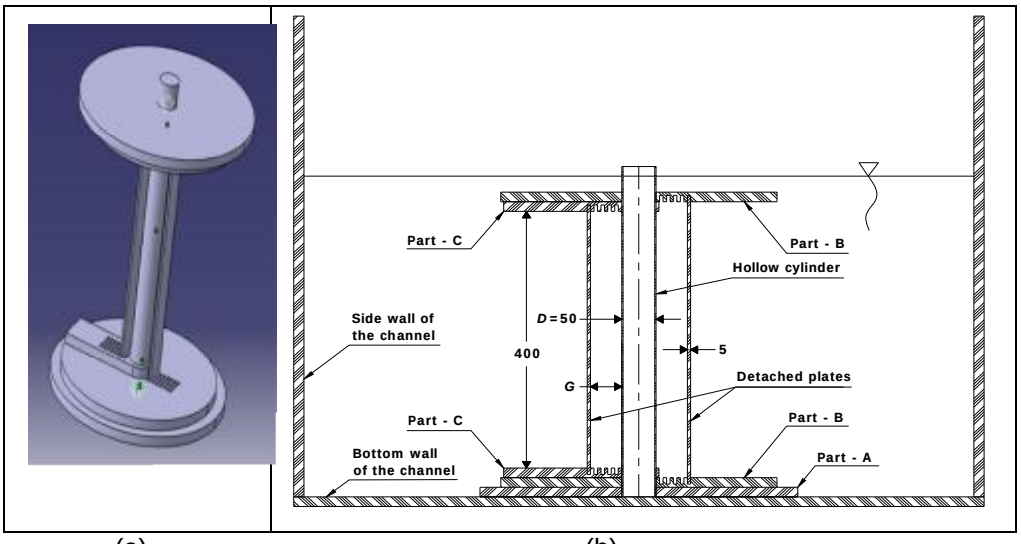
Bir akış içerisinde bulunan cisimlerin arkasında oluşan daimi olmayan girdaplar ve bu girdapların meydana getirdiği dinamik kuvvetler uygulamada dikkat edilmesi gereken önemli faktörlerden biridir. Bu kuvvetler, cisim üzerinde titreşim meydana getirir ve titreşim cismin doğal frekansıyla çakıştığı anda rezonans devreye girerek malzemede yorulmaya ve sonrasında yapısal hasarlara yol açabilir. Cisimlerin arkasında oluşan bu akış yapısının kontrolü, bahsi gecen olumsuzluklardan dolayı son yıllarda bir hayli önem kazanmıştır.

Bir silindir etrafındaki akış aerodinamik veya hidrodinamik ile uğraşan birçok araştırmacının ilgi odağı olmayı başarmıştır. Rüzgâr türbinlerinin direkleri, aydınlatma direkleri, köprü bacakları, fabrika veya güç santrallerinin bacaları, fenerler, kıyı ötesi yapılar gibi pratikteki birçok nesne etrafındaki akışkan hareketi, silindir etrafındaki ile büyük oranda benzerlik göstermektedir.

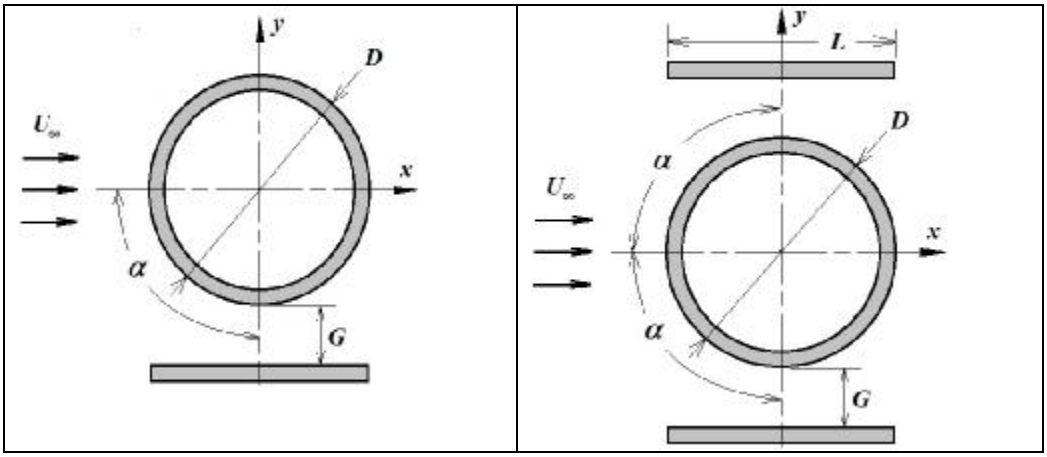
Akış içerisine yerleştirilmiş bir cisim arkasında oluşan girdap yapısının sebep olduğu problemlerin önlenebilmesi için daimi olmayan akış yapısının kontrol altına alınması ve arka bölgedeki akışın değerlerinin azaltılması gerekmektedir. Cisimler etrafındaki akışın kontrol yöntemleri aktif ve pasif kontrol olmak üzere ikiye ayrılır. Kontrol amacıyla sisteme dışarıdan enerji veriliyorsa, bu aktif kontroldür. Pasif kontrolde ise akış yapısını değiştirmek için dışarıdan enerji verilmesi söz konusu değildir, bunun yerine kontrol amacıyla cisim üzerinde geometrik şekil değişikliklerine gidilir. Pasif kontrol yöntemleri arasından ilk akla gelenlerden biri silindir arkasına plaka yerleştirerek kopan girdapları kontrol etmektir.

Çalışma, bir cisim üzerine etkiyen ve cisim veya sistem için uygun olmadığı belirlenmiş kuvvetlerin, herhangi bir enerji gereksinimi olmadan, azaltılmasının altında yatan fiziksel temelleri araştırmaya ve uygun şartları belirlemeye yöneliktir. Bu çalışmanın belirli ve uygun bir sisteme, tek başına bilimsel, teknolojik veya ekonomik bir katkısının olma ihtimalinin düşük olduğu önceden belirtilmelidir ancak uygun bir sistemin bir bileşeninin veya bir alt-sisteminin performansını arttırmak kaydı ile sisteme istenilen katkılarda bulunabilir.

Bu çalışmanın temel amacı, bir silindir etrafındaki akışın silindir etrafında yer alan plaka ve yay yardımıyla faklı açılarla yerleştirilerek girdap dökülmesinin kontrol edilmesi ve cisim üzerindeki ortalama ve yüksek salınımlı kuvvetleri azaltacak en uygun parametreleri tayin etmektir (Şekil 1a, 1b, 1c ve 1d).



(a) (b)



(c) (d)

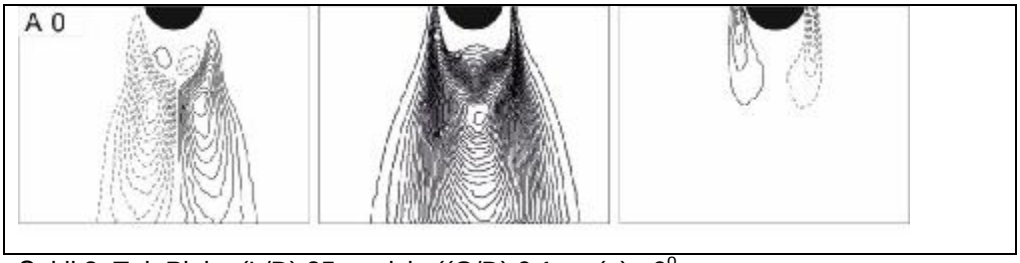
Şekil 1. Deneysel çalışmanın gösterilmesi

Şekil 1'de görülebildiği gibi çalışmadaki temel parametreler plaka ve yay'ın silindire olan mesafesi (G), düz plakaların büyüklüğü (L) ve hücum açısı (α) olarak belirlenmiştir. Hem direkt olarak silindirin iz bölgesi kontrolü hem de silindir yüzeyindeki sınır tabaka kontrolüne imkân veren bu yöntemin parametrik çalışma sonucunda en uygun şekli ve konumu tayin edilecektir. Çalışmadan kullanılan silindir ve plakalar akrilik malzemeden üretilmiştir. Çalışmada kullanılan silindirin çapı 50mm ve cidar kalınlığı 2mm, diğer kullanılan malzemelerin kalınlığı 5mm'dir. Deneylerde kullanılan plaka uzunlukları (L/D) 0.5, 0.8, 1 ve silindir arasındaki açıklıklar (G/D) 0,1, 0,3, 0,5, 0,7, 0,9 olup plakaların açısı (α)=0^o başlayıp 10° artırımlarla 180^o kadar deneyler yapılmıştır. Deneyler plakanın tek ve çift şekilde silindirin etrafında yerleştirilmesiyle gerçekleştirilmiştir.

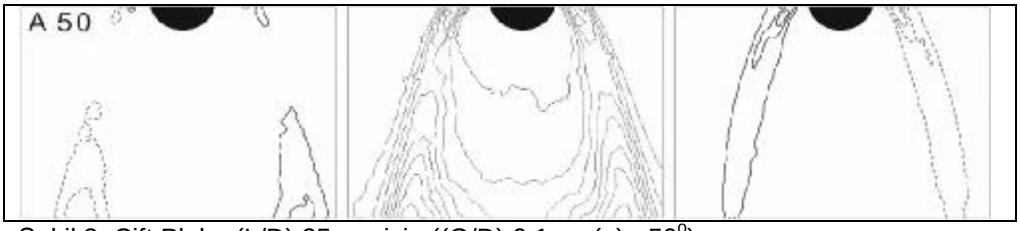
Deneyler Çukurova Üniversitesi Makine Mühendisliği Enerji Laboratuvarında gerçekleştirilmiştir. Deneyler kurulu bulunan su kanalında parçacık görüntüleme tekniği kullanarak veriler elde edilmiştir.

Deneyler Reynold 7500 değerinde yapılmış ve deney sonuçları Reynolds Kayma gerilmeleri (RSS), Türbülans Kinetik Enerji konturları (TKE), ve girdap konturları (ω) açıklanmıştır.

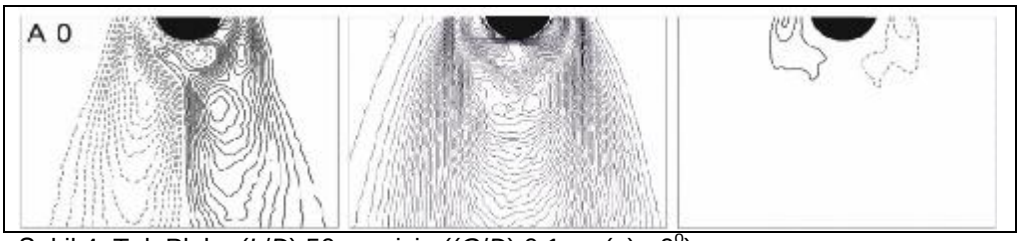
Şekil.2, 3, 4 ve 5'de yapılan deneylerin sonuçların hazırlanan grafiklerde açıklanmıştır.



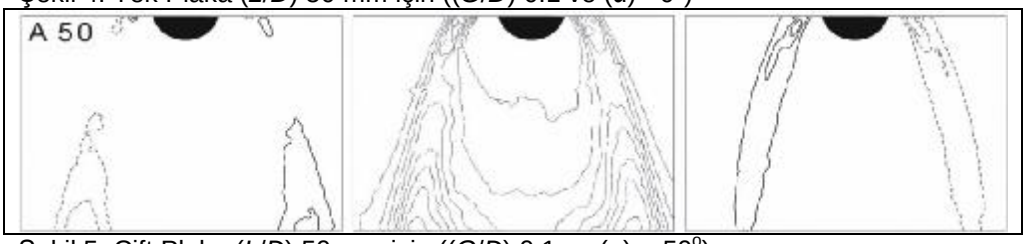
Şekil 2. Tek Plaka (L/D) 25mm için ((G/D) 0.1 ve (α)= 0^o



Şekil 3. Çift Plaka (L/D) 25mm için ((G/D) 0.1 ve (α)= 50^o)



Şekil 4. Tek Plaka (*L*/*D*) 50 mm için ((*G*/*D*) 0.1 ve (*α*)= 0^o)



Şekil 5. Çift Plaka (*L*/*D*) 50 mm için ((*G*/*D*) 0.1 ve (*α*) = 50^o)

ACKNOWLEDGEMENTS

This list endless if I have to thank all the people that made possible this work. My first and sincere thanks goes to my advisor Prof. Dr. Hüseyin AKILLI for his support, guidance and encouragement. Beginning and starting of this work would not have been possible without his long-sightedness and supervision.

I would like to thank Prof. Dr. Beşir ŞAHİN for his continues support, help and encouragements. Knowing and feeling his support during my Ph.D. thesis helped me a lot to my self-confidence.

I owe special thanks to Erhan FIRAT for creating research opportunities. I really appreciate his providing everything necessary to complete this work and keeping me on the right track.

I am especially in debt to my dear friends Durmuş Ali BİRCAN, Arif ÖZBEK, Göktürk ÖZKAN, Engin PINAR, Tahir DURHASAN and others for continuous moral support, help and excellent friend ship.

I also thank all members of Mechanical Engineering stuff for their grateful helps throughout my experiments.

Last but not least, I would like to thank my wife Serap EKİNCİ and my son Efe EKİNCİ.

CONTENTS **PAGE**

ÖZ.....I
ABSTRACT ……...…..II
GENİŞLETİLMİŞ ÖZET…….....III
ACKNOWLEDGEMENTS…….……..…VII
CONTENTS……...……..……...…..VIII
LIST OF TABLES……..……..….XII
LIST OF FIGURES……..……....XIV
NOMOCULTURE.....…….…..XX
l. INTRODUCTION……..……1
1.1. Flow past a Bluff Body …….....1
1.2. Vortex Shedding……..4
1.2.1 Mechanism of Vortex Shedding……..……..5
1.2.2. Kármán and Kelvin-Helmholtz (Shear Layer) Vortices …….……..…6
1.2.3.Strouhal Number……..…….…….9
1.3. Flow Control……...…….9
1.3.1. Active Control……..…..……10
1.3.2. Passive Control……..…..…11
1.4. The Aim of the Study…….....……13
1.5. Statement of Contribution to Original Knowledge……..……..….13
1.6. Structure of the Thesis……..14
2. LITERATURE SURVEY ……...15
2.1. Studies on Flow Control Methods……...……..…15
2.1.1. Studies on Passive Control……..…15
2.1.2. Studies on Active Control ……..…….....…24
3. MATERIAL AND METHOD…….……29
3.1. Water Channel System……29
3.2. Digital Particle Image Velocimetry(DPIV)……..30

3.3. Experimental Model……35
3.4. Physical Quantities and Dimensionless Numbers……...……...….38
3.5. Measurement of Uncertainty……...……40
4. RESULT AND DISCUSSION…..……..43
4.1. The Effect of Single Detached Plate for Plate Length of 0.5 On The Flow Control…….……..45
4.2. Comparison of Flow Control of Single Plate Arrangement for L/D= 0.5 Case……...…….....……..…63
4.3. The Effect of Dual Detached Plate for Plate Length of 0.5 On The Flow Control……...……..64
4.4. Comparison of Flow Control of Dual Plate Arrangement for L/D= 0.5 Case……..……...….75
4.5. The Effect of Single Detached Plate for Plate Length of 1 On The Flow Control ……..…..….76
4.6. Comparison of Flow Control of Single Plate Arrangement for L/D= 1 Case…….……...….92
4.7. The Effect of Dual Detached Plate for Plate Length of 1 On The Flow Control……...…….93
4.8. Comparison of Flow Control of Dual Plate Arrangement for L/D= 1 Case…….……..103
4.9. The Effect of Arc Shaped Single Detached Plate On The Flow Control....104
4.10. Comparison of Flow Control of Single Plate Arrangement for L/D= 0.8 Case……...…….118
4.11. The Effect of Arc Shaped Dual Detached Plate On The Flow Control…119
4.12. Comparison of Flow Control of Dual Plate Arrangement for L/D= 0.8 Case……..……127
4.13. Spectral Analysis for Effective Control Cases…….....128
4.13.1. FFT Analysis for Bare Cylinder ……...……..…129
4.13.2. FFT Analysis for Normalized Plate Length (*L*/*D*) of 0.5……..…130

4.13.3. FFT Analysis for Normalized Plate Length (*L*/*D*) of 1…..……133
4.13.4. FFT Analysis for Normalized Plate Length (*L*/*D*) of 0.8…….....135
5.5. CONCLUSIONS AND RECOMMENDATIONS……..…….....139
REFERENCES……..……..143
CURRICULUM VITAE…..…….…….....155

LIST OF TABLE **PAGE**

Table 3.1. Main parameters…….……...…...……..37

LIST OF FIGURES **PAGE**

Figure 1.1. A schematic of flow separation……..……..2
Figure1.2 . Regions of disturbed flow around a circular cylinder ……....2
Figure 1.3. Effect of Reynolds number on the near wake of a circular cylinder in steady upstream cross-flow…….4
Figure 1.4. Schematic of vortex shedding mechanism from cylinder…..…….....5
Figure 1.5. The Kelvin-Helmholtz vortices and the Karman vortices from circular Cylinder……...7
Figure 1.6. Variation of normalized shear layer frequency with Re……..8
Figure 1.7. Classification of flow control methods…… 10
Figure 3.1. A view from the upstream reservoir…….…….29
Figure 3.2. The components of the water channel……...30
Figure 3.3. Principles of PIV……...…31
Figure 3.4. Seeding material……...…….33
Figure 3.5. Laser unit……...……33
Figure 3.6. CCD camera with lens……..……..……...33
Figure 3.7. The interface of the DynamicStudio v3.20 software…….34
Figure 3.8. Three-dimensional view of the cylinder-plate system…….…..36
Figure 3.9. Cross-Sectional view of the experimental set-up.....……...36
Figure 3.10. Cylinder with single and dual detached plates…….……...37
Figure 4.1. The spatial distribution of time-averaged Reynolds shear stress $<u'v'>$, turbulent kinetic energy$<TKE>$ and vorticity contours, $<\omega>$ for gap ratio of 0.1 and bare cylinder case……...48-49
Figure 4.2. The spatial distribution of time-averaged Reynolds shear stress $<u'v'>$, turbulent kinetic energy$<TKE>$ and vorticity contours, $<\omega>$ for gap ratio of 0.3 and bare cylinder case……...51-52

Figure 4.3. The spatial distribution of time-averaged Reynolds shear stress $<u'v'>$, turbulent kinetic energy$<TKE>$ and vorticity contours, $<\omega>$ for gap ratio of 0.5 and bare cylinder case…….…....54-55
Figure 4.4. The spatial distribution of time-averaged Reynolds shear stress $<u'v'>$, turbulent kinetic energy$<TKE>$ and vorticity contours, $<\omega>$ for gap ratio of 0.7 and bare cylinder case……...57-58
Figure 4.5. The spatial distribution of time-averaged Reynolds shear stress $<u'v'>$, turbulent kinetic energy$<TKE>$ and vorticity contours, $<\omega>$ for gap ratio of 0.9 and bare cylinder case… …….……61-62
Figure 4.6. All results of experiment at single plate arrangement in the detached plate length of 0.5 in terms of TKE_{max}…..…..…..…..…..…..…..…64
Figure 4.7. The spatial distribution of time-averaged Reynolds shear stress $<u'v'>$, turbulent kinetic energy$<TKE>$ and vorticity contours, $<\omega>$ for gap ratio of 0.1 and bare cylinder case……...66
Figure 4.8. The spatial distribution of time-averaged Reynolds shear stress $<u'v'>$, turbulent kinetic energy$<TKE>$ and vorticity contours, $<\omega>$ for gap ratio of 0.3 and bare cylinder case…….……...68
Figure 4.9. The spatial distribution of time-averaged Reynolds shear stress $<u'v'>$, turbulent kinetic energy$<TKE>$ and vorticity contours, $<\omega>$ for gap ratio of 0.5 and bare cylinder case…….…...70
Figure 4.10. The spatial distribution of time-averaged Reynolds shear stress $<u'v'>$, turbulent kinetic energy$<TKE>$ and vorticity contours, $<\omega>$ for gap ratio of 0.7 and bare cylinder case…….…….....72
Figure 4.11. The spatial distribution of time-averaged Reynolds shear stress $<u'v'>$, turbulent kinetic energy$<TKE>$ and vorticity contours, $<\omega>$ for gap ratio of 0.9 and bare cylinder case…….…….....74
Figure 4.12. All results of experiment at dual plate arrangement in the detached plate length of 0.5 in terms of TKE_{max}……..75

Figure 4.13. The spatial distribution of time-averaged Reynolds shear stress $\langle u'v' \rangle$, turbulent kinetic energy $\langle TKE \rangle$ and vorticity contours, $\langle \omega \rangle$ for gap ratio of 0.1 and bare cylinder case…….....78-79
Figure 4.14. The spatial distribution of time-averaged Reynolds shear stress $\langle u'v' \rangle$, turbulent kinetic energy $\langle TKE \rangle$ and vorticity contours, $\langle \omega \rangle$ for gap ratio of 0.3 and bare cylinder case…….....81-82
Figure 4.15. The spatial distribution of time-averaged Reynolds shear stress $\langle u'v' \rangle$, turbulent kinetic energy $\langle TKE \rangle$ and vorticity contours, $\langle \omega \rangle$ for gap ratio of 0.5 and bare cylinder case…….....84-85
Figure 4.16. The spatial distribution of time-averaged Reynolds shear stress $\langle u'v' \rangle$, turbulent kinetic energy $\langle TKE \rangle$ and vorticity contours, $\langle \omega \rangle$ for gap ratio of 0.7 and bare cylinder case…….....87-88
Figure 4.17. The spatial distribution of time-averaged Reynolds shear stress $\langle u'v' \rangle$, turbulent kinetic energy $\langle TKE \rangle$ and vorticity contours, $\langle \omega \rangle$ for gap ratio of 0.9 and bare cylinder case…….....90-91
Figure 4.18. All results of experiment at single plate arrangement in the detached plate length of 1 in terms of TKE_{max}…….92
Figure 4.19. The spatial distribution of time-averaged Reynolds shear stress $\langle u'v' \rangle$, turbulent kinetic energy $\langle TKE \rangle$ and vorticity contours, $\langle \omega \rangle$ for gap ratio of 0.1 and bare cylinder case…….....94
Figure 4.20. The spatial distribution of time-averaged Reynolds shear stress $\langle u'v' \rangle$, turbulent kinetic energy $\langle TKE \rangle$ and vorticity contours, $\langle \omega \rangle$ for gap ratio of 0.3 and bare cylinder case…….....96
Figure 4.21. The spatial distribution of time-averaged Reynolds shear stress $\langle u'v' \rangle$, turbulent kinetic energy $\langle TKE \rangle$ and vorticity contours, $\langle \omega \rangle$ for gap ratio of 0.5 and bare cylinder case…….....98
Figure 4.22. The spatial distribution of time-averaged Reynolds shear stress $\langle u'v' \rangle$, turbulent kinetic energy $\langle TKE \rangle$ and vorticity contours, $\langle \omega \rangle$ for gap ratio of 0.7 and bare cylinder case…….....100

Figure 4.23. The spatial distribution of time-averaged Reynolds shear stress $<u'v'>$, turbulent kinetic energy$<TKE>$ and vorticity contours, $<\omega>$ for gap ratio of 0.9 and bare cylinder case…….....102
Figure 4.24. All results of experiment at dual plate arrangement in the detached plate length of 1 in terms of TKE_{max}…….103
Figure 4.25. The spatial distribution of time-averaged Reynolds shear stress $<u'v'>$, turbulent kinetic energy$<TKE>$ and vorticity contours, $<\omega>$ for gap ratio of 0.1 and bare cylinder case…….....105
Figure 4.26. The spatial distribution of time-averaged Reynolds shear stress $<u'v'>$, turbulent kinetic energy$<TKE>$ and vorticity contours, $<\omega>$ for gap ratio of 0.3 and bare cylinder case…….....107-108
Figure 4.27. The spatial distribution of time-averaged Reynolds shear stress $<u'v'>$, turbulent kinetic energy$<TKE>$ and vorticity contours, $<\omega>$ for gap ratio of 0.5 and bare cylinder case…….....110-111
Figure 4.28. The spatial distribution of time-averaged Reynolds shear stress $<u'v'>$, turbulent kinetic energy$<TKE>$ and vorticity contours, $<\omega>$ for gap ratio of 0.7 and bare cylinder case…….....113-114
Figure 4.29. The spatial distribution of time-averaged Reynolds shear stress $<u'v'>$, turbulent kinetic energy$<TKE>$ and vorticity contours, $<\omega>$ for gap ratio of 0.9 and bare cylinder case…….....116-117
Figure 4.30. All results of experiment at single arc shaped plate arrangement in the detached plate length of 0.8 in terms of TKE_{max}……..…118
Figure 4.31. The spatial distribution of time-averaged Reynolds shear stress $<u'v'>$, turbulent kinetic energy$<TKE>$ and vorticity contours, $<\omega>$ for gap ratio of 0.1 and bare cylinder case…….....120
Figure 4.32. The spatial distribution of time-averaged Reynolds shear stress $<u'v'>$, turbulent kinetic energy$<TKE>$ and vorticity contours, $<\omega>$ for gap ratio of 0.3 and bare cylinder case…….....122

Figure 4.33. The spatial distribution of time-averaged Reynolds shear stress <$u'v'$>, turbulent kinetic energy<*TKE*> and vorticity contours, <ω> for gap ratio of 0.5 and bare cylinder case…….....123
Figure 4.34. The spatial distribution of time-averaged Reynolds shear stress <$u'v'$>, turbulent kinetic energy<*TKE*> and vorticity contours, <ω> for gap ratio of 0.7 and bare cylinder case…….....125
Figure 4.35. The spatial distribution of time-averaged Reynolds shear stress <$u'v'$>, turbulent kinetic energy<*TKE*> and vorticity contours, <ω> for gap ratio of 0.9 and bare cylinder case…….....126
Figure 4.36. All results of experiment at dual plate arrangement in the detached plate length of 0.8 in terms of TKE_{max}……..…127
Figure 4.37. The variation of Strouhal number with Reynolds number for a circular Cylinder……..…..129
Figure 4.38. Spectral analysis of streamwise velocity fluctuations for bare cylinder …….....130
Figure 4.39. Spectral analysis of streamwise velocity fluctuations for effective single detached plate arrangement cases for *L*/*D*=0.5……...131
Figure 4.40. Spectral analysis of streamwise velocity fluctuations for dual detached plate arrangement effective cases for *L*/*D*=0.5…….....132
Figure 4.41. Spectral analysis of streamwise velocity fluctuations for effective single detached plate arrangement cases for *L*/*D*= 1…….134
Figure 4.42. Spectral analysis of streamwise velocity fluctuations for effective dual detached plate arrangement cases for *L*/*D* =1…….135
Figure 4.43. Spectral analysis of streamwise velocity fluctuations for effective single detached plate arrangement cases for *L*/*D*=0.8…….…….137
Figure 4.44. Spectral analysis of streamwise velocity fluctuations for effective dual plate arrangement cases for *L*/*D*=0.8……....138

NOMENCLATURE

D	: Diameter of the cylinder (mm)
f	: Frequency (Hz)
L/d	: Normalized length of the plate
L	: Length (mm)
Re	: Reynolds number
St	: Strouhal number
t	: Time (s)
TKE	: Turbulent kinetic energy
Tu	: Turbulence intensity
u, v, w	: Streamwise, transverse and spanwise components of velocity (m/s)
U	: Resultant velocity (m/s)
un	: Uncertainty
VR	: Velocity Ratio
Acronyms	
VIV	: Vortex-Induced Vibration
Operators	
<…>	Time-averaged
Greek symbols	
α	: Angle of incidence (°)
μ	: Viscosity of fluid (kg/m/s)
ρ	: Density of fluid (kg/m^3)
υ	: Kinematic viscosity of fluid (m^2/s)
ω	: Vorticity (1/s)

1. INTRODUCTION

1.1. Flow Past a Bluff Body

The flow past a bluff body has been studied extensively owing to its practical importance in engineering and fundamental significance in fluid mechanics. The nature of the flow over a bluff body has been the subject of extensive investigation for many years. Experimental, numerical and theoretical analysis have all been applied to studying cases such as the canonical flow over a circular cylinder, and to other cases like flow over square, triangular, rectangular, or elliptic cylinders.

In engineering practice, a circular cylinder, which is one of the structure components employed mostly, is a typical bluff body. A bluff body is define as bodies that when subjected to a stream of fluid, suffers separation of large part of its surface or defined as bodies that are not streamline shape so that separation occurs (Williams, 2002). The problem about the viscous flow past bluff bodies, a very complicated physical phenomenon, which is of great important value for academic research and a strong background for engineering application, has long been the subject of interest for fundamental studies in fluid dynamics. With the development of many aspects of engineering industries, fluid-structure interactions became one of the most challenge problems for modern fluid mechanics.

Flow approaching a circular cylinder is forced to deviate from its uniform straight path to move around the cylinder. At very low Reynolds numbers (*Re*), the flow is tangent to the surface of the cylinder and streamlines are symmetric. At $Re<5$, the flow field is steady and known as creeping flow. As Reynolds number increases, inertia force effects increase in comparison to viscous forces. As the inner boundary layer has lower velocity, it is more sensitive to the pressure gradient and thus the stagnation or reverse flow starts from this region. The boundary layer separates due to

the adverse pressure gradient generated because of the divergent geometry of the flow on the rear side of the cylinder. The vorticity in the boundary layer is fed into the shear layer forcing the latter to roll up into a vortex. Thus, the shear layer is formed as shown in Figure 1.1. In the same way, a vortex rotating in the opposite direction is formed on the other side of cylinder.

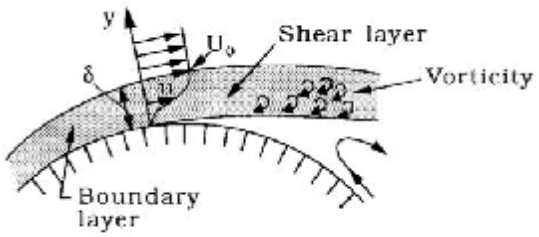


Figure 1.1. A schematic of flow separation

At low Reynolds number the flow is steady and laminar. With increasing Reynolds number the flow becomes unsteady in two-dimensional periodic manner with regular vortex shedding forming a Kármán vortex street in the wake. At even higher Reynolds numbers (*Re*>190) the flow becomes three-dimensional, and finally becomes chaotic and turbulent. For a given geometry the transition between these states occur at precise values of the Reynolds number based on the body thickness.

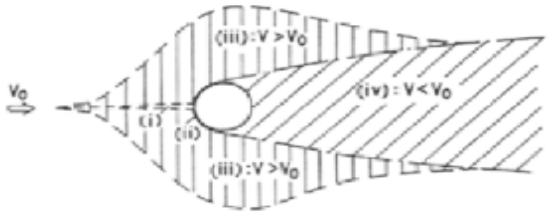


Figure 1.2. Regions of disturbed flow around a circular cylinder (Zdravkovich, 1997)

When a fluid flows past a circular cylinder, a region of disturbed flow is always formed around the cylinder (Zdravkovich, 1997). Figure 1.2 shows the division of the disturbed flow regions. Region (i) is narrow region of retarded flow, (ii) denotes the region where the two boundary layers attached to the surface of the cylinder. Region (iii) depicts two sidewise regions of displaced and accelerated flow, and region (iv) is one wide region of separated flow called wake (Zdravkovich, 1997). The wake region is characterized by vortex shedding processes. For a turbulent unbounded, plane wake, the spanwise length scale of vortices is roughly proportional to the width of the wake and the vortices exhibit strong 3D components (Lloyd and Stnsby, 1997).

The flow pattern and the drag on a cylinder are functions of the Reynolds number. A more thorough depiction of the wake structure dependence on Reynolds number can be seen in Figure 1.3. (a) creeping flow, $Re<5$; (b) attached recirculation zone, Re 5 to 40; (c) low, transitional and high Reynolds numbers laminar and transitional vortex shedding, $Re=40$ to 350; (d) subcritical regime, $Re=350$ to 2×10^5; (e) critical regime, $Re=2\times10^5$ to 7×10^4; (f) supercritical regime, $Re=7\times10^5$ to 3.5×10^6 (g) transciritical or post-critical regime, $Re>3.5\times10^6$. The Reynolds number ranges specified are approximate, since the upper and lower limits are sensitive to experimental conditions, and differ from one study to another.

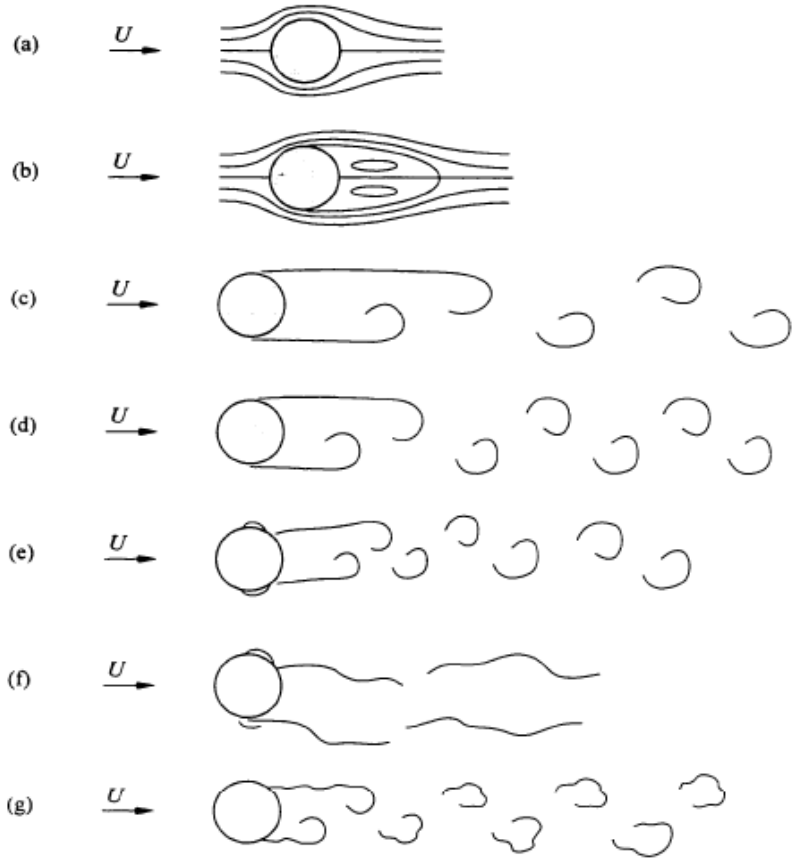


Figure 1.3. Effects of Reynolds number on the near-wake of a circular cylinder in steady upstream croos-flow.

1.2. Vortex Shedding

The central feature of bluff body wake is the shedding of vortices from the separated shear layers after a certain (low) value of the Reynolds number. The shedding of vortices is alternated between the top and bottom shear layers formed on the body. The essential mechanisms of vortex formation from the separted shear layers can be explained by the growth of disturbances in two infinite, initially parellel vortex in an inviscid incompressible fluid (Abernathy and Kronauer, 1962). The presence of two shear layers, rather than the bluff body itself, is primarily responsible for

vortex shedding. The presence of the body however modifies the process by allowing feedback between the wake and the shear layers.

The vortex shedding induces forces that may result in transverse and inline oscillations. This phenomenon is known as vortex induced vibration (VIV). VIV occurs in a large variety of engineering fields such as civil and mechanical engineering where cylindrical structures are commonly used. Examples are undersea pipelines, drilling risers, transmission lines and suspension bridges cables exposed to ocean or wind currents, etc.

1.2.1. Mechanicsm of Vortex Shedding

Figure 1.4 illustrates the vortex formation by means of filament lines the rolling–up shear layers (Gerrard, 1966). The arrows show the path of the fluid at later times during the entrainment process. The fluid is (a) largely engulfed into growing vortex and (c) partly entrained by the shear layer upstream of vortex. Some of the fluid (b) finds its way into the interior of the vortex-formation region. During their formation the growing vortices draw in fluid from the base region, and the removal of entrained fluid is balanced by an induced reverse flow into formation region (Bearman and Treuman, 1972). It is further suggested that the enterainment process also provides a form of feedback to stabilize the vortex shedding.

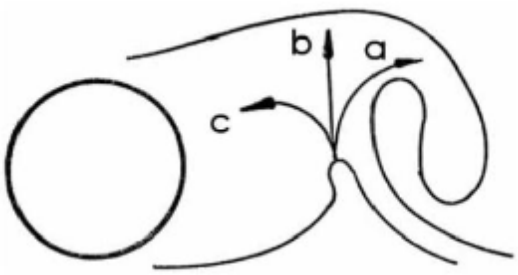


Figure 1.4. Schematic of vortex shedding mechanism from the cylinder (Gerrard, 1964)

Since Roshko (1955) first measured the period of Kármán vortex shedding behind a bluff body, researchers have been steadily investigating vortex shedding and nearwake flow as reported in the reviews by Berger & Wille (1972), Lin & Pao (1979), Bearman (1984), Oertel (1990), Griffin & Hall (1991), Coutanceau & Defaye (1991), and Williamson (1996, 2004). Furthermore, efforts have been made to alter and suppress vortex shedding.

1.2.2. Kármán and Kelvin-Helmholtz (Shear Layer) Vortices

Two types of streamwise vortices have been reported in the laminar and transitional wakes of cylinders. At a sufficiently high value of Reynolds number, so-called “transition waves” appears in the shear layer separating from the surface of the cylinder. These waves are detectable in the region of the wake extending from the separation point on the body to the first appearance of the large-scale Kármán vortex.

As a result, a vortex is shed from the cylinder when the local pressure changes each time. Therefore, the cylinder is subjected to a fluctuating drag and lift in addition to the mean drag and lift. The drag, lift and vortex shedding frequency are normally expressed in non-dimensional forms as the drag coefficient (C_D), the lift coefficient (C_L) and the Strouhal number (St). These three non-dimensional parameters depend on the nature of both the approaching flow and the cylinder. When the cylinder is located near a plane boundary, the bed proximity and the velocity gradient in the boundary layer, as well as the turbulent characteristics of the boundary layer, also have some influence on these parameters.

When the value of Reynolds number is sufficiently high, then these transition waves take the form of train of Kelvin-Helmholtz vortices shown in Figure 1.5. In the bluff body community, these small-scale vortices are often referred to as Bloor-Gerrard vortices. It can be noted that it is also called shear layer vortices. The onset of “transition waves” is expected to be

strong function of the disturbance level of the free stream, in view of the fact that they arise from convective-type instability, as described by Ho and Huerre (1984). Bloor (1964) detected the small-scale vortices for the range of Reynolds number Re>1300, however, Ünal and Rockwell (1988) first noted these vortices at Re_D=1900. Wu et al. (1994) discussed the possible influence of background disturbance levels and observed these waves over the range of Reynolds numbers $1000 \leq Re \leq 3000$.

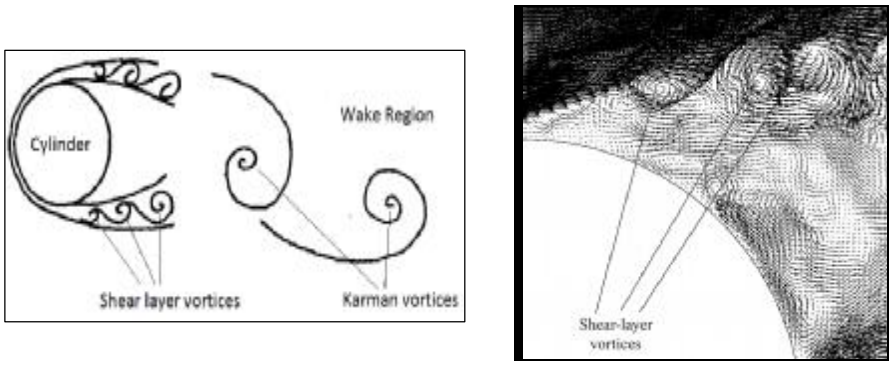


Figure 1.5. The Kelvin-Helmholtz (shear layer) vortices and the Kármán vortices from circular cylinder (Williamson, 1996; Dong et al., 2008)

Kelvin-Helmholtz vortices in the shear layer are an essential feature of the transition from a laminar to turbulent state. As a consequence of this transition process, the first Kármán vortex formed from the cylinder at Re_D=5000 is essentially turbulent.

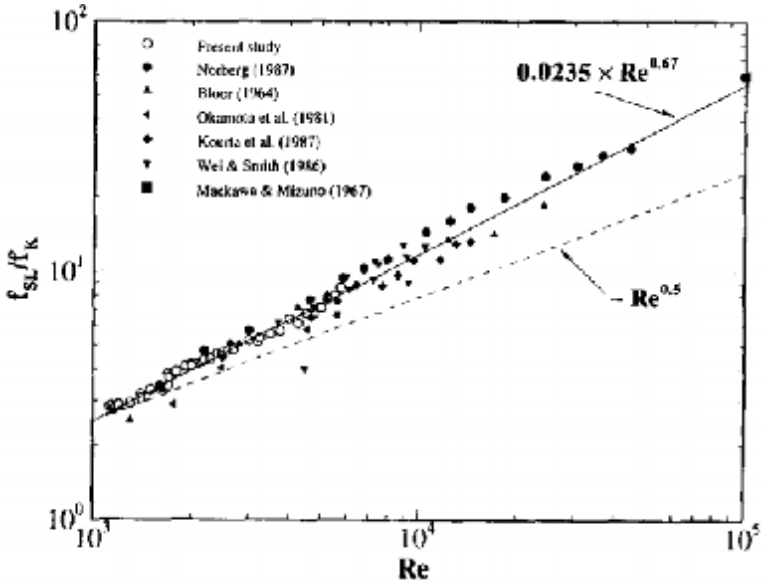


Figure 1.6. Variation of normalized shear layer frequency (the shedding frequency ratio of shear layer vortices to Kármán vortices) with *Re*. (Williamson, 1997)

With regard to the normalised frequency of the instability (f_{SL}/f_K), and following the original work of Bloor (1964), almost all previous investigators have assumed a variation of the form $Re^{0.5}$. There is no question that this is of the right order, although even a cursory glance of actual data points from these investigations does not precisely support the $Re^{0.5}$ variation. We shall briefly discuss these matters below. For clarity, the frequencies are defined by f_{SL} which is the shear layer frequency, and f_K, which is the Kármán vortex frequency. $f_{SL}/f_K = A \times Re^p$ is distinctly greater than 0.5 in each and every case. All the compiled data has been plotted in Fig. 1.6. The least-squares best-fit to the data is $f_{SL}/f_K = 0.0235 \times Re^{0.67}$ and the line for $Re^{0.5}$, although clearly of the right order, does not precisely fit the measured data. One might note that the data extend over a large range from *Re*=1,200 up to *Re*=100,000.

1.2.3. Strouhal Number

The frequency of vortex shedding has a possible relationship with the flow velocity. This relationship is characterized by the Strouhal number

$$St = f_K D/V \tag{1.1}$$

where f_K is the frequency of a complete cycle of vortex shedding for the body at rest (also referred to as Strouhal frequency). Kármán vortex shedding frequency can be mesaured by placing a velocity probe downstream of (wake) the body. D is a characteristic structure dimension perpendicular to the direction of flow. V is the velocity of approaching flow. The Strouhal number of a stationary cylinder in a subsonic flow is a function of Reynolds number, surface roughness and freestream turbulence.

1.3. Flow Control

Flow over a bluff body is a common occurrence associated with fluid flowing over an obstacle or with the movement of a natural or artificial body. Evident examples are the flows past an airplane, a submarine and an automobile and wind blowing past a bridge and a high-rise building. At much lower Reynolds numbers, the flow over a bluff body is highly viscous, and the force exerted on the body is mainly attributed to skin friction. However, when the Reynolds number exceeds a critical value, vortex shedding occurs in the wake, resulting in a significant pressure drop on the rear surface of the body. This vortex shedding occurs over a wide range of Reynolds numbers. This vortex shedding occurs over a wide range of Reynolds numbers causing serious structural vibrations, acoustic noise and resonance, enhanced mixing, and significant increases in the mean drag and lift fluctuations. Therefore, the effective control of vortex shedding is important in engineering applications, in general.

There are lots of schemes for classifying flow control methods. Here, we considered energy expenditure scheme. The control device can be passive, requiring no auxiliary power, and active, requiring an auxiliary power, based on this scheme. In the past, many passive and active methods were introduced to control vortex shedding behind a bluff body, such as a circular cylinder and a blunt-based bluff body. Examples include end plates, splitter plates, geometric modifications in the trailing edge, base bleed, axial slit, electrohydrodynamic and magnetohycrodynamic body forces, heating, oscillation in line with the incident flow, and rotary oscillation.

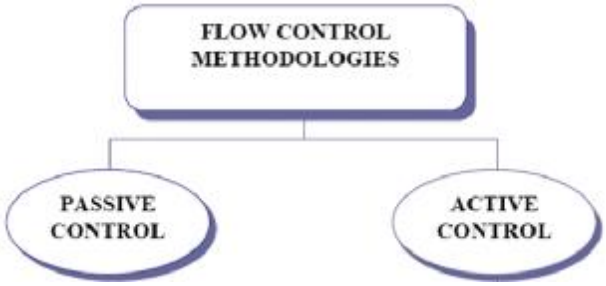


Figure 1.7. Classification of flow control methods.

1.3.1. Active Flow Control

Active control methods, applying some sorts of energy into the flow, have been developed in order to solve vortex shedding problem among others. The aim of active control is to exploit the instability of the wake, which is the cause of the vortex formation, to indirectly modify the mean wake velocity profile and drag.

There are two primary advantages to active flow control that are not achievable by passive techniques. First active flow control technology leverages and controls a natural stability of the flow to attain a large effect using small localized energy input. Control is most effective when the control input is introduced locally at a high receptivity region. Secondly, active control can be used to control complex, dynamical processes like

turbulence production in turbulent boundary layers to reduce skin friction and hence viscous drag where the reduction is proportional to the surface area covered by the actuators. On the other hand, to put energy from outside is the disadvantage of the active control techniques. There are various active control techniques such as; feedback control, electro-magnetic control, rotating circular cylinder, wake heating, suction and blowing.

As can be seen from the figure 1.7, the flow control can involve passive or active methods. But during the last decade, more emphasis has been on the development of active control methods in which energy, or auxiliary power, is introduced into the flow. Active control schemes can be divided into predetermined or interactive methods. A predetermined method of control involves the introduction of steady or unsteady energy inputs without consideration for the state of the flow field. Examples of predetermined active flow control include jet vectoring using piezoelectric actuators (Smith and Glezer, 1997) and post stall lift enhancement and form drag reduction using oscillatory blowing (Seifert and Pack, 1999a).

In interactive methods of flow control, the power input to the actuator (controller) is continuously adjusted based on some form of measurement element (sensor). The control loop for interactive control can be either a feed forward (open) or feedback (closed) loop. In the feed forward control loop, the sensor is placed upstream of the actuator. Therefore the measured flow field parameter and the controlled flow field parameter will differ as flow structures come over stationary sensors and actuators.

1.3.2. Passive Flow Control

Passive control techniques modify a flow without external energy expenditure. Passive control techniques control the vortex shedding by modifying the shape of the bluff body or by attaching additional devices in

the flow stream. Passive control techniques include geometric shaping to manipulate the pressure gradient, the use of fixed mechanical vortex generators for separation control, and placement of longitudinal grooves or riblet on a surface to reduce drag.

Passive control techniques are widely used for flow control applications. They have same advantages of being easier to implement, less expensive in cost, and more stable. The methods have proved successful particularly in offshore explorations and marine hydraulics.

Roshko(1954) and Zdravkovich(1981) are among the first investigators, Zdravkovich(1981) presents control techniques that can be classified into three categories:

(i) The control of shear layer by surface protrusion (tripping wire, fin, helical strakes, helical wires, studs, etc.), which affects flow separation lines (James and Truong, 1972); this can be further subdivided into omnidirectional and unidirectional. The omnidirectional techniques are those not affected by the direction of flow velocity; for example, helical strakes and helical wires. The unidirectional are those effective only for a given direction of flow velocity; for example, straight fins. The full shrouds are omnidirectional, while incomplete shrouds become unidirectional.

(ii) The control of the entrainment layers by shrouds (perforated gauze, axial rods, etc.) that supply irrotational fluid to the entrainment layers (Knell, 1969)

(iii) The instability control of wakes by near-wake stabilizers (splitter plate, guiding plates, base-bleed, slits cut along the models, etc.) that reduce the interaction of two opposite shear layers (Roshko, 1954, Bearman, 1965, Wood, 1967, Aplet, West and Szewczyck, 1973).

1.4. The Aim of the Study

The vortex flow casueses adverse effects on a large number of enginnering applications. Therefore, control of vortex shedding has a great importance since it causes reductions in the time-varying flow-induced forces acting on the bluff bodies and many studies have been carried out in the past to establish a method to control the vortex shedding which can be observed easily when fluids flows over a bluff body.

The motivation of this thesis stems from the study of Galvao et al. (2008) who employed passive flow control using two-dimensional hydrofoils to reduce vortex-induced vibrations (VIV) and drag on a cylinder. The aim of this study is to assess the effect of single and dual plates on the near-wake flow structure of a single circular cylinder in the subcritical flow regime.

In the study, velocity field measurements will be conducted in the wake of test models; velocity statistics and streamline topology will compared with that of the single circular cylinder. Main parameters are angle of rotation (α), number of plate (single or dual), normalized plate length (L/D) and normalized gap length (G/D). The effects of these parameters for experiments will be explained by means of the Reynolds Shear Stress contours (RSS), Turbulent Kinetic Energy (*TKE*) contours, and spanwise vorticity contours (ω_z).

1.5. Statement of Contribution to Original Knowledge

The subject of this research was the near-wake flow structure of two-dimensional (2D) circular cylinder subjected to cross-flow. The contributions of the thesis to original knowledge include that this is the first parametric investigation of the cylinders with single and dual plates in steady cross-flow. The findings serve as useful guidelines for researchers or product developers.

1.6. Structure of the Thesis

The present thesis is divided into 5 chapters, including this introduction:

Chapter 2 presents a brief introduction to a literature review about various flow control methods and their effectiveness in suppressing vortex shedding. Some similar passive control techniques were also revised in the chapter.

Chapter 3 describes the experimental set-up employed in this study, comprising flow facility, experimental techniques and models. Furthermore, physical quantities, dimensionless numbers utilized in the thesis were also described as well as uncertainty analysis.

Chapter 4 presents preliminary results for turbulence statistics and wake characteristics in the near-wake of various test models with respect to angles of rotation (α), number of plate (single or dual), normalized plate length (L/D) and normalized gap length (G/D).

Chapter 5 concludes the thesis summarizing the main findings and contributions of the present study. It also suggests further works to advance the present investigation.

2. LITERATURE SURVEY

2.1. Studies on Flow Control Methods

Flow control methods have been used for many years to control the fluid flow. The ability to manipulate a flow passively or actively is of immense technological importance. Here, we will present some active and passive flow control methods.

2.1.1. Studies on Passive Control

One of the first reports on periodic vortex formation suppression using a circular cylinder connected with a splitter plate was presented by Roshko (1954) at a Reynolds number of 1.45×10^4. He also showed that, by positioning this splitter plate at different fixed distances in the fully developed cylinder-wake, the Strouhal number (St) diminishes as the distance between the cylinder and the plate increases up to a limit position ($G \approx 2.7D$). He also observed that a splitter plate of chord $5D$, attached to the cylinder, results in suppression of shedding. A plate of chord $1D$ does not inhibit formation of vortices but changes the shedding frequency slightly. Roshko (1955) observed flow changes at $Re_d=1.45\times10^5$ when splitter plates were inserted behind a cylinder. When the plate was attached on the cylinder base and the length of the splitter plate (l) was larger than $5d$, the vortex shedding disappeared, and thus drag was significantly reduced. On the other hand, he also observed flow changes as the plate of $l=d$ moved downstream. When the splitter plate was located downstream less than $4d$, the Strouhal number decreased and the base pressure increased as the splitter plate moved downstream. However, when the splitter plate was located farther downstream, the flow field did not show much difference from the natural vortex shedding. Every et al. (1982) compared several devices used to limit vortex shedding from cylinders and cables used in marine applications. They found that even very short splitter plates significantly reduce the wake width and a minimum drag coefficient is reached at $L \approx D$. A “flexible” splitter

plate, also known as a flag, was shown to suppress the oscillation of foundation piles. Experiments on flow over a circular cylinder with splitter plate were conducted by Unal and Rockwell (1988) in the *Re* range of $140 < Re < 1600$. The flow patterns observed were divided into two separate regions: pre-vortex formation regime and post-vortex formation regime. The pre- and post-vortex formation regimes were characterized by the absence and presence of large-scale vortices upstream of the plate's tip respectively. The unsteady pressure forces acting on the plate were found to change drastically when the plate was moved from the one regime to another. An experimental investigation was carried out by Mansingh and Oosthuizen (1990) to study the effect of a splitter plate on the two-dimensional wake of a bluff body with fixed separation points. This experimental study has shown that the characteristics of the wake downstream of a bluff body with fixed separation points can be considerably altered by placing a splitter plate on the wake centerline downstream of the bluff body. The effect of splitter plates on the wake flow characteristics of a rectangular cylinder with a splitter plate shows a relatively small change in Reynolds number. The behavior of a circular cylinder with attached splitter plate, under conditions where the entire cylinder/splitter plate body is free to rotate about the cylinder's axis, has been studied by Cimbala et al. (1991). Under their conditions, the splitter plate did not align itself with the free stream, but instead migrated from the centerline position to a nonsymmetric equilibrium position. Theoretically, the splitter plate could move to either side of the centerline with the same probability. Cimbala and Garg (1991) studied the influence of splitter plate on a freely rotatable cylinder, and reported that splitter plate of $L/D<5$ were not aligned with the free-stream flow. The formation length and the frequency of von Kármán vortex shedding were completely different between the rotatable plate and a fixed one when $L/D<2$. For greater L/D, they behaved in the same way even though the rotatable cylinder-plate combinations were not aligned with the free-stream flow. The inverse relationship between the formation length and the shedding frequency was found to be

applicable for the rotatable cylinder also. Roshko (1993) controlled the flow around a circular cylinder by attaching a splitter plate behind the cylinder and investigated the suppression of vortex shedding. When the gap between the cylinder and splitter plate was large, the effect of the splitter plate became strong. The parameter that had the greatest effect on the vortex shedding was the gap width rather than the length of splitter plate. Lin and Wu (1994) conducted a numerical study for the Re_D=100 flow to see the effect of a splitter plate. They found that a splitter plate of length 2D attached to the cylinder is sufficient to completely suppress vortex shedding. It was also found that a splitter plate whose upstream edge is located at more than 2.5D from the cylinder is ineffective of suppressing vortex shedding. Hasan and Budair (1994) investigated the effect of length and location of a splitter plate detached from a circular and square cylinder for $1.2\times10^4<Re_D<3.0\times10^4$. They found that when the splitter plate is located close to the cylinder, the shear layer instability tone plays a role in controlling the frequency characteristics of the flow. The shear layer instability tone disappears for large gap between the plate and cylinder, but the wake instability remains. Lin and Wu (1994) found that a splitter plate having a length of 2D attached to the cylinder could suppress the vortex shedding and when the plate was located more than 2.5D from the base of the cylinder, vortex suppression was not obtained for Re=100. Akilli et al. (2005) investigated the effect of splitter plate on the suppression of vortex shedding in shallow water using the Particle Image Velocimetry (PIV) technique. Splitter plates with a length of 50 mm, which is equal to the diameter of the cylinder (D), were used during the experiments. Gap distance between the base of the cylinder and the leading edge of the splitter plate ranged from 0 to 2D. Velocity vector field and corresponding vorticity contours and streamline topology and Reynolds stress concentrations were used to explain the characteristics of the flow. The splitter plates having different thicknesses presented the same influence on the flow characteristics. The splitter plate has a substantial effect on suppression of the vortex shedding for the gap ratio between 0 and 1.75D. In these gap ratios, shear

layers extend up to the trailing edge of the splitter plate preventing the entrainment of the free-stream flow into the base region. For G/D=1.75, the normalized Reynolds stress has a peak value of 0.0158 which is approximately 8.5 times smaller than the concentrations occurring for a bare cylinder. After passing the splitter plate, the flow starts to oscillate with smaller frequency compared to the natural frequency of the bare cylinder. When the splitter plate was located at 2D location, no effect of the splitter plate was observed. Akıllı et al. (2008) investigated experimentally passive control of vortex shedding behind a circular cylinder by splitter plates of various lengths attached on the cylinder base in shallow water flow (Re=6,300). At this study the length of the splitter plate was varied from L/D=0.2 to L/D=2.4 in order to see the effect of the splitter plate length on the flow characteristics. Instantaneous and time-averaged flow data clearly indicate that the length of the splitter plate has a substantial effect on the flow characteristics. They found the flow characteristics in the wake region of the circular cylinder sharply change up to the splitter plate length of L/D=1.0 and above this plate length, small changes occur in the flow characteristics. Stappenbelt (2010) investigated the proposed utility of splitter-plate wake stabilization as a passive control mechanism for vortex-induced vibration (VIV) mitigation for low aspect ratio cylinders. His experiments of stationary cylinder show the effectiveness of splitter plates in reducing lift and drag coefficients, C_D and C_L for a cylinder in uniform flow. On the other hand, rigid attached splitter plates are capable of entirely eliminating vortex shedding in fixed cylinder investigations. Assi et al. (2010) studied on a pair of circular cylinders to investigate the effectiveness of pivoting parallel plates as wake-induced vibration suppressors. Measurements of amplitude of vibration and average drag are presented for a circular cylinder, free to respond in the cross-flow direction, with mass ratio of 2 and a damping level of 0.7% of critical damping. Reduced velocities were up to nearly 30, with associated Reynolds numbers up to 2.3×10^4 and the results presented are for a centre-to-centre separation of cylinders of 4 diameters. They

showed how vortexinduced vibration and wake-induced vibration of the downstream cylinder of a tandem pair can be practically eliminated by using free to rotate parallel plates. They also presented the results for a single splitter plate and helical strakes for comparison, however they were found not to be effective in suppressing wake-induced vibration. Gozmen et al. (2013) conducted an experimental work on the control of vortical flow of circular cylinder using a splitter plate having different lengths and heights. They found that as the ratio of hp/hw increases, the effect of the splitter plate on the suppression of the vortex shedding increases. Flow characteristics and the examination of spectra indicated that Kármán vortex shedding is attenuated pronouncedly for the cases of $L/D \geq 1$ and $h_p/h_w \geq 0.75$. The transverse Reynolds normal stress is more effective on the attenuation of turbulent kinetic energy than the streamwise Reynolds normal stress, $\langle u'u'/U^2 \rangle$. They also found that the value of peak transverse Reynolds normal stress, $\langle u'u'/U^2 \rangle$ is reduced to 90% of that of the bare cylinder at most.

Naudascher and Rockwell (1994) used surface modifications to alter the loading and structural vibration of a circular cylinder. They modified the surfaces of cylinders in numerous ways, for example by applying straight and helical wires, staggered wires, and collars and rings.

Mahir and Rockwell (1996) investigated the wake of two side-by-side cylinders (G/D=3.0), both forced to vibrate laterally. In the lock-in state, they observed a variety of flow patterns, which depended on the phase relationship between the two vibrating cylinders. The power spectral density function corresponding to the flow patterns was nevertheless almost the same. However, information on the flow when the neighboring cylinder is vibrating is scarce.

Nakamura (1996) carried out experiments on flow over several bluff body shapes attached with a splitter plate. The *Re* of the experiments ranged from 300 to 5,000. When the splitter plate is attached to the bluff body, the vortex shedding characteristics is changed from Kármán shedding (which is a double-layer instability) into impinging shear layer instability (which is a single-layer

instability). It was reported that *St* based on streamwise distance of the body was only weakly dependent on *Re* and sectional geometry.

Lam and Lin (2010) simulated the turbulent flow past wavy cylinders at *Re* = 3,000 using the large eddy simulation (LES). Simulations were performed for eleven wavy cylinder models with different combinations of wave amplitude, a/D_m, and spanwise wavelength, λ/D_m. It was demonstrated that all the values of mean drag coefficients and fluctuating lift coefficients of the wavy cylinders are smaller than that of the single circular cylinder. Compared with a circular cylinder, the drag coefficient reduction up to 18% was obtained for the wavy cylinder with a/D_m = 0.152 and λ/D_m = 1.894. A maximum reduction of the fluctuating lift coefficient up to 94% was obtained at a/D_m = 0.152 and λ/D_m = 1.515. They pointed out that the values of wave steepness (a/λ) are not directly related to the magnitude of drag reduction, but it may significantly control the vortex structures and hence suppress the fluctuating lift force.

Jung and Yoon (2014) investigated the flow over a twisted cylinder at *Re* = 3,000 using large eddy simulation (LES) based on finite volume method (FVM). They stated that the twisted cylinder achieved reductions in mean drag of approximately 13% and 5% compared with the results for smooth and wavy cylinders, respectively. Furthermore, RMS value of the fluctuating lift coefficient of the twisted cylinder showed a tremendous decrease of approximately 96% compared with the smooth cylinder. The vortex shedding from the twisted cylinder was considerably suppressed.

Wei and Chang (1999) studied turbulence effect on the interaction of wake and base-bleed flow downstream of two circular cylinders arranged side-by-side. They found that free stream turbulence had an effect of changing the relation between the gap ratio and the wake behavior. However, the biasing characteristic of the gap flow was not substantially affected by free stream turbulence.

Lee and Lee (2001) investigated the flow structure over a semicircular riblet surface. They measured the near-wall turbulent structures over semicircular (U-

type) grooves of s=3mm using particle image velocimetry (PIV) velocity field measurement technique and found how the semicircular riblet reduces the drag acting on the surface. As an extension of this study to a bluff body, we tested the U- and V-grooved cylinders having the same groove spacing of s=3 mm in the present study.

Igarashi and Terachi (2002) made an experimental study on drag reduction of flat plate normal to airstream by flow control using a rod. They chosen chord lenght of the plate, D, was 50 mm and the diameter of the rod, d, ranged from 2 to 20 mm. and the distance between the axes of the rod and plate, L/D, was varied from 1.0 to 2.6. The Reynolds number ranged from 19,000 to 77,000. According to the result of experiments they reported that the larger the rod diameter, the more efficient is the drag reduction. The maximum reduction of total drag coefficient that includes the additional force from the rod is about 20-30 % for d/D=0.4 and L/D=2.0 in comparision to the value obtained without the rod.

Interference effects on vortex-induced vibrations of two side-by-side elastic cylinders, fixed at both ends (with no deflection and displacement) in a cross-flow, were experimentally investigated by Wang et al.(2003). The dynamic responses of the cylinders were measured using two fiberoptic Bragg grating (FBG) sensors. Simultaneously, a single hot wire was used to measure the velocity in the wake. It has been previously observed that violent resonance occurs when transverse cylinder spacing ratio, G/D, is either large (2.0) or small (>1.2), but not for intermediate cylinder spacing, i.e., G/D=1.2∼2.0. The interrelationship between the vortical structures generated by the two cylinders is also investigated and interpreted in terms of different vortex generation mechanisms. The different fluid dynamics around each cylinder is further found to be responsible for a deviation between the natural frequencies of the combined fluid-cylinder system associated with each cylinder.

Zhou et al. (2015) compared the flow structures downstream of the smooth, grooved and dimpled cylinders at Re ranged from 7,400 to 80,000. It was shown

that the recirculation lengths, vertical distances between foci and horizontal distances between focus and cylinder's center of the smooth, grooved and dimpled cylinders were reduced as *Re* increased from 7,430 to 17,980. The recirculation regions behind the grooved and dimpled cylinders are smaller than that of the smooth cylinder. Besides, mean drag coefficients also lower than that of the single cylinder.

Self-issuing jets from holes periodically located along the span of a square cylinder have been studied by Aydın et al. (2010) for a Reynolds number range from 200 to 1,000. It was stated that jets emanating from these holes lead to changes of the near-wake characteristics of a square cylinder. It was added that, the nature of changes is shown to depend on the jet spacing λ/D and *Re*. For *Re* of 200 and 300, there were indications that the self-issuing jets effectively create a mild geometric disturbance in the form of a wavy trailing end. For *Re* = 400 and 500, jets issuing from the holes did not show a direct interaction with shear layers originating from the upper and lower surfaces of the cylinder. At higher *Re*, 750 and 1,000, direct interaction of shear layers from self-issuing jets and the cylinder led to a reduction in the formation length of large scale vortices with no appreciable variation in *St* with respect to the reference case of the plane cylinder. Fu and Rockwell (2005) found that vortex formation in the near wake of shallow flow past a circular cylinder could be substantially delayed by base bleed through a very narrowslot. The wake structures associated with this delay changed dramatically with the dimensionless momentum coefficient of the slot bleed. Baek and Karniadakis (2009) indicated that a slot of sufficiently large width positioned in a modified cylinder could cause a strong jet flow into the near wake, which changed the vortex-shedding pattern remarkably. Meanwhile, the instantaneous flow field did not show periodic vortex shedding when the slot was larger than the critical width.

Kuo and Chen (2009) revealed the wake flow structures behind a circular cylinder manipulated by two small control cylinders and elucidate the primary

mechanism that leads to a reduction of the lift and the pressure drag on the main cylinder. They found that when the control cylinders lie within $0.8 \leq X_C/D \leq 3.0$, the fluctuating lift on the main cylinder shows a 70–80% reduction without completely suppressing the vortex street.

Kunze and Brücker (2012) presented experiments on separation control using flexible self-adaptive hairy-flaps. They investigated the wake-flow behind a circular cylinder without and with flexible hairy-flaps at the aft-part of the cylinder. Flow dynamics and hair motion were measured by particle image velocimetry and image processing in a range of Reynolds number $5{,}000<Re<31{,}000$. The experiments and POD analysis show that the hairy-flaps alter the natural vortex separation cycle in such a way that the vortices do not shed in a zigzag like arrangement as in the classical von Kármán vortex street but in line in a row with the cylinder wake axis. Thus, the wake-deficit is largely reduced. Furthermore, they have found that the flow fluctuations are considerably reduced about 42% in streamwise and 35% in transversal direction compared to the reference case without hairy-flaps, too.

The numerical study of Xiao et al. (2012) examined the potential of cylinder wake vortex control using a downstream undulating foil. They showed that the proper placement of foil, with its chord length equal to the upstream cylinder diameter, can result in a suppression of cylinder vortex shedding and an improvement in downstream foil propulsion. The detailed flow field analysis revealed that, such benefit is strongly linked to the interaction between the cylinder wake vortex and the reversed Kármán vortex street, which is shedding continuously at the foil leading edge associated with foil undulation locomotion.

Ünal and Altar (2010) investigated the effects of the angular position of streamwise vortex generators on the near-wake flow structure of a circular cylinder at 41,300. It was stated that the vortex formation and recirculation lengths were higher than that of the single cylinder, regardless of angular position. The recirculation region was lengthened and wake width was decreased. This is a clear

indication of delayed flow separation. As angle of vortex generators increased from 50° to 70°, vortex formation and recirculation lengths were increased, maximum rms values of the fluctuating streamwise and transverse velocities were reduced.

Ozkan et. al. (2012) examined the change in flow characteristics downstream of a circular cylinder surrounded by an outer permeable cylinder in shallow water using particle image velocimetry technique. In their study, five different outer cylinder diameter and four porosities were used to understand the effect of diameter and porosity on flow characteristics. The best results were taken at outer cylinder ranging from 1.6 to 2 and ranging from 0.4 to 0.6 to have a better flow control in the near-wake.

2.1.2. Studies on Active Control

Jukes and Choi (2009) used dielectric barrier discharge (DBD) plasma actuators to control the flow around a circular cylinder at Re = 15,000. They placed the actuators at the top and bottom of the cylinder close to the natural separation points, where they were activated in a pulsed mode with nondimensional frequency in the range 0.1-2 with duty cycle of 1-40%. It was shown that maximum drag reduction occurred with nondimensional frequency of 2.0 and plasma force coefficient of 0.32%, where drag coefficient and lift fluctuations were reduced by 32% and 72%, respectively. The drag coefficient and lift fluctuations were only reduced by 23% and 44% when the plasma was fired continuously. It was suggested that even higher levels of drag reduction may be possible through further increase in nondimensional frequency or plasma force coefficient. On the other hand, drag coefficient was increased by up to 7.5% and lift fluctuations increased by 87% when the plasma was formed at a frequency close to the natural vortex shedding frequency. The energy efficiency of active flow control mechanism (DBD surface plasma) for drag reduction was found to be 1-2%. The maximum efficiency 2.4% occurred at nondimensional frequency of 1.0 and plasma force coefficient of 0.045%, where drag coefficient and lift fluctuations were reduced by

12.8% and 62.3%, respectively. The moving surface boundary-layer control (MSBC) injects momentum in the boundary layer of circular cylinder which delays separation and decreases the fluctuating transverse velocity in the wake.

Korkischko and Meneghini (2012) located two small rotating cylinders to the sides of the main cylinder, in this respect. The diameter of the control cylinders is d_c/D=0.06 and the gap between the main and controlling cylinders is g/D=0.07. The velocity ratio range was 5-10, the Reynolds numbers were in the range of 1,600-7,500 and the reduced velocity varied from 3.7 to 17 in the study. For the velocity ratio of 5, the mean drag coefficient of the cylinder was 60% lower than that of the single cylinder. A significant decrease in the maximum amplitude (one degree-of-freedom in the transverse direction) for the controlled cylinder was observed.

Ingham (1983), Badr et al. (1989) and Ingham and Tang (1990) numerically investigated the rotating cylinder flow in the laminar steady regime (Re_D<47) for relatively small rotational speeds. They found that, although vortex shedding does not occur in the wake, the rotation delays and even inhibits the boundary-layer separation.

Griffin and Votaw (1972) concluded that, when the cylinder vibrates transversely to the oncoming flow, the vortex frequency adjusts itself to the forcing frequency. An increase in the relative amplitude, A/D, where A is the vibration amplitude and D is the cylinder diameter, induces an increase in the drag and a reduction in the longitudinal distance of the vortices until they disappear completely at some threshold amplitude.

Wu et al. (1989) and Wu (1990) carried out study which showed that, when the forcing frequency is equal to that of the natural vortex shedding frequency of the cylinder, the shed vortices in the wake become more organized, and both the unsteady lift and drag components reach their maximum. Wu (1990) also suggested that the drag could decrease below that of a stationary cylinder when the frequencies are mismatched.

The possible drag reduction and the corresponding variation of the flow field around a circular cylinder are studied by Fujisawa and Takeda (2003) in a wind tunnel using flow control with acoustic excitation, which was supplied internally through a slit to the flow over the cylinder. In the study, the control parameters were chosen as the slit angle, the forcing Strouhal number and the excitation amplitude. The results indicate that the drag was reduced about 30% in comparison with a stationary cylinder, when the control parameters are optimized at Re = 9,000. It was expressed that this condition was obtained when the acoustic excitation was given just behind the separation point with the frequency near the unstable frequency of the separating shear-layer. With larger amplitude of the acoustic excitation, the drag reduction was strengthened; however, it was saturated at larger values of excitation amplitude. Furthermore, the velocity fluctuations and the Reynolds stress in the near wake of the cylinder were strongly diminished under acoustic excitation.

Baz and Ro (1991) used an electromagnetic actuator installed inside a cylinder to exert a force on the cylinder. The actuator was driven by a feedback hotwire signal measured in the wake, thus increasing damping to the cylinder and effectively reducing the vortex-induced vibration at the occurrence of resonance, when the vortex shedding frequency, f_S, coincided with the natural frequency, f_N of the system.

Baz and Kim (1993) made attempts to control the vibration of a cylinder in a cross-flow. In their studies, surface-bonded piezo-ceramic patches were activated by a closed-loop control system to exert a force on the cylinder under resonance, that is, the vortex shedding frequency coincided with the natural frequency of the cylinder. The control increased the flow structure system damping and subsequently reduced the vortex-induced vibration.

Tokumaru and Dimotakis (1993) experimentally investigated flow past a circular cylinder with both net steady rotation and forced oscillations at $Re_D \approx 10^3$ by suggesting the so-called virtual vortex method. They found that a higher cylinder

aspect ratio yields a higher maximum lift coefficient in the case of steady rotation and the addition of forced rotary oscillations to the steady rotation increases or decreases the lift coefficient.

Nosenchuck and Brown (1993) measured a reduction of skin friction of up to 90% by means of chessboardlike arranged electrodes/magnets to induce a wall-normal Lorentz force in a flat plate boundary layer. The injection of an electrolyte generated a non-uniform electrical conductivity. Spanwise oscillating Lorentz-force (Berger et al., 2000) was successfully used to reduce the skin friction in a turbulent boundary layer. A considerable scatter of results was found even on very similar arrangements. This could result from inadequate calculations of the Lorentz force in numerics or difficulties with established measurement techniques.

There have been some researches to apply the magnetic fields to control the vortical structure in the wake. They investigated the effect of magnetic fields on the flow structure past a cylinder. Lahjomri et al. (1993) carried out an experimental study and showed that an aligned magnetic field leaded to the suppression of vortex shedding.

Shatrov et al. (1997) and Mutschke et al. (1997) and Mutschke et al. (1998) and Mutschke et al. (2001) investigated the flow instability in the wake in the presence of magnetic fields from their numerical studies. They carried out the stability analysis using the numerical simulation techniques for the time-dependent two- and three-dimensional flow. Depending on the magnitude of applied magnetic fields in the two-dimensional flow region, the vortex shedding can be suppressed or eliminated and as a result the flow becomes stabilized.

Shiels and Leonard (2001) carried out numerical simulations, using a two-dimensional high-resolution viscous vortex method, over a range of Re_D=150-15,000 to verify the experimental observation of drag reduction by Tokumaru and Dimotakis (1991). They found that boundary layer bursting causing the formation of a multipole vorticity structure, triggered by appropriate rotary oscillation (for example, Ω=2 and St_f=1), leads to a time-averaged separation delay and thus drag

reduction. This control mechanism was found to be effective only at high Reynolds number ($Re_D \geq 3000$), apparently because the viscosity suppressed the multipole growth in the case of low Reynolds number. As reviewed in details above, the previous studies have numerically or experimentally investigated lock-on phenomena, occurring through interactions between the rotary oscillation and natural vortex shedding, and their accompanying characteristics.

Glezer and Amitay (2002) show that synthetic jets on selected positions over the cylinder can give a delay of separation for different Reynolds number (i.e., both for a turbulent and a laminar boundary layer). They argued that this delay was caused by increased mixing within the boundary layer. In addition, the interaction between the jet and the cross flow has a profound effect both on the separated shear layer and on the wake; the magnitude of the Reynolds stresses is reduced indicating that the delay in separation is not merely the result of a transition to turbulence in the boundary layer.

A nonlinear adjoint-based optimal control approach of cylinder wake by electromagnetic force is investigated numerically by Zhang et al. (2010). They constituted a cost functional representing the balance of the regulated quantities with different weights and interaction parameter N (Lorentz force), where the regulated quantities related with flow and force are taken as targets of regulation and the Lorentz force, (as interaction parameter N), is taken as a control input. They observed that under the action of optimal $N(t)$, the flow separation is suppressed fully, so that the oscillations of drag and lift are suppressed and the total drag coefficient decreases dramatically. For the different regulations, the control effects have some differences due to the different values of optimal inputs corresponding to the different adjoint flow fields.

3. MATERIAL AND METHOD

3.1. Water Channel

Particle image velocity (PIV) experiment was performed in a large-scale, recirculating water channel located in the Fluid Mechanics Laboratory at Çukurova University (Figure 3.1). The water channel test section has the following dimensions: a length of 8,000 mm, a width of 1,000 mm and a depth of 750 mm (Figure 3.2). It was constructed of transparent Plexiglas. It was interconnected to upstream and downstream fiberglass reservoirs. The water channel also has honeycomb screen arrangement, which is located at the entrance of 2 to 1 contraction. These reservoirs and honeycomb screen arrangements are used to maintain the turbulence intensity in the section below 1.45%. The water flow speed was controlled by a 15 kW axial flow pump. Pump rotation speed was controlled by an ABB variable frequency controller unit.



Figure 3.1**.** A view from the upstream reservoir

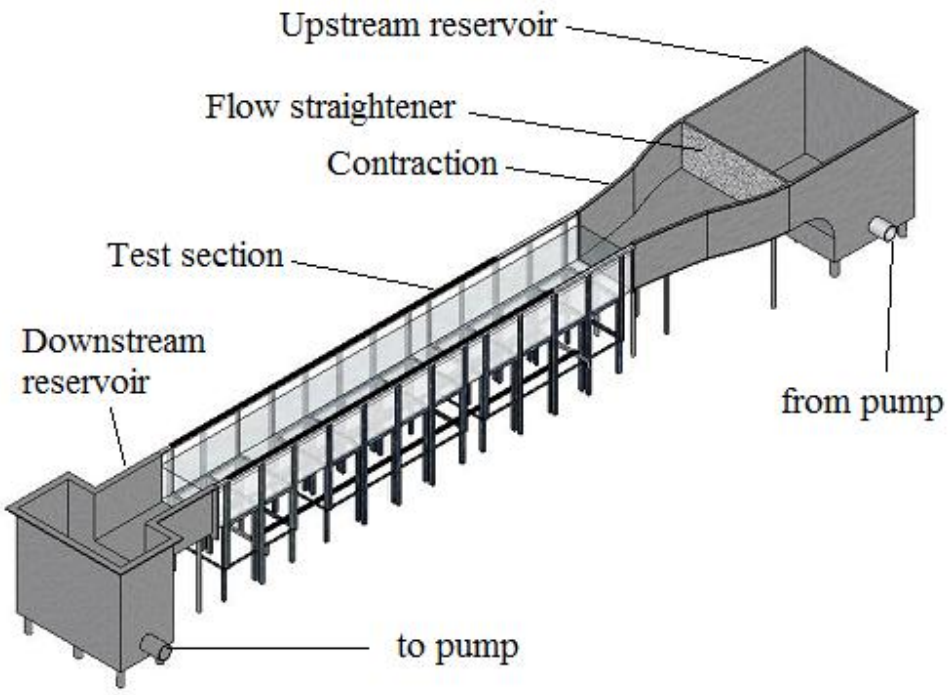


Figure 3.2**.** The components of the water channel

3.2. Digital Particle Image Velocimetry (DPIV)

The theory of PIV was introduced by Adrian (1988) in the late 1980s with the first experimental implementations following shortly afterwards (Kean et al. 1990 and Kean et al. 1991). At the stage, due to hardware limitations, a single photographic frame was multiply exposed and analyzed using an auto-correlation technique. However, improved speed of photographic recording soon allowed images to be captured on separate frames for analysis by cross-correlation (Kean et al., 1992). The introduction of digital camera technology to PIV enabled the direct recording of particle images (Willert et al., 1991), at the expense of reduced resolution, resulting in the development of digital PIV Westerweel, 1997). As well as these hardware advances, many new algorithms have been developed in the last decade, increasing the accuracy and speed of PIV analysis. One key advantage of

the PIV technique over other conventional techniques such as LDV or hotwire anemometry is ability to obtain instantaneous flow-field information is important for probing the structure of turbulent flow fields (Westerweel et al. 1996; Meinhart and Adrian 1995).

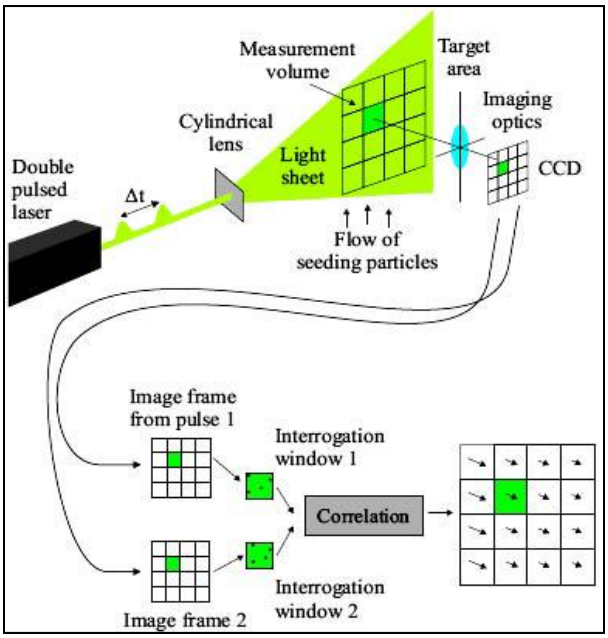


Figure 3.3. Principles of PIV (Schiwietz and Westermann, 2004)

DPIV is a non-intrusive measurement technique used to simultaneously determine the velocities at many points in a flow field (Figure 3.3). The PIV technique for velocity measurement consists of two main steps: visualization and image processing.

The first step is to seed the flow with suitable particles in order to trace the fluid motion. Then a pulse of laser light sheet illuminates a thin slice of the flow field at the desired plane, and the positions of particles in that plane are determined by detecting the light scattered by particles on a digital video or photographic camera positioned at right angles to the light sheet. After a very short time period

Δt (typically in μs), the particles are illuminated again by a second pulse of laser light sheet, and their new positions are recorded. Using the information on these two superimposed camera images, the particle displacement, Δx are determined for all particles, and the magnitude of velocity of the particle in the plane of the laser light sheet is determined from $\Delta x/\Delta t$. The direction of motion of the particles is also determined from the two positions so that two components of velocity in the plane are calculated (Cengel and Cimbala, 2007).

Seeding is, in general, easier in water than in air. Lower velocity and accelerations combined with the higher density and viscosity of liquid mean larger, more easily detectable particles can be used. The flow medium was seeded with 10 μm, silver-coated hollow glass spheres (S-HGS; Figure 3.4). They have a density of approximately 1,400 kg/m^3. Although the density of the seeding materials is higher than that of the water, they could remain suspended in the water for several hours. The thin silver coating further increases the reflectivity. In order to detect the movement of seeding particles, desired area of the flow field was illuminated by a light-sheet (New Wave Research, Solo 120XT). The 2 mm thick laser light sheet was parallel to the bottom wall of the channel and illuminated the mid-depth of the channel flow. The double pulsed Nd:YAG laser system provided a maximum laser energy output 2 × 120 mj/pulse and has a laser source with a wavelength of 532 nm (Figure 3.5). A CCD (Charge Coupled Device) camera has a spatial resolution of 1,600 × 1,200 pixels (Dantec Dynamics, FlowSense 2M) and equipped with a lens has a focal length of 60 mm (Nikon AF Micro-Nikkor 60 mm f/2.8D) was used in order to record the movement of seeding particles (Figure 3.6). It has a maximum operation frequency of 15 Hz in double-frame mode. Its sensors are generally more sensitive to be damaged by reflected laser radiation. In our case, the camera shows some dead pixels probably originating from that. A synchronization unit was used to generate trigger pulses for the camera and laser light source.



Figure 3.4. Seeding material (Dantec Dynamics)



Figure 3.5. Laser unit



Figure 3.6. CCD camera with lens

DynamicStudio v3.20 software was used for the acquisition and analysis of the images (Figure 3.7). After images and related data were acquired, adaptive correlation method based on iterative procedure with 2 refinement steps, 2 pass per step was applied. The camera images were subdivided into interrogation areas of 32 × 32 pixels; the first and second camera frames were correlated to estimate the average displacement vector. The initial or the final position of the seeding particle may be outside the interrogation area especially near the interrogation area edges; therefore, cannot contribute to the velocity calculation at these locations. In order to prevent this problem, overlapping interrogation areas were selected with a horizontal and vertical overlap of 50%.

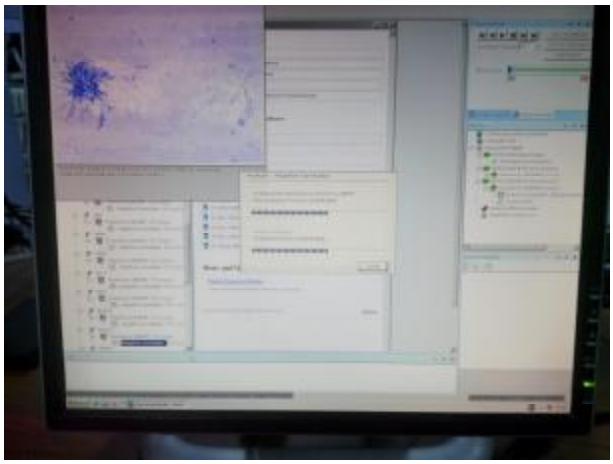


Figure 3.7. The interface of the DynamicStudio v3.20 software

In each test, 1,000 instantaneous images were captured and recorded to obtain time-averaged quantities such as velocity, vorticity, etc. Totally 7,326 (99 × 74) velocity vectors were acquired (at a sampling rate of 10 Hz) for an instantaneous velocity field. Spurious (bad) velocity vectors (less than 3%) due to the dead pixel of the camera, reflection and refraction of the laser sheet and any other non-black object detectable by camera except seeding particles were detected by applying the local-median filter technique, and were replaced by interpolated

vectors that calculated by means of bilinear least-squares fit technique between neighboring vectors.

The flow around the cylinder and dual detached plates is nominally two-dimensional. Therefore, one field of view (FOV) was used during the experiments. The selected FOV allows revealing turbulence statistics in the wake of the cylinder-plate system. The FOV covered an area of 216.43 mm × 162.32 mm. The magnification factor of the camera was 18.58. The effective grid size was 2.16 mm × 2.16 mm. By the way, the streamwise, cross-stream and spanwise directions were denoted by *x*, *y* and *z*, respectively.

3.3. Experimental Model

The three-dimensional view of the experimental model is shown in figure 3.8. Hollow Plexiglas cylinder of 50±0.1 mm diameter and 2 mm wall thickness was used in this investigation. Besides, detached plates were also made of Plexiglas material. To prevent the deflection of the plates due to the gravity and hydrodynamic forces, slightly thicker plates were employed. The thicknesses of the plates were 5 mm. Models considered in the present study were oriented vertically in the channel (Figure 3.9). There were clearance fits between the assembled mating parts (Cylinder and Part-A; Cylinder and Part-B; Cylinder and Part-C; Plate and Part-B; Plate and Part-C). The amount of designed deviation between two mating dimensions in a fit (allowance) was relatively small. That is, cylinder could not move freely inside holes of the parts. Here, Part-A, -B and -C were used to adjust the rotation angle of the detached plates (α) with respect to horizontal centerline of the cylinder. Models inserted into the channel produced a blockage area of 5% and aspect ratio of 8.

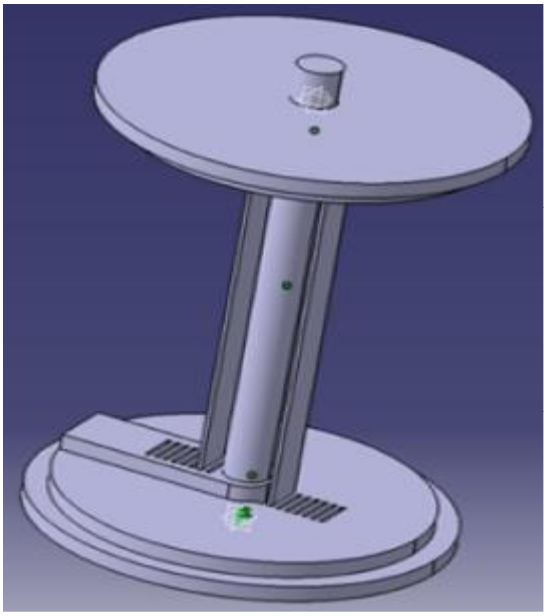


Figure 3.8. The three-dimensional view of the cylinder-plate system

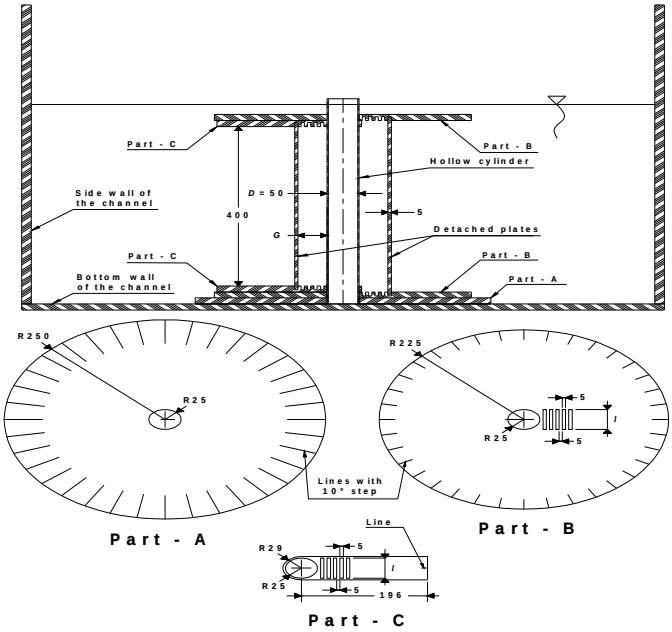


Figure 3.9. Cross-sectional view of the experimental setup and top view of some components of the system. All units are in mm. Part – A, – B and – C have a thickness of 15 mm.

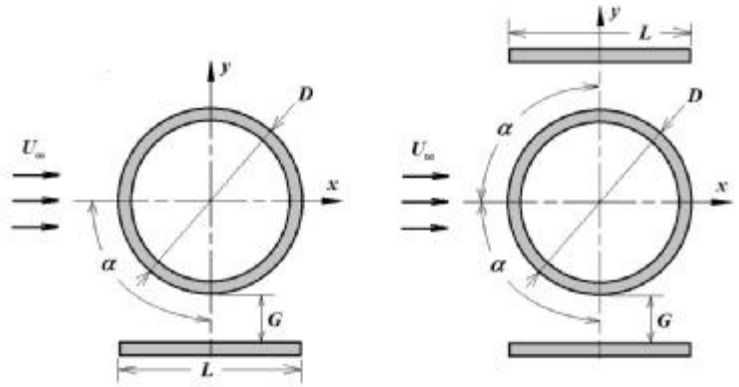


Figure 3.10. Cylinder with single and dual detached plates

Three major parameters defined for the cylinder and plate system (Figure 3.10). First parameter is the normalized gap between the cylinder surface and the plate surface (*G*/*D*). Here, gap is equal to the difference between the shortest line between the cylinder center and the inner surface of the plate, and radius of the cylinder. Besides, inner surface of the plate always perpendicular to the shortest line irrespective to the rotation angle. The second parameter is the rotation angle. It represents the angle between the shortest line and the –*x* axis. The last parameter is the normalized length of the plate (*L*/*D*). The values of these parameters and more were given in Table 3.1.

Table 3.1. Main parameters

Cylinder diameter	50 mm
Wall thickness of the cylinder	2 mm
Thickness of the plates	5 mm
Normalized length of the plate (*L*/*D*)	25 mm, 50 mm
Normalized gap between the plate and the cylinder (*G*/*D*)	0.1, 0.3, 0.5, 0.7, 0.9
Angle of rotation (α)	0^o to 180^o (by 10° step)

3.4. Physical Quantities and Dimensionless Numbers

In turbulent flow, velocity, pressure, density, temperature, etc. at a point fluctuate with time in an apparently random fashion. Moreover, turbulent flow is generally three-dimensional and rotational. Thus, any instantaneous component of velocity or other quantities can be regarded as consisting of a time-averaged value plus a random fluctuation. For instance, streamwise component of the velocity can be expressed as

$$u(t) = \langle u \rangle + u'(t) \quad \text{(m/s)} \tag{3.1}$$

In the above equation, the angle brackets denote an average with respect to time and the prime denotes fluctuation. The magnitude of instantaneous and time-averaged resultant velocity vectors at a point in the measurement plane can be expressed as

$$U(t) = (u(t)^2 + v(t)^2 + w(t)^2)^{1/2} \tag{3.2}$$

$$\langle U \rangle = (\langle u \rangle^2 + \langle v \rangle^2 + \langle w \rangle^2)^{1/2} \tag{3.3}$$

The time-averaged streamwise velocity component can be expressed as

$$\bar{u} = \left[\frac{\Delta t}{\Delta t + t_f - t_i} \right] \sum_{t=t_i}^{t_f} u(t) \quad \text{(m/s)} \tag{3.4}$$

where Δt is time step or sampling period, t_i is initial time and t_f is the final (ending) time. The root-mean-square (RMS) value of the fluctuating streamwise velocity component can be expressed as

$$u_{RMS} = \sqrt{\left[\frac{\Delta t}{\Delta t + t_f - t_i}\right] \int_{t=t_i}^{t_f} (u(t) - \bar{u})^2} \quad \text{(m/s)} \tag{3.5}$$

Turbulence intensity in the streamwise direction can be expressed as

$$Tu_x = \frac{u_{RMS}}{U_\infty} \times 100 \tag{3.6}$$

where U_∞ (m/s) is the freestream velocity of the fluid. Normalized time-averaged turbulent kinetic energy per unit mass of the fluid can be calculated by the following formula by assuming the flow to be locally isotropic (Sheng et al., 2000).

$$< TKE > = 0.75 \times \frac{(< u'u' > + < v'v' >)}{U_\infty^2} \tag{3.7}$$

The Reynolds number is the dimensionless number which gives a measure of the ratio of inertial (resistant to change or motion) forces to viscous (heavy and gluey) forces. It can be expressed as

$$\mathrm{Re} = \frac{\rho \times U_\infty \times L_{Ch}}{\mu} \tag{3.8}$$

where ρ (kg/m^3) is the density of fluid, L_{Ch} (m) is the characteristic length and μ (kg/m/s) is the dynamic viscosity of the fluid. The characteristic length becomes D for the circular cylinder in cross-flow. The Strouhal number (St) is a dimensionless flow parameter which gives important information about the integrity of the flow pattern and can be expressed as

$$St = \frac{f_K \cdot D}{U_\infty} \tag{3.9}$$

where f_K (Hz) is the vortex shedding frequency. On two-dimensional vector map, spanwise vorticity at a grid position (m, n), is computed from the local circulation ζ_z.

$$\begin{aligned} z_z(m,n) = {} & \frac{1}{2}\Delta x\left[u(m-1,n-1)+2u(m,n-1)+u(m+1,n-1)\right]+ \\ & \frac{1}{2}\Delta y\left[v(m+1,n-1)+2v(m+1,n)+v(m+1,n+1)\right]- \\ & \frac{1}{2}\Delta x\left[u(m+1,n+1)+2u(m,n+1)+u(m-1,n+1)\right]- \\ & \frac{1}{2}\Delta y\left[v(m-1,n+1)+2v(m-1,n)+v(m-1,n-1)\right] \end{aligned} \tag{3.10}$$

$$w_z(m,n) = \frac{z_z(m,n)}{4\,\Delta x\,\Delta y} \quad (1/s) \tag{3.11}$$

where Δx is the grid spacing (physical distance between grid points) in the x-direction and Δy is the grid spacing in the y-direction. As one can see from the Eq. 3.11, the local ω_z about a given grid point (m, n) was computed along the path of the four nearest neighbors by using first-order central difference approximation.

3.5. Measurement of Uncertainty

In the present study, an uncertainty analysis was carried out on relevant parameters using the procedures described by Kline and McClintock (1953) and Holman (1994). The total percent uncertainties (*un*) for Reynolds number (*Re*), Strouhal number (*St*), normalized gap between the plate and the cylinder (*G/D*) and normalized length of the plate (*L/D*) took the form of;

$$un_{\mathrm{Re}} = \left[\left(un_{U_\infty}\right)^2 + \left(un_D\right)^2 + \left((-1)\times un_\upsilon\right)^2\right]^{1/2} \tag{3.12}$$

$$un_{St} = \left[\left(un_f \right)^2 + \left(un_D \right)^2 + \left((-1) \times un_{U_\infty} \right)^2 \right]^{1/2} \quad (3.13)$$

$$un_{U_\infty} = \left[\left((0.5) \times un_{DP} \right)^2 + \left((-0.5) \times un_{\rho} \right)^2 \right]^{1/2} \quad (3.14)$$

$$un_{L/D} = \left[\left(un_L \right)^2 + \left((-1) \times un_D \right)^2 \right]^{1/2} \quad (3.15)$$

$$un_{G/D} = \left[\left(un_G \right)^2 + \left((-1) \times un_D \right)^2 \right]^{1/2} \quad (3.16)$$

The CCD camera was carefully aligned and positioned at 90° and parallel to the field of interest in the laser plane by using spirit level with an accuracy of ±0.057°. The percent uncertainties in the time-averaged streamwise (un_u) and transverse (un_v) velocities were estimated to be less than ±3%. The PIV experiments were carried out at a water temperature of 23±1°C and local pressure of 100±1 kPa. The total percent uncertainty in the density of water (un_ρ) originated from the temperature (±1°C) and ambient pressure (±1 kPa) variations were estimated to be less than 0.03%. The total percent uncertainty in the kinematic viscosity of water (un_υ) originated from the temperature (±1°C) and ambient pressure (±1 kPa) variations were estimated to be less than 2.4%. The diameter of the test model (D) is accurate within 0.1 mm. The length and the thickness of the plates (D) are also accurate within 0.1 mm. Thus, total percent uncertainty in the Reynolds number (un_{Re}) was estimated to be less than 3.85% (Eq. 3.12).

The maximum percent uncertainties in the L/D and G/D were estimated to be less than 0.45% and 2%, respectively.

The maximum percent uncertainty in the vortex shedding frequency (un_f) originated from the frequency resolution of the power spectrum was estimated to be less than 1.3%. Thus, total percent uncertainty in the Strouhal number was less than

3.28% (Eq. 3.13). The total uncertainty in the rotation angle (α) was estimated to be less than 2°. The percent uncertainties in the time-averaged spanwise (un_z) were estimated to be less than 6%. The water level (H) was maintained at 500±2 mm.

4. RESULT AND DISCUSSION

Reynolds shear stresses (RSS) evaluated from PIV data are presented in this section and were calculated by the multiplication of fluctuations in streamwise (u') and spanwise (v') directions. Taking the average of the multiplications gives the time averaged Reynolds shear stress. The obtained values are divided by the square of depth averaged freestream velocity (U_∞^2) in order to make better comparisons. In the physical point of view, the RSS define the amount of momentum transferred from one layer of the fluid through another layer by the effect of fluctuations in all directions; Thus, the greater amount of this momentum transfer means that the flow in that region is highly turbulent and complex; however, the fluid layers are alternately changed by each other by the time. It can be concluded that if the amount of RSS is high in the wake of a cylinder then the vortex formation and unsteady shedding of these vortices are inevitable downstream of the cylinder; therefore, reducing the RSS in the wake of a cylinder has great importance in the suppression of vortex shedding and consequent effects; such as Kármán vortex street and vortex induced vibrations (VIV). Here, the solid and dashed lines represent the positive and negative concentrations, respectively. Throughout the figures, the minimum of positive and maximum of negative values of RSS contours are +0.01 and -001 respectively, while the increment is 0.01.

Turbulent kinetic energy (*TKE*) concentrations are presented in this section for gap ratios and plate angles. The values of *TKE* have been made dimensionless by dividing them with the square of the depth-averaged freestream velocity for better comparison. In two dimensional PIV, the values of $< u'u' >$ and $< v'v' >$ can be calculated in the usual manner (by subtracting the mean values of the velocity components from their instantaneous values and then by averaging the products) from the 1,000 instantaneous data. Assuming isotropic flow, the third fluctuating velocity component can be estimated by a 2D approximation (Sheng et al. 2000),

the third component has been supposed to be equal to the half of ($< u'u' > + < v'v' >$), and then *TKE* can be calculated with the following expression

$$TKE = 4/3\ (< u'u' > + < v'v' >) \tag{4.1}$$

Both the minimum and incremental values of dimensionless *TKE* is 0.01 for all *TKE* contours throughout the thesis, and for each figure the results of the bare cylinder case (BC) is given as a reference to compare the results. The results of the detached plate experiment are explained by means of the Reynolds shear stress, turbulent kinetic energy contours, and spanwise vorticity contours for the Reynold number of 7,500.

The detached plate is one of the simplest passive control devices where a thin, flat, two-dimensional plate is placed over the bluff body. The aims of this study are to inspect in detail the variations in flow structure for a cylinder with different plate angles, and to identify the critical gap ratio (*G*/*D*). In the present section, the results are demonstrated and analyzed for Reynolds number of 7,500 with respect to the cylinder diameter. All of the experiments are performed in the gap ratios of 0.1, 0.3, 0.5, 0.7 and 0.9, and with the plate angle of α=0^o to α=180^o as well. The detached plate length of 0.5 has 25mm length and 20mm thickness. In this section, the detached plate length (*L*/*D*) 0.5 is investigated and analyzed by means of Reynolds shear stress, turbulent kinetic energy contours, and spanwise vorticity contours.

We used a case of a cylinder without a plate as the reference called the bare cylinder case (BC). When analyzing of the control cases, between from case α=0^o to case α=90^o is called Regime I and the cases of α=90^o to α=180^o is called Regime II. The primary shear layers and vorticity contours are generated by the cylinder, and the secondary shear layers and the secondary vorticity contours are generated

by the detached plate. For each case, the rotation angle of the plate is shown as case A.

4.1. The Effect of Single Detached Plate for Plate Length of 0.5 On The Flow Control

In this section, the figures of the results are shown by means of Reynolds shear stress, turbulent kinetic energy contours, and spanwise vorticity contours. The first column of the figure shows time-averaged Reynolds Shear Stress (RSS) $<u'v'>$, the second column and third column show time-averaged Turbulent Kinetic Energy$<TKE>$ contours and vorticity contours$<\omega>$ for various plate angles, respectively, as well as the bare cylinder case.

The results of experiment Figure 4.1 shows the RSS, *TKE* and vorticity contours for a gap ratio of 0.1 as well as a bare cylinder case. The shear layers are being formed by upper and lower shoulders of the cylinder in the bare cylinder case. The selected and analyzed cases show the control or suppression of vortex shedding for the gap ratio of 0.1. The flow characteristics of case $\alpha=0^o$ are similar to the bare cylinder case. The shear layers of the system are symmetrical and the contours of *TKE* and vorticity are incomparable with bare cylinder case, clearly. It is expected that the plate and the cylinder act like a single bluff body because the clearance of the plate and the cylinder is not great enough.

The cases in Regime I show the same flow pattern in terms of RSS, *TKE* and vorticity contours for the gap ratio of 0.1. With case $\alpha=80^o$, the secondary shear layer and vorticity contours are observed. As shown in the vorticity of case $\alpha=90^o$, the negative contours of the detached plate interact with the primary vorticity contours. After case $\alpha=90^o$, the center of the shear layers elongates from the near wake to far wake region and also the vorticity contours get longer in the wake region. As the plate angle increases, the formation of shear layers formation is being changed with the increased cross-section area of the body. In the case $\alpha=90^o$, the asymmetrical shear layers are shown clearly.

The secondary shear layer is effective on the negative shear layer of the cylinder in cases α=120^o to 140^o. But the secondary shear layer has no power to divide the negative shear layer of the cylinder. As seen in the vorticity section, the vorticity contours generated by the near trailing edge of the plate elongates with the positive vorticity contours of the cylinder in the wake region for the *G*/*D* of 0.1.

After case α=100^o, the vortex shedding occurs behind the detached plate and the flow is separated by the plate. In Figure 4.1, for the bare cylinder case, the vorticity contours have a small length. But with the increased plate angle, the length of the vorticity contour reach a maximum value like the positive vorticity contour of the system in case α=110^o .It can be said that case α=110^o, case α=120^o, and α=130^o are effective for suppressing the vortex shedding in the near wake of the cylinder. The value of ***TKE*** in the bare cylinder case is 0.498, the value of ***TKE*** for case α=110^o is 0.149.

In Regime I, the positive vorticity contour of the cylinder is dominant over the negative vorticity contour of the cylinder in the wake region and the positive vorticity contour of the cylinder has been elongated as well. In Regime II, the vorticity contours of the cylinder and the plate interact with each other and have a comparable same length.

After case α=90^o, the symmetrical shape is changed due to the effect of the increased plate angle on the negative shear layer of the cylinder. After case α=80^o, the secondary vorticity shear layer appears. The secondary vorticity contours affect the negative vorticity contours of the cylinder in the wake region. In case α=130^o and α=140^o, the momentum of the flow in the gap between cylinder and plate does not have enough power to separate the lower vorticity contours of the cylinder.

As explained previously, due to the lower momentum of the flow, the secondary vorticity contour lacks the power to separate the primary vorticity contour in the wake region, for example case α=130^o and case α=140^o in the *G*/*D* of 0.1.

Comparing case α=0^o and α=180^o, the formation of both negative and positive shear layers appear similar to the bare cylinder case. As expected, case α=180^o is similar to the bare cylinder case in terms of shape and intensity, but, the values of RSS and *TKE* are still lower than in the bare cylinder case. In the case α=180^o, the formation of the vortex shedding is further from the cylinder in the wake region than the formation of the vortex shedding in the bare cylinder case.

The control of the vortex shedding occurs in cases α=100^o, α=110^o, α=120^o and α=130^o, but the suppression of vortex shedding does not occur. It can be said that using the detached plate for the control and suppression of vortex shedding with the gap ratio of 0.1 is suitable for the larger plate angles in Regime II with a plate length of 0.5.

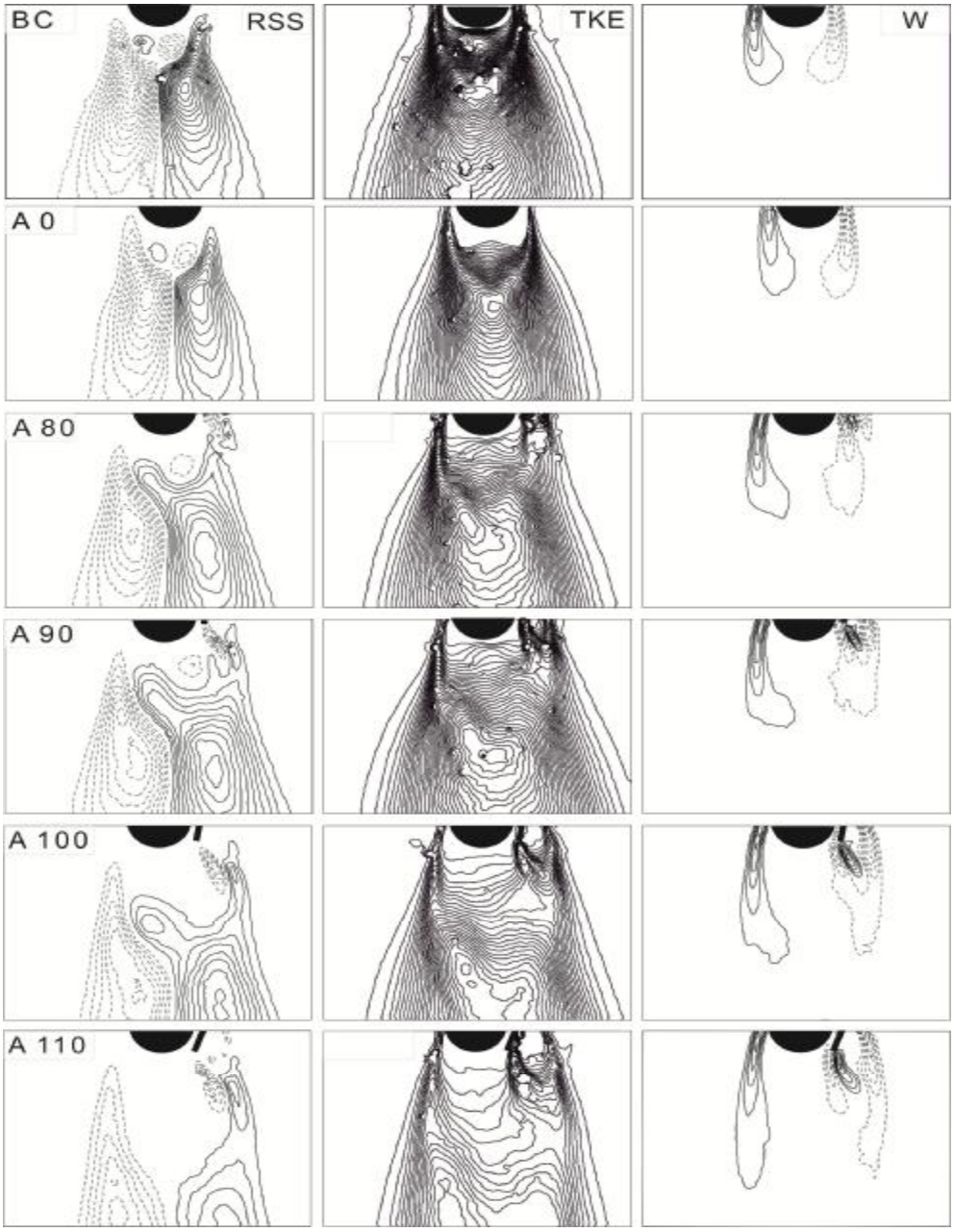


Figure 4.1. The spatial distribution of time-averaged Reynolds shear stress $\langle u'v' \rangle$,turbulent kinetic energy$\langle TKE \rangle$ and vorticity contours,$\langle \omega \rangle$ for gap ratio of 0.1 (continue)

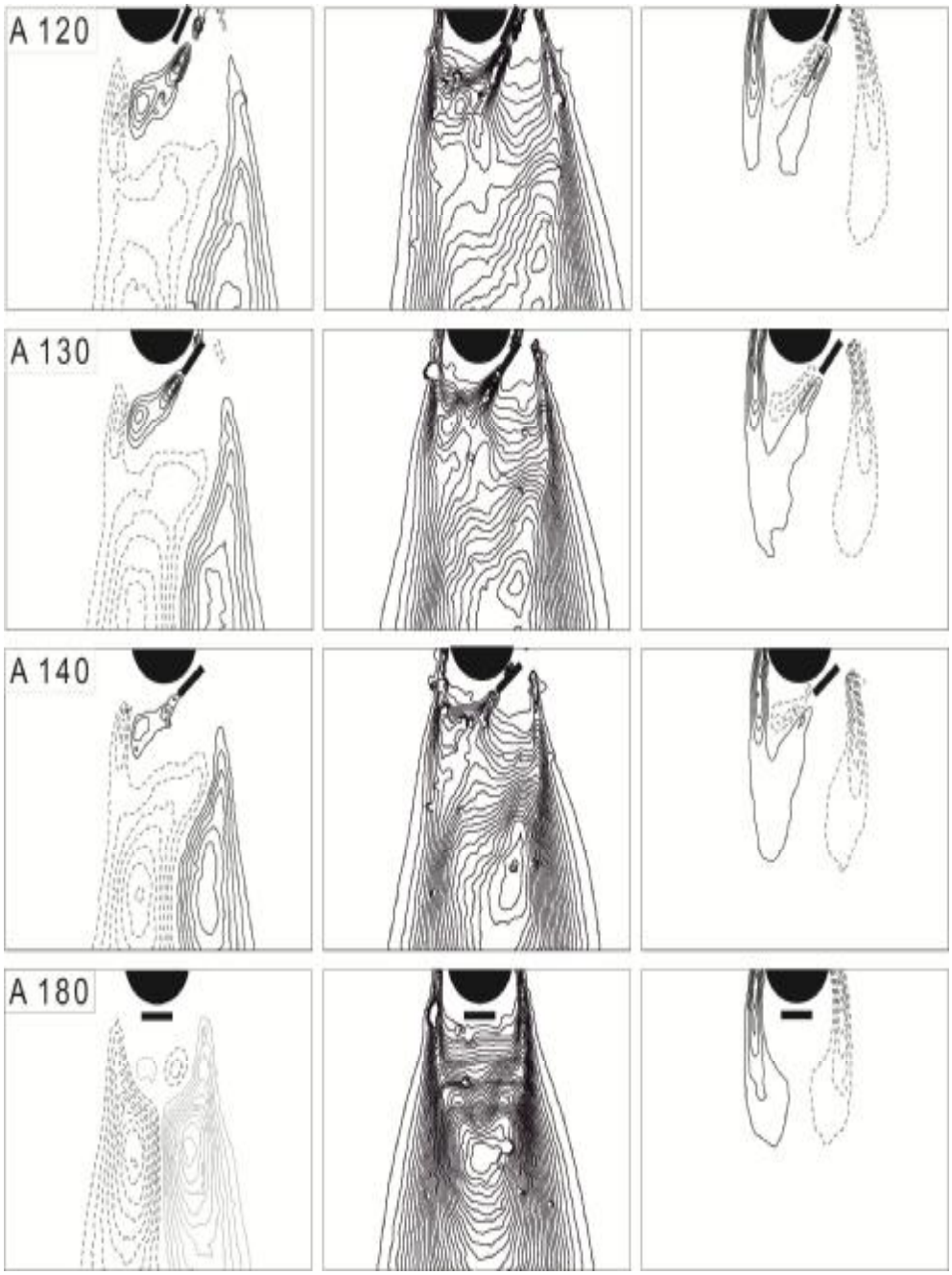


Figure 4.1. The spatial distribution of time-averaged Reynolds shear stress $\langle u'v' \rangle$,turbulent kinetic energy$\langle TKE \rangle$ and vorticity contours,$\langle \omega \rangle$ for gap ratio of 0.1

Figure 4.2 shows the results of the experiments for the gap ratio of 0.3. The gap between plate and cylinder is minimal in the case α=0^o so that the detached plate and cylinder behave like a single bluff body. The formation of the shear layer is typically the same in the bare cylinder case. But for the case α=0^o, the vorticity contours of the system are smaller than in the bare cylinder case. After the case α=0^o, the shear layers elongate in the wake region due to the increased plate angles in Regime I and the better control cases are case α=20^o and α=30^o for the *G*/*D* of 0.3. For the case α=20^o, the RSS value is 0.049 and the *TKE* value is 0.189. These values are evident for the controlling of the shedding vortex respect to bare cylinder case. The positive vorticity contours of the cylinder are larger in the case α=20^o and case α=30^o and the length of the vorticity contours decreases. When the plate appears in the wake region at case α=90^o, the interaction of the secondary shear layer and the positive shear layers of primary disturbs in the wake region.

In Regime II for the case α=90^o and case α=100^o, the secondary shear layer is formed in the trialing edges of the plate. For case α=140^o, the jet flow is observed and the flow causes a change in the negative shear layers of the cylinder. For the case α=110^o and α=140^o, the center of the shear layer moves in the far wake region.

In Regime II, two vorticity contours are observed. One of them is generated by the cylinder, the other is generated by the detached plate. For the case α=140^o, the existing plate in the wake region disturbs the shear layer of the cylinder and the center of the shear layer elongates. In case α=180^o, the flow pattern of the shear layers of the system is still similar to the bare cylinder case but the length of the vorticity contours is longer compared to the bare cylinder case.

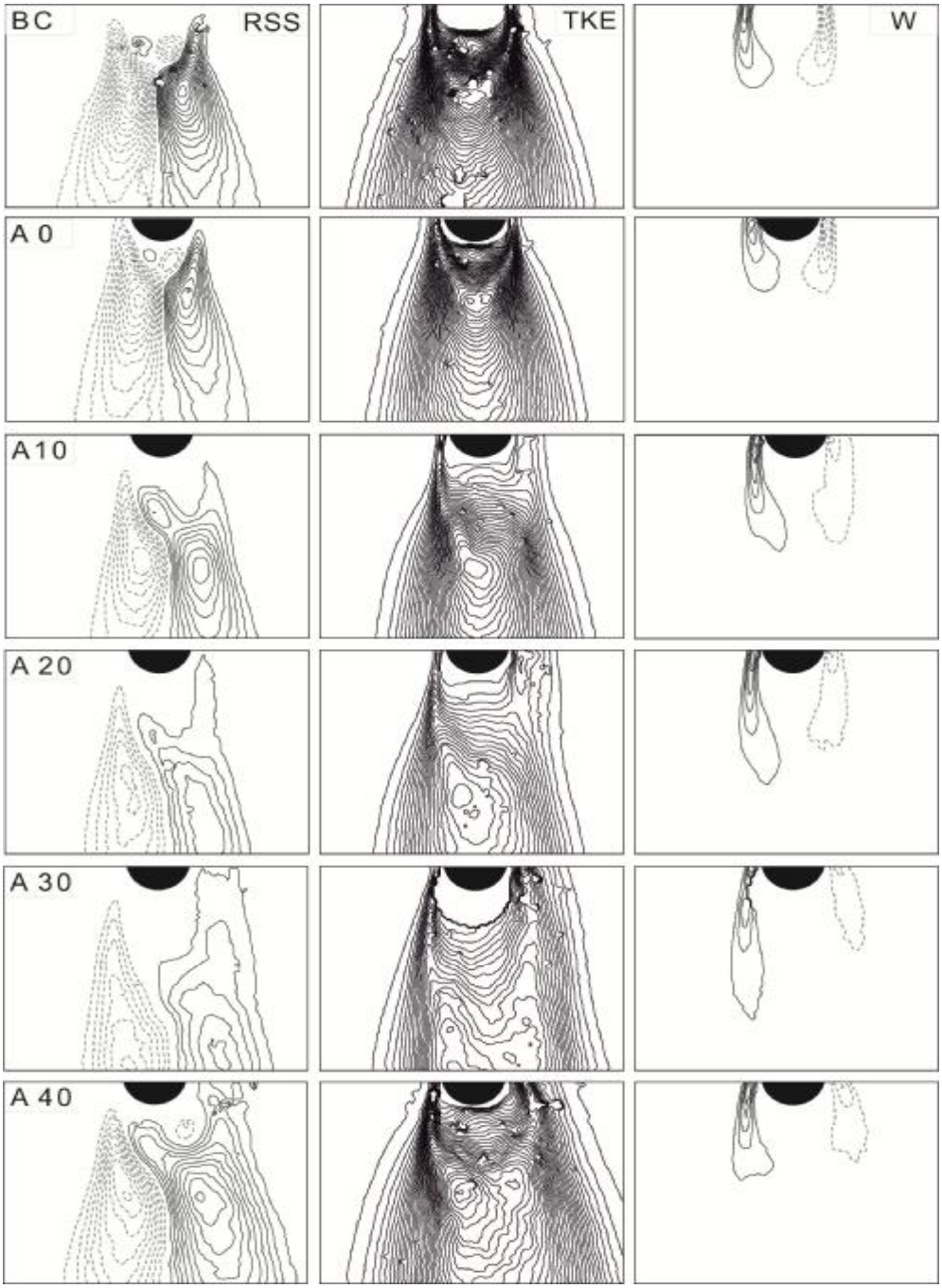


Figure 4.2. The spatial distribution of time-averaged Reynolds shear stress $\langle u'v' \rangle$,turbulent kinetic energy$\langle TKE \rangle$ and vorticity contours,$\langle \omega \rangle$ for gap ratio of 0.3 and bare cylinder case (continue)

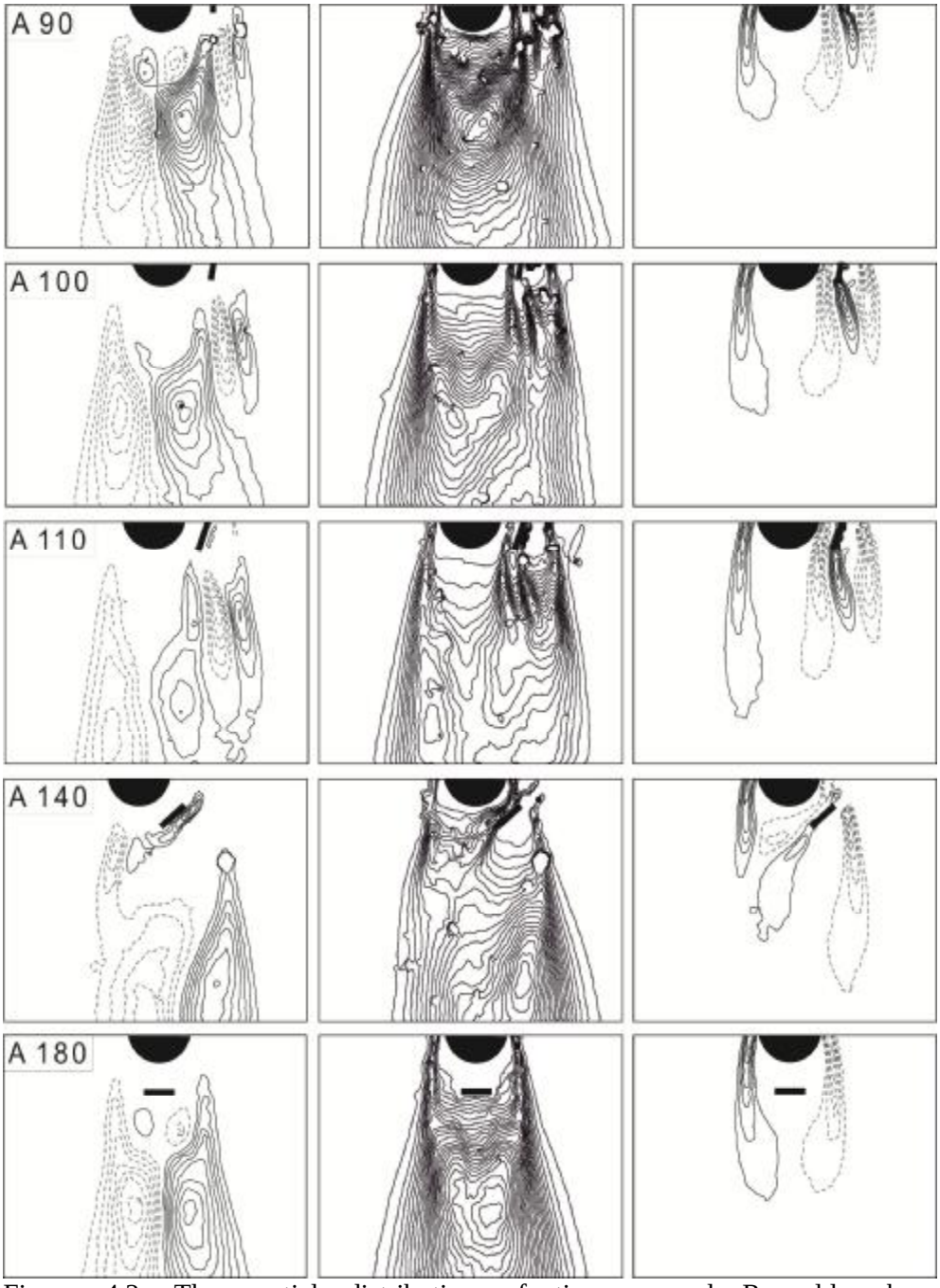


Figure 4.2. The spatial distribution of time-averaged Reynolds shear stress $<u'v'>$,turbulent kinetic energy$<TKE>$ and vorticity contours,$<\omega>$ for gap ratio of 0.3

Figure 4.3 shows the RSS, *TKE* contours and vorticity contours for a gap ratio of 0.5 as well as the bare cylinder case. The width of the shear layers and the length of the vorticity contours of the system are smaller according to gap ratio of 0.3 for case $\alpha=0^o$. The clearance between the cylinder and the detached plate is to permit more flow so that the center of the shear layers of the system elongates in the wake region. Due to an increased *G*/*D*, the positive vorticity contours of the cylinder increase and the controlled vortex shedding is observed in case $\alpha=10^o$ and $\alpha=20^o$ for Regime I.

As in the gap ratio of 0.3, the case $\alpha=20^o$ is the best controlled case for gap ratio of 0.5. Moreover, in the case of $\alpha=20^o$ and $\alpha=30^o$ characteristics are similar to the *G*/*D* of 0.3 shown by the flow formation. The values of RSS and *TKE* are 0.026 and 0.143, respectively in the case $\alpha=20^o$ for the gap ratio of 0.5 and these values are the smallest value in the all gap ratios in the plate length of 0.5. It can be concluded that the best controlled case is case $\alpha=20^o$ in the gap ratio of 0.5. The values of RSS and *TKE* of bare cylinder case are 0.158 and 0.500. These values are comparable with case $\alpha=20^o$ in the gap ratio of 0.5; the increment of the decreasing RSS values is approximately eighty percent.

In Regime II, the shear layers and vorticity contours generated by the front and rear trailing edge of the plate interact with the primary shear layers and vorticity contours in the wake region. The negative secondary vorticity contours are larger than the other vorticity contours. The vorticity contours elongates the maximum value in the wake region for case $\alpha=180^o$ compared to the gap ratios of 0.1 and 0.3. Due to plate interaction, the vorticity contours and shear layers are affected so that the shear layers of the system elongate in the far wake region.

When the plate is placed vertically along the centerline of the cylinder in the upstream, the detached plate has an effect on flow because the flow is obstructed by the detached plate. This situation is estimated because the plate does not permit the streams to flow freely (Roshko, 1954).

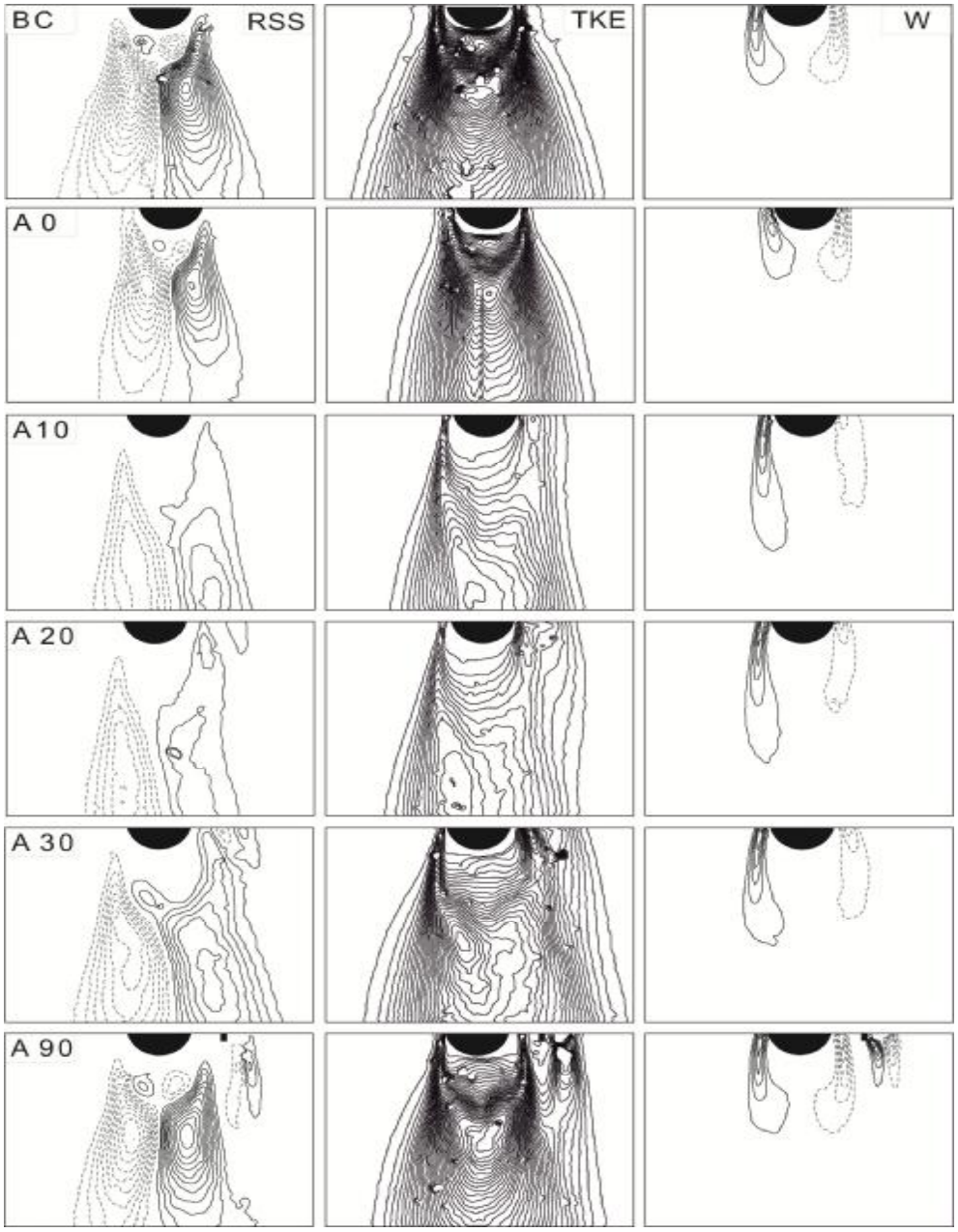


Figure 4.3. The spatial distribution of time-ave.Reynolds shear stress $\langle u'v' \rangle$, turbulent kinetic energy$\langle TKE \rangle$ and vorticity contours,$\langle \omega \rangle$ for gap ratio of 0.5 and bare cylinder case (continue)

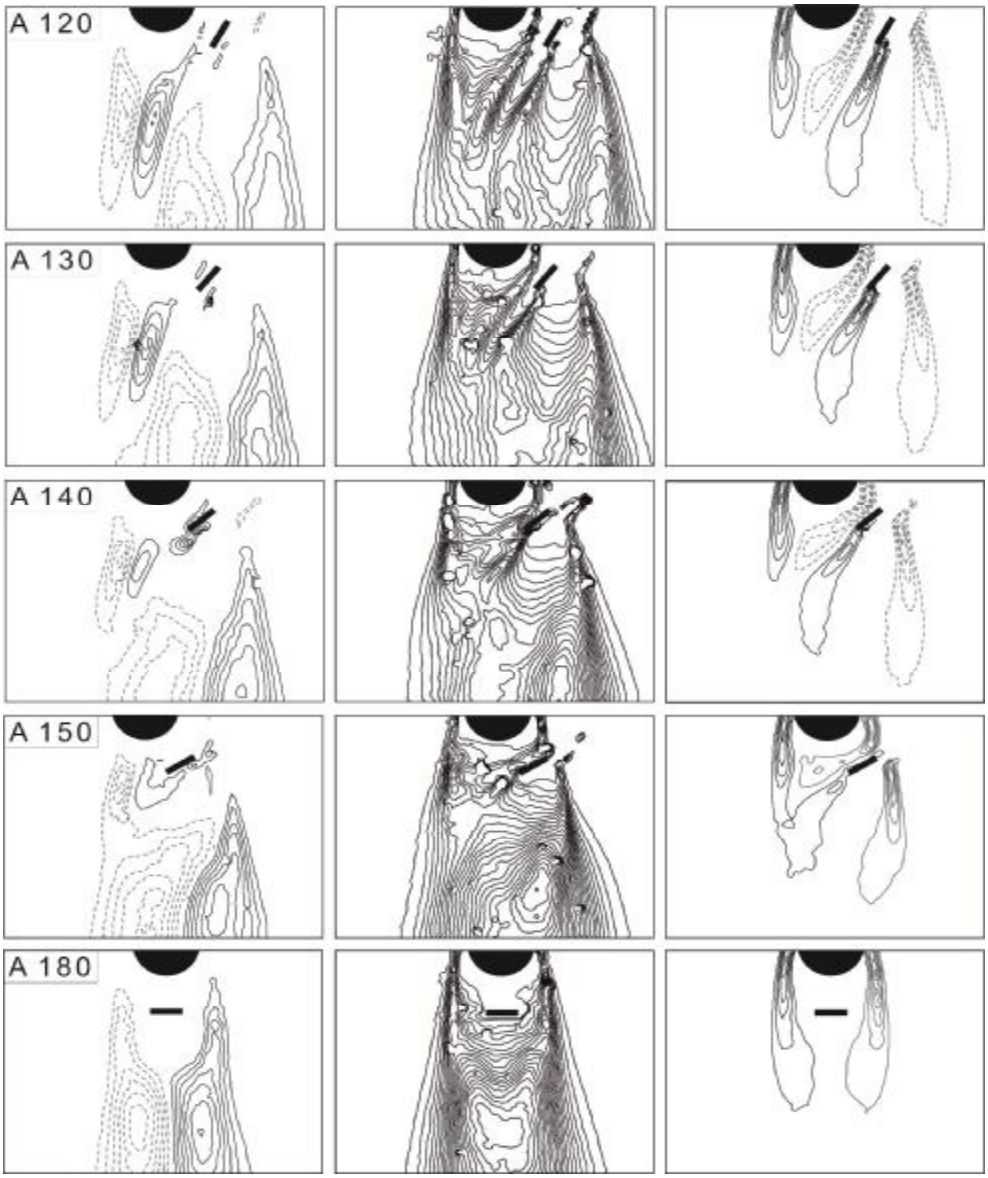


Figure 4.3. The spatial distribution of time-ave.Reynolds shear stress $\langle u'v' \rangle$, turbulent kinetic energy$\langle TKE \rangle$ and vorticity contours,$\langle \omega \rangle$ for gap ratio of 0.5

Case α=10^o has a longer length of positive vorticity contour than the upper negative vorticity contours. The negative shear layer of the cylinder and the shear layers of the plate move together. The flow characteristics of cases α=10^o and α=20^o show similarity in flow characteristics in the gap ratios of 0.5 and 0.3. while the most effective intervals of plate angles is 10^o≤α≤30^o in Regime I and 120^o≤α≤140^o in Regime II for the gap ratio of 0.7 in the figure 4.4.

For case α=130^o, α=140^o and α=150^o, it can be concluded that the increased gap ratio permits the flow to transfer much more momentum through the gap between the cylinder and the detached plate. For this reason, the vorticity contours do not interact with each other easily. In Regime II, for case α=180^o, the shear layers of the cylinder are reattached to the plate causing the length of the vorticity contour to get smaller in the figure 4.4.

Generally, as the horizontal distance between cylinder and plate is increased in the wake region, the interaction between upper and lower shear layers of the cylinder has been decreased. Then, together the plate and cylinder act as single body (Roshko, 1954).

It can be concluded that the lower concentration and value of RSS and *TKE* are generated by the upstream detached plate because the entire front surface of the cylinder is subjected to a low pressure which is found to be remarkably uniform through the cavity region for the gap ratio of 0.7 (Zhang, 2005).

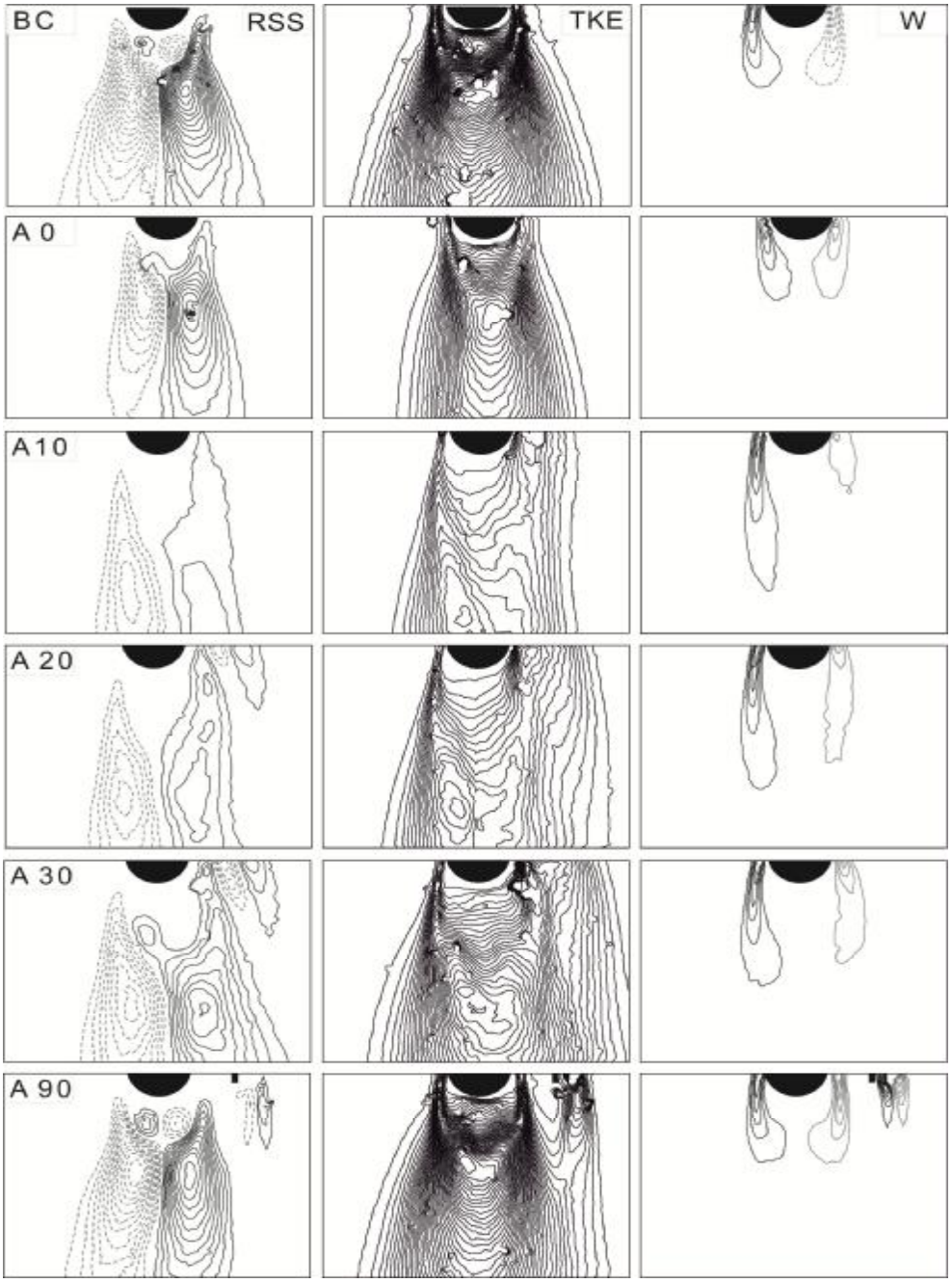


Figure 4.4. The spatial distribution of time-averaged Reynolds shear stress $\langle u'v' \rangle$,turbulent kinetic energy$\langle TKE \rangle$ and vorticity contours,$\langle \omega \rangle$ for gap ratio of 0.7 and bare cylindercase (continue)

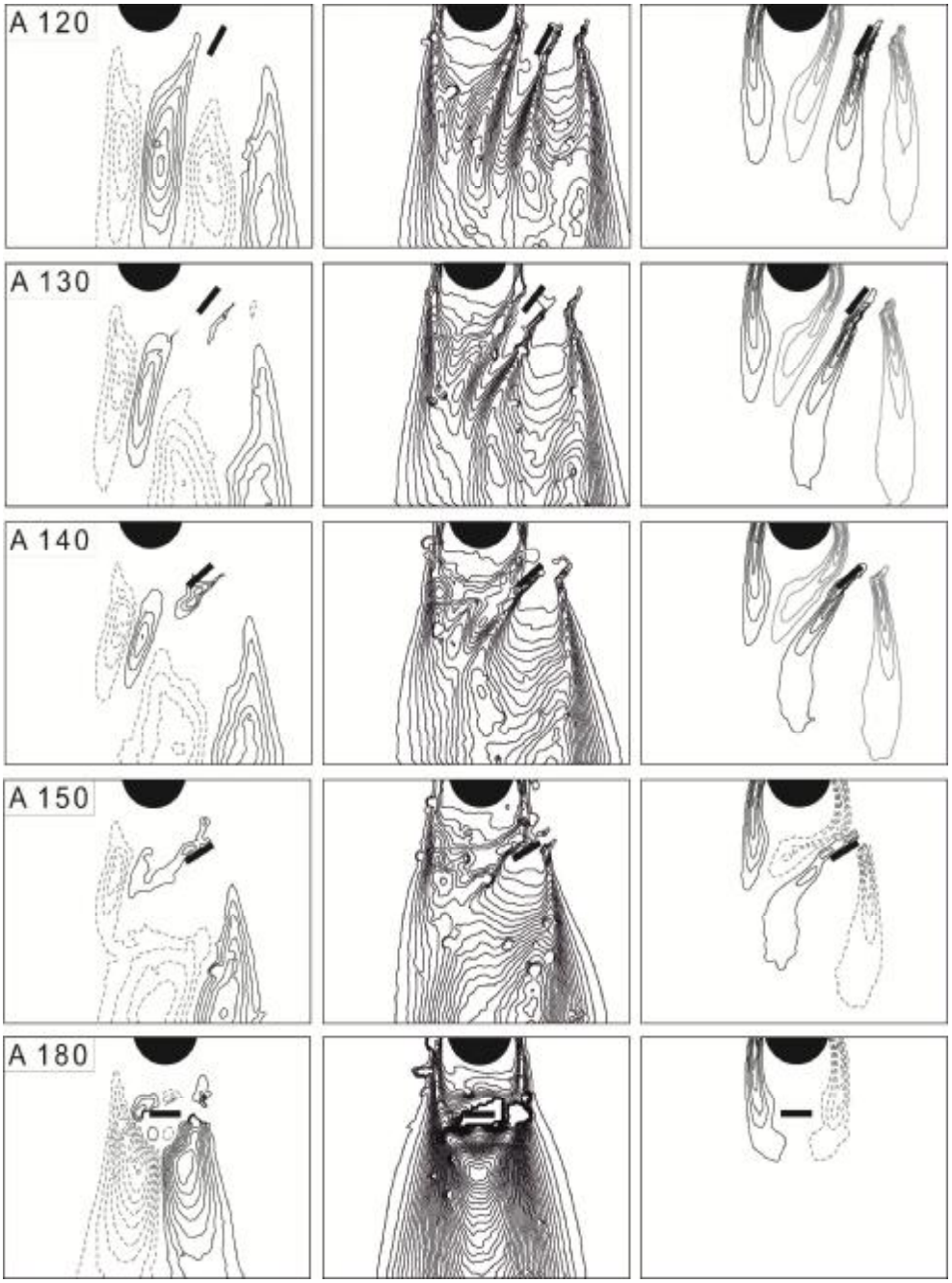


Figure 4.4. The spatial distribution of time-averaged Reynolds shear stress $\langle u'v' \rangle$, turbulent kinetic energy $\langle TKE \rangle$ and vorticity contours, $\langle \omega \rangle$ for gap ratio of 0.7

For case α=20^o, the controlling of vortex shedding is satisfied in the all gap ratios except gap ratio 0.1. It can be seen that case α=140^o and case α=160^o are the best examples for controlled vortex shedding in Regime II. As expected, the vorticity contours of the detached plate do not interact with those of the cylinder in the smaller plate angles of the Regime I. As the gap ratio increases, the momentum of flow passing through the gap is also increases so that the interaction between the plate and cylinder is seen clearly in Regime II. The primary and secondary vorticity contours interact in all the gap ratios in the wake region and the shear layers of the detached plate and the cylinder interact as well. In Regime I, the positive vorticity contours of the cylinder are dominant over the negative vorticity contours in the wake region and the positive vorticity contours have been elongated as well in case α=10^o and case α=20^o in figure 4.5

For Regime I, the separated shear layers from the cylinder interact with the plate, therefore it can be concluded that the shear layer plate interaction occurs before they roll up to form large scale vortices which has also been found in the study by Ali et al. (2010).

As in the G/D of 0.7, the effective intervals of plate angles show similar flow characteristics to the gap ratio of 0.9 in figure 4.5. In Regime II, the shear layers of case α=150^o are generated by the trailing edges of the detached plate and the lower shear layers of the plate affect the negative shear layers of the cylinder. For case α=160^o, similar flow pattern behavior is observed.

The wake region downstream of the cylinder elongates as a result of the interaction between plate and cylinder in the bare cylinder case for all gap ratios. Behind the base of the cylinder, a well-organized flow structure is observed, and it is almost the similar to the case of the bare cylinder.

When the gap ratios are increased, the interactions between shear layers and the plate become more intensive. Consequently the secondary vortices develop along the edges of plate. Then the secondary vortices slowly merge with the growing primary vortices of the same sing of notation.

Another different determination is shown in the case $\alpha=0^o$ where has positive vorticity contours than other cases. For the case $\alpha=0^o$, while the length of the vorticity contour decreases in the gap ratio of 0.7, the vorticity contour elongates in the gap ratio of 0.9. With an increasing gap distance, the separation of shear layers from the plate roll up into discrete vortices, and then impinges on the cylinder at lower plate angles in Regime I. For Regime I, it can be concluded that the shear layers from the cylinder rolling up impinges the plate in the larger plate angle.

It is also observed that there is an incipient small scale vortex engulfing the near surface of the cylinder due to the face-wide vertical flow induced by the shear layers. The flow field near the plate is more complex. This is due to an interaction between the fully developed vortex and the plate or vortex-plate interaction. The plate divides the oncoming vortex in two parts. The plate pushed the vortex formation region further downstream from the cylinder when the gap is increased. The weak region, behind the plate, was classified as the end-plate affected region, and outside of this region as unaffected region. As expected, the detached plate completely loses its effectiveness by increasing a G/D of 0.9 and observed in between the cylinder and the detached plate in Regime II.

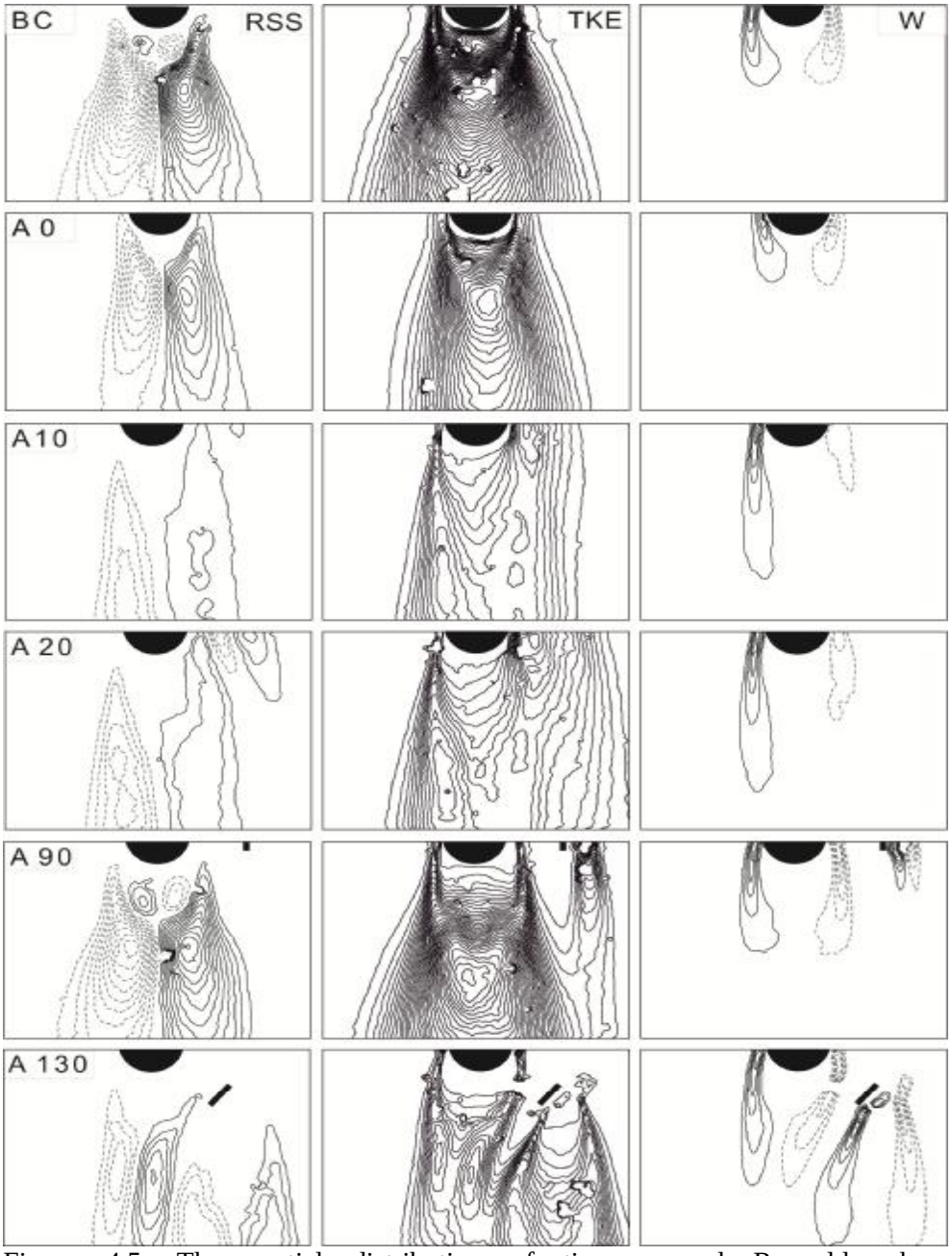


Figure 4.5. The spatial distribution of time-averaged Reynolds shear stress $\langle u'v' \rangle$,turbulent kinetic energy$\langle TKE \rangle$ and vorticity contours,$\langle \omega \rangle$ for gap ratio of 0.9 and bare cylinder case (continue)

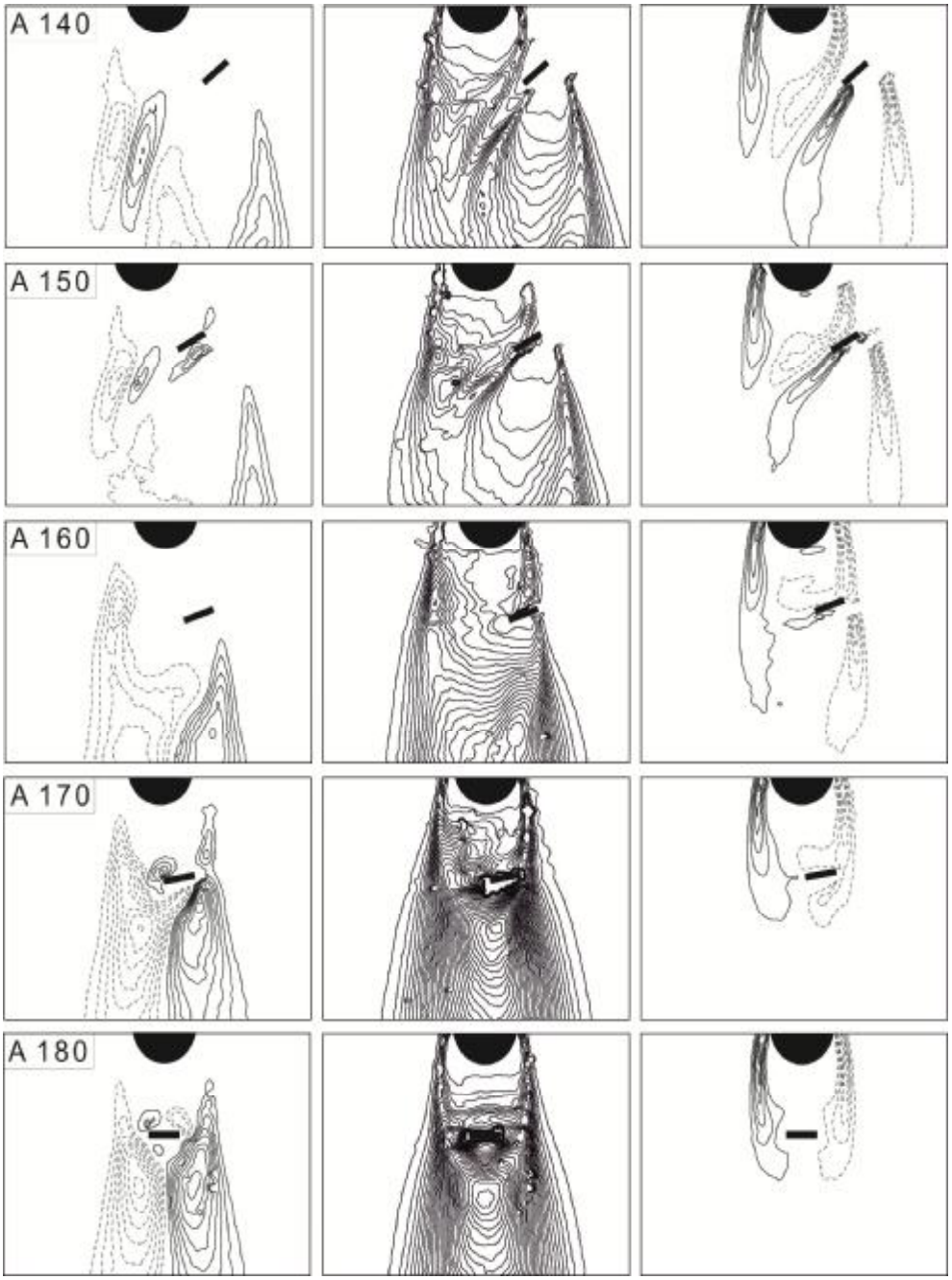
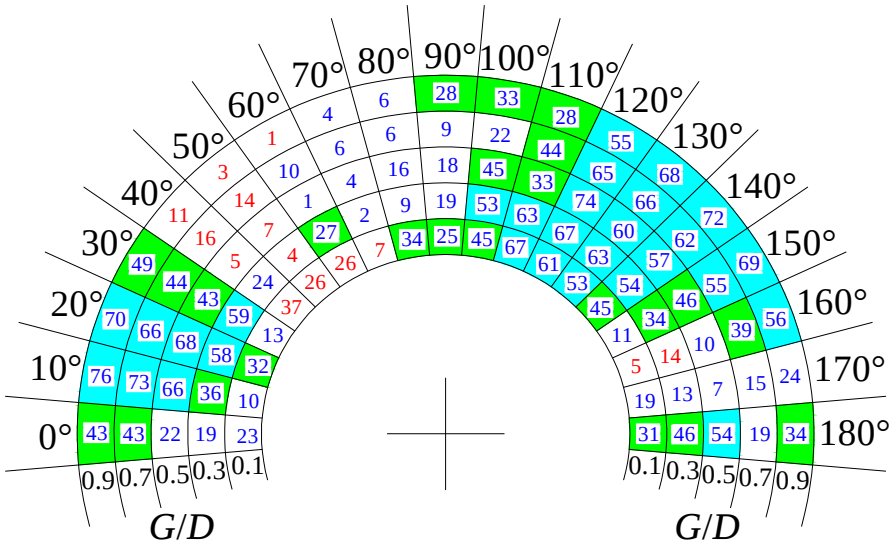


Figure 4.5. The spatial distribution of time-averaged Reynolds shear stress $\langle u'v' \rangle$, turbulent kinetic energy $\langle TKE \rangle$ and vorticity contours, $\langle \omega \rangle$ for gap ratio of 0.9

4.2. Comparison of Flow Control of Single Plate Arrangement for L/D= 0.5 Case

All experiments of single detached plate arrangement are shown in Figure 4.6. These numbers are calculated for the percentage of increasing or decreasing TKE_{max} respect to TKE_{max} value of bare cylinder case. Red numbers show increasing of percentage according to bare cylinder case. Blue numbers show decreasing of percentage according to bare cylinder case. Green background color shows the decreasing value of TKE_{max} in between 25% and 50%. Blue background color shows the decreasing of TKE_{max} in between 50% and 100%. For the gap ratio of G/D of 0.1, the maximum decreasing in TKE_{max} is shown in case 110^o at larger angle plate arrangement. The maximum decreasing in TKE_{max} is occurred in case 120^o. The case 10^o and case 20^o are the best example for control of vortex shedding expect gap ratio of G/D of 0.3. For larger angle plate arrangement, case 120^o, 130^o and 140^o is satisfied to control of vortex shedding. Generally, to control or suppressing of vortex shedding the single detached plate can be used in downstream detached plate arrangement.



Single plate with a
length of 25 mm

Figure 4.6. All results of experiment at single plate arrangement in the detached plate length of 0.5 in terms of TKE_{max}

4.3. The Effect of Dual Detached Plate for Plate Length of 0.5 On The Flow Control

For the dual detached plate arrangements, the flow characteristics of the plate length of 0.5 are similar compared to the gap ratio of 0.1 for single plate experiments, but the flow pattern is not the same shape due to twin plates' arrangement in Regime I. It is expected that the dual plates and cylinder act as a single bluff body because of the low clearance *G*/*D*.

The control of vortex shedding is observed in case α=80°. The symmetrical flow pattern is shown and the length of the vorticity contours is greater than the bare cylinder case in Regime I. The center of the system's shear layer elongates in the far wake region. The secondary shear layer and vorticity contours are observed with case α=90°. The center of the shear layer of the system is still far from the

center of the cylinder and the dual detached plates along with the cylinder act as a single bluff body. The secondary shear layer by the trailing edge of the plate affects the primary shear layer. The secondary shear layer pushes moves the center of the primary shear layer into the far wake region for case $\alpha=100^{o}$ in figure 4.7. As expected, there is an interaction between the dual detached plates and the cylinder in Regime II.

For the gap ratio of 0.1, due to the jet flow, the primary and secondary shear layers begin to interact with each other in the greater plate angle of case $\alpha=100^{o}$ and case $\alpha=110^{o}$ in figure 4.7. The primary shear layer pushes to the secondary shear layer generated by the far trailing edge of the plate in case $\alpha=110^{o}$ and case $\alpha=120^{o}$ so that the interaction between the plate and the cylinder is observed, clearly. The different observation is seen them in the single detached plate, because of a small gap between plate and cylinder. The jet flow affects the shear layers and vorticity contours in the wake region so that they begin to elongate into the far wake region.

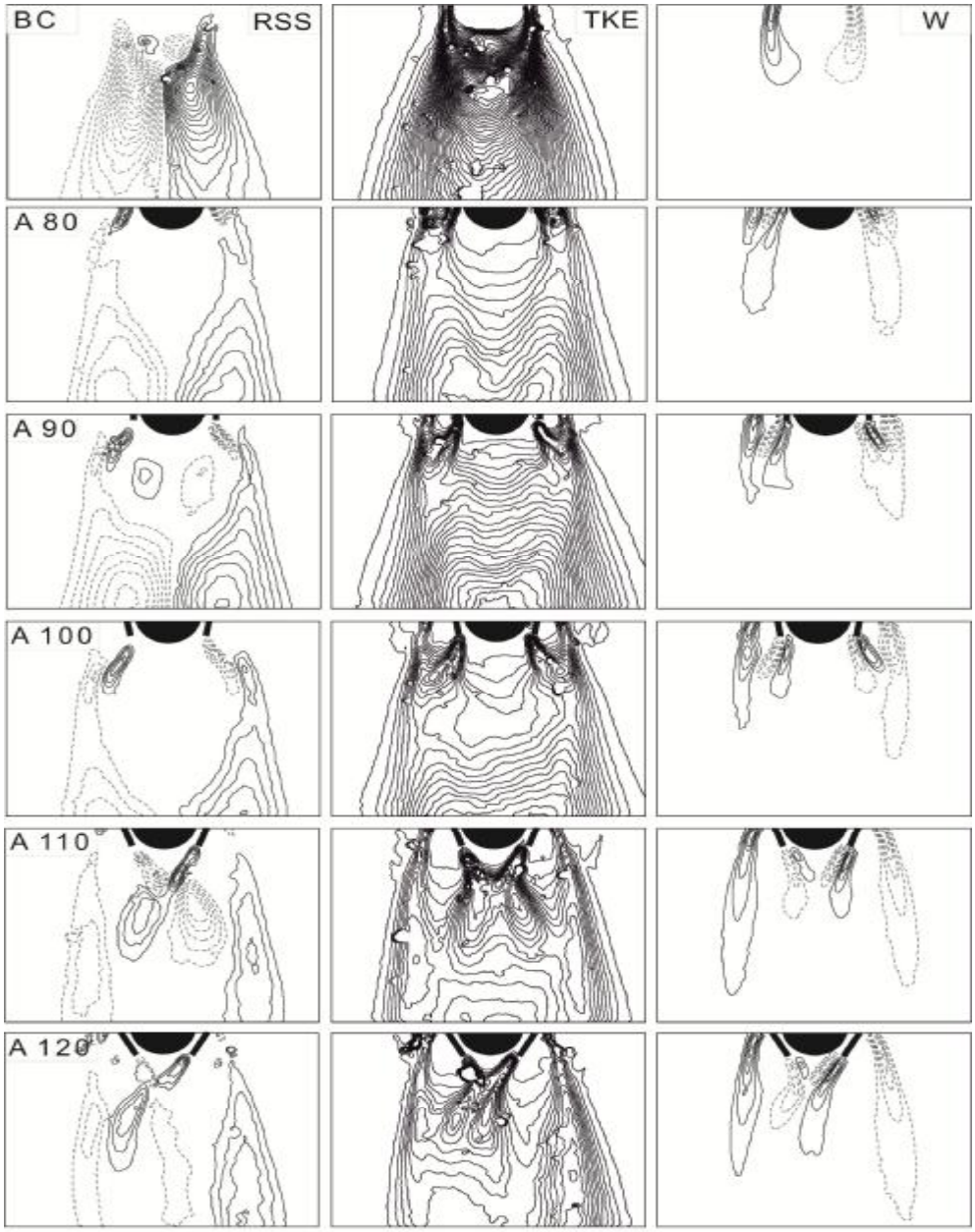


Figure 4.7. The spatial distribution of time-averaged Reynolds shear stress, $\langle u'v' \rangle$, turbulent kinetic energy, $\langle TKE \rangle$, and spanwise vorticity contours, $\langle \omega \rangle$, for gap ratio of 0.1 and bare cylinder case

The shear layer of the system elongates in far the wake region for case α=50^o in figure 4.8. Due to plate angle and gap ratio, the vorticity contours of the system elongate and also move away from the rear cylinder. The secondary shear layers disrupt the upstream flow causing the primary shear layers to elongate. The intensity and concentration of the ***TKE*** is lower than in the other cases for the gap ratio of 0.3. The obstruction and deflection of the incoming flow caused by the dual detached plate forms to two symmetrical streams in the wake region.

As expected, due to the twin plate's arrangement for the larger plate angles, the shear layer and vorticity contours are shown in the wake region. There are six shear layers and vorticity contours generated by the cylinder and by the far and rear trailing edge of the plate shown in the figure 4.8.

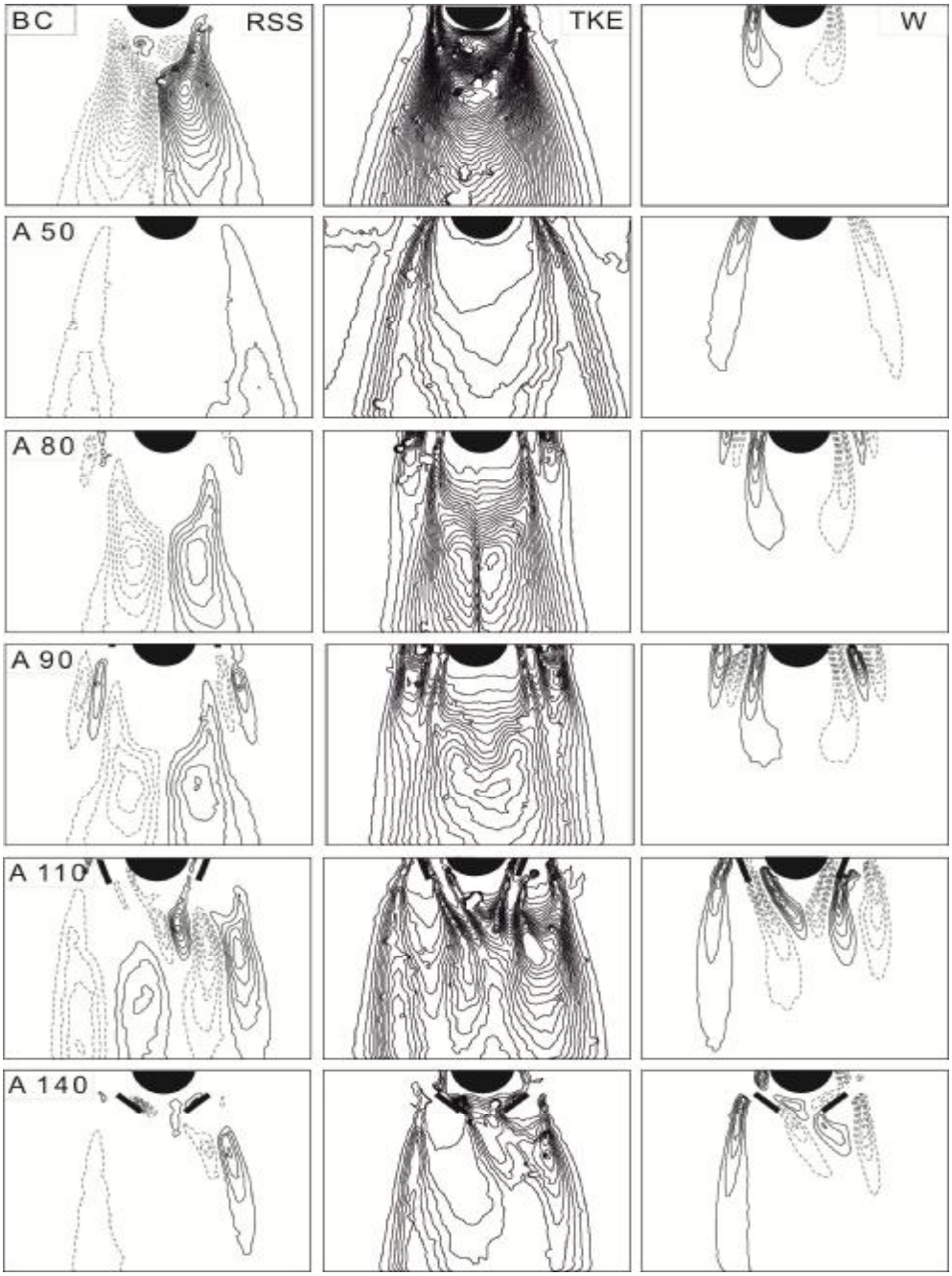


Figure 4.8. The spatial distribution of time-averaged Reynolds shear stress, $\langle u'v' \rangle$, turbulent kinetic energy, $\langle TKE \rangle$, and spanwise vorticity contours, $\langle \omega \rangle$, for gap ratio of 0.3 and bare cylinder case

The different flow pattern is observed for case α=30^o in the gap ratio of 0.5. The shear layers of the plate and cylinder act together in case α=30^o. This situation can be explained as the dual detached plate and the cylinder behave the single bluff body. The similar flow pattern is observed for case α=30^o in the gap ratio of 0.7.

Due to the increased cross-sectional of the system in upstream region, the width of the *TKE* increases in case α=50^o. The interesting situation is observed in the analyzing of cases. For case α=60^o, although the flow characteristic of gap ratio 0.3 is similar in case α=50^o, the case α=50^o has the different flow characteristic according to same case in the gap ratio of 0.3 in figure 4.9. The same trend is observed for case α=150^o. The case α=150^o shows the similarity of flow characteristic of the case α=140^o in the gap ratio of 0.3. A large amount of the downstream advancing momentum significantly delays the vortex formation farther downstream, leading to a more symmetric flow structure in the near wake region of the cylinder in case α=150^o in figure 4.9.

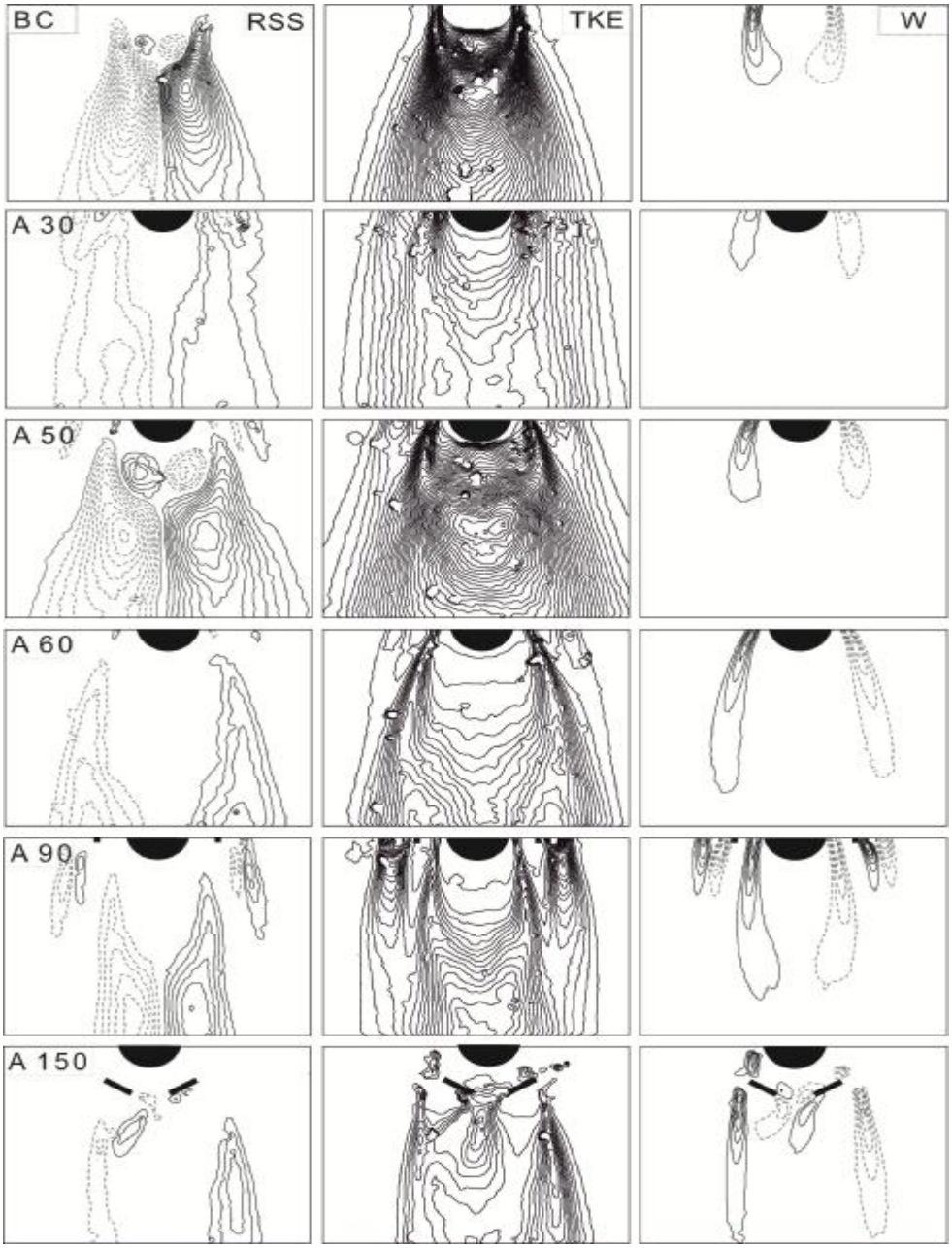


Figure 4.9. The spatial distribution of time-averaged Reynolds shear stress, $\langle u'v' \rangle$, turbulent kinetic energy, $\langle TKE \rangle$, and spanwise vorticity contours, $\langle \omega \rangle$, for gap ratio of 0.5 and bare cylinder case

The flow characteristic of case α=30^o is similar for the gap ratio of 0.7 according to case α=30^o in the gap ratio of the 0.5. All selected and analyzed cases have almost same flow characteristics in figure 4.10 respect to figure 4.9. The primary and secondary shear layers move together in the case α=30^o in the Regime I. As the width of the *TKE* decrease, the length of vorticity contours elongates in Regime I. The center of the shear layers is located in the far wake region in the gap ratio of 0.7 and the intensity and values of the RSS have lower rates than the other cases for case α=60^o. It can be concluded that the case α=60^o and case α=150^o in the gap ratio *G*/*D* of the 0.7 are the indication of the control and suppressed cases in the *L*/*D* of 0.5.

The higher plate angle in the wake region is obstacle for the beginning of shear layers of the cylinder because of the dual detached plate for case α=150^o. The center of systems shear layer is located behind the plates in the far wake region. The cases of α=140^o and α=150^o in the gap ratio of 0.3, and 0.5, 0.7 and 0.9 are examples of this situation.We can say that the higher plate angles in the dual detached plates for the Regime II are well defined for the control cases. Although the lower plate angles is satisfied to control in the Regime I, the width and intensity of *TKE* have lower concentrations in the Regime I than the larger plate angle in the Regime II.

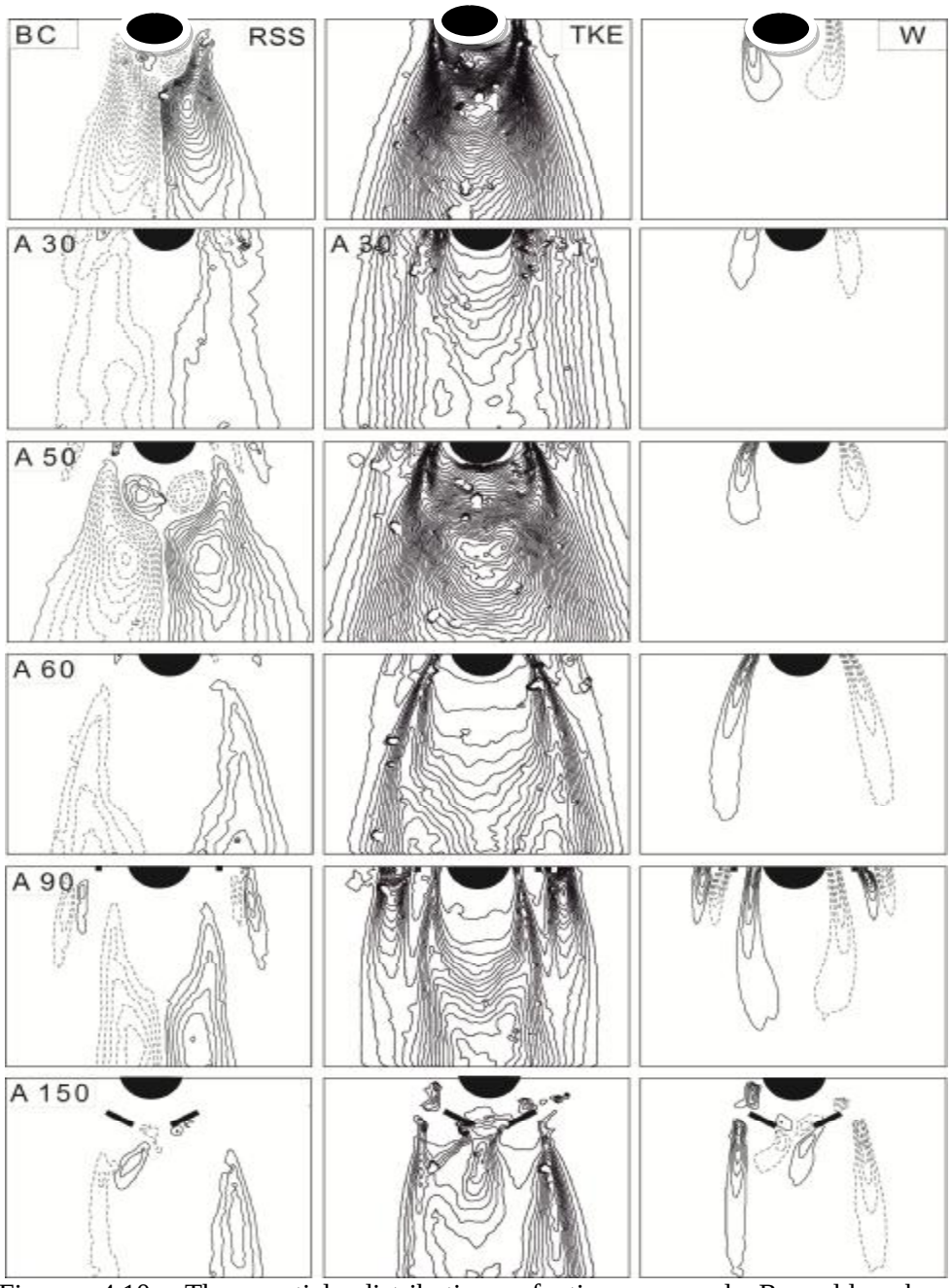


Figure 4.10. The spatial distribution of time-averaged Reynolds shear tress, $\langle u'v' \rangle$, turbulent kinetic energy, $\langle TKE \rangle$, and spanwise vorticity contours, $\langle \omega \rangle$, for gap ratio of 0.7 and bare cylinder case

It is observed that the intensity and amplitude of the ***TKE*** has been increased at the case α=30^o in figure 4.11. The secondary and primary shear layer does not move with primary shear layer in wake region. Compared to bare cylinder case, the maximum value of the Reynolds shear stress layers is still lower.

As respect to the controlling and suppressing of the vortex shedding, the results of some cases in the single detached plate (L/D=0.5) show that the interaction of the shear layer of cylinder and plate is more effective than lower plate angle in the Regime II. But the trend is not observed in the dual detached plate's experiments.

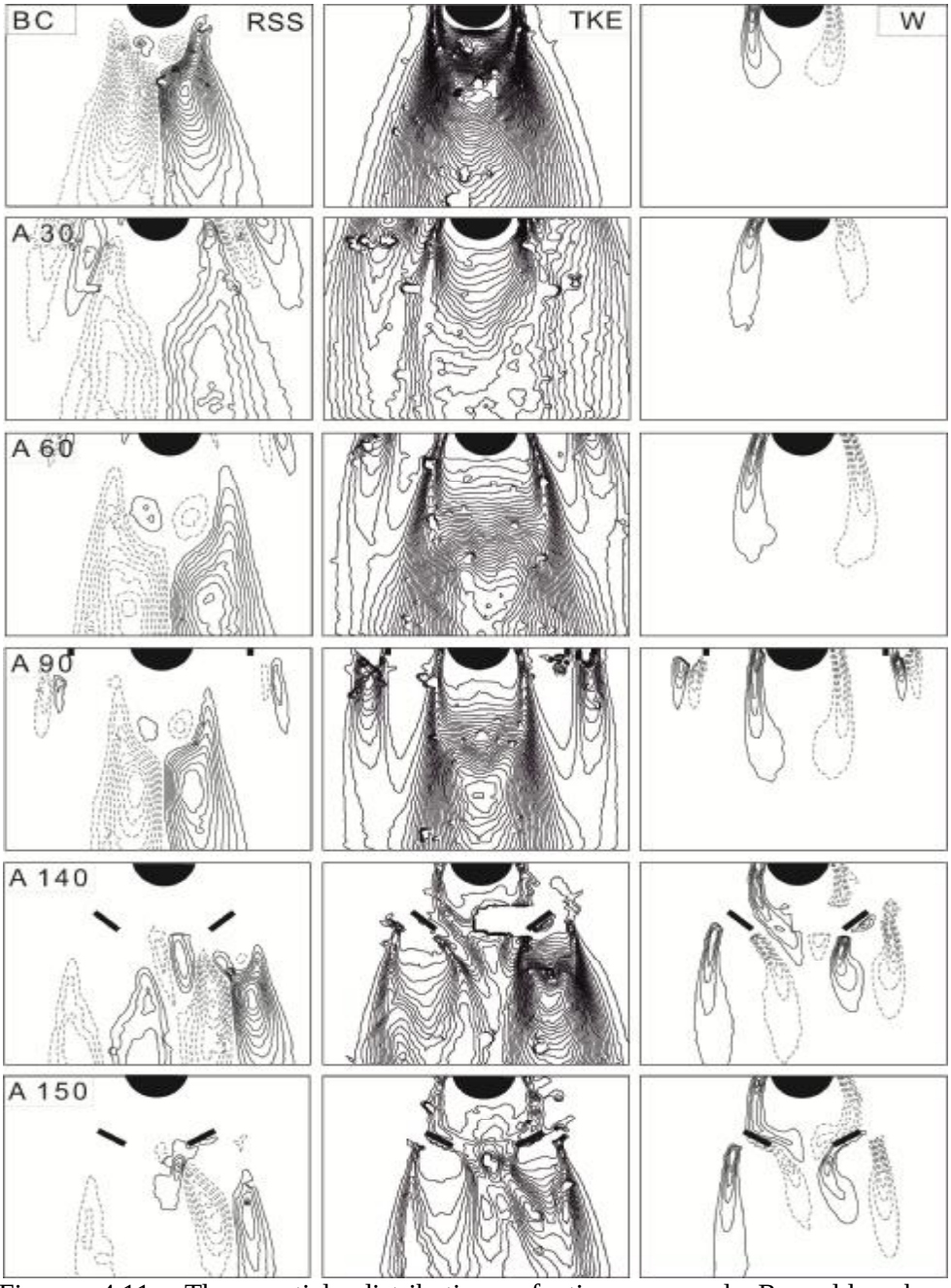


Figure 4.11. The spatial distribution of time-averaged Reynolds shear stress $\langle u'v' \rangle$,turbulent kinetic energy$\langle TKE \rangle$ and spanwise vorticity contours, $\langle \omega \rangle$ for gap ratio of 0.9 and bare cylinder case

4.4. Comparison of Flow Control of Dual Plate Arrangement for L/D= 0.5 Case

All experiments of dual detached plate arrangement are shown in figure 4.12. For the gap ratio of *G*/*D* of 0.1, the maximum decreasing in TKE_{max} is shown in case 130^o at larger angle plate arrangement. The maximum decreasing in TKE_{max} is occurred in case 140^o. Case 30^o is the best example for control of vortex shedding. For larger angle plate arrangement, case 90^o is satisfied to control of vortex shedding all gap ratios. Generally, to control or suppressing of vortex shedding the single detached plate can be used in upstream detached plate arrangement.

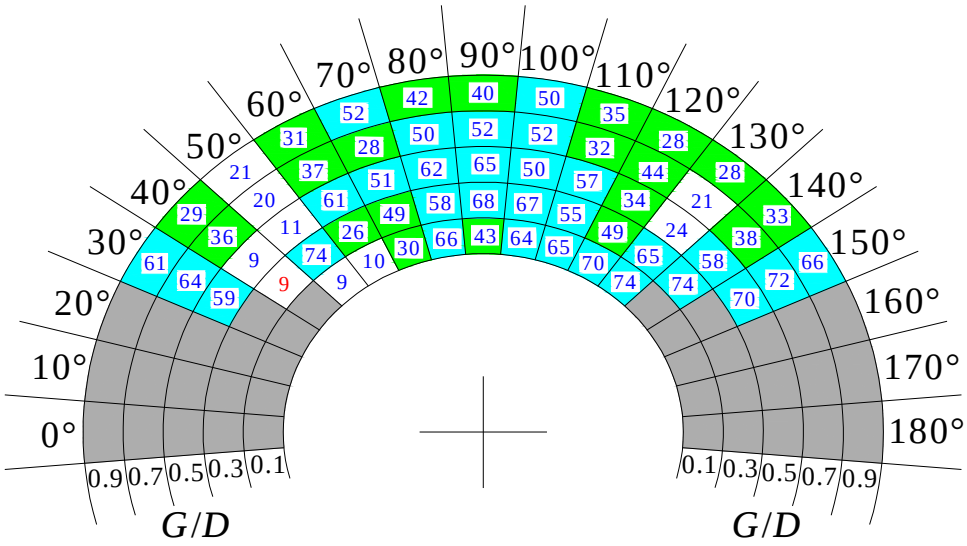


Figure 4.12. All results of experiment at dual plate arrangement in the detached plate length of 0.5 in terms of TKE_{max}

4.5. The Effect of Single Detached Plate for Plate Length of 1 On The Flow Control

Generally, the flow patterns of the detached plate length of 1 are almost similar to the result of the detached plate length of 0.5. Due to increased plate length, the width of shear layers of the system is larger according to the detached plate length of 0.5 for case $\alpha=0^o$. The intensity and concentrations of the shear layer and *TKE* of the system is higher than the detached plate length of 0.5. This variety depends on the larger plate length. The shear layers and turbulent kinetic energy intensify immediately behind cylinder. As seen in the figure 4.13, the width of the RSS and *TKE* are higher than other gap ratios for the gap ratio of 0.1. The vorticity contours of the case $\alpha=0^o$ do not be formed exactly in the gap ratio of 0.1. The vorticity contours of cylinder for the case $\alpha=0^o$ is break downed by the upstream detached plate and the small clearness between the detached plate and the cylinder.

Due to plate length, the detached plate behave a shield to flow freestream lines so that the flow is speared from the detached plate and cylinder but the detached plate is not effective in the upstream region in the gap ratio of 0.1 for lower detached plate angle. Increasing the plate angle in Regime I, the primary vorticity contours get to interact with secondary vorticity contours in case $\alpha=80^o$ in figure 4.13. Due to cross-sectional area, the width of the *TKE* contours is getting smaller until case $\alpha=90^o$ and later *TKE* contours increase in wake region.

The shear layers of the cylinder elongate in weak region for the case $\alpha=90^o$. The secondary vortices are effective in Regime II especially case $\alpha=110^o$. At the case $\alpha=90^o$, The positive shear layer of the plate is affective for the positive shear layers of the cylinder so that the positive shear layers of the cylinder and the secondary shear layers act together. The rupture is occurred in the near wake region so that the intensity of vortex shedding is higher in the other cases for case $\alpha=110^o$. The interaction of the primary and secondary shear layers are seen clearly in case $\alpha=160^o$. The detached plate act a bluff body so the secondary vorticity contours

highly interact with the primary vorticity contours in the case α=160^o. As expected, case α=180^o has symmetrical flow patterns in figure 4.13. The intensity and width of case 180^o is still lower than bare cylinder case.

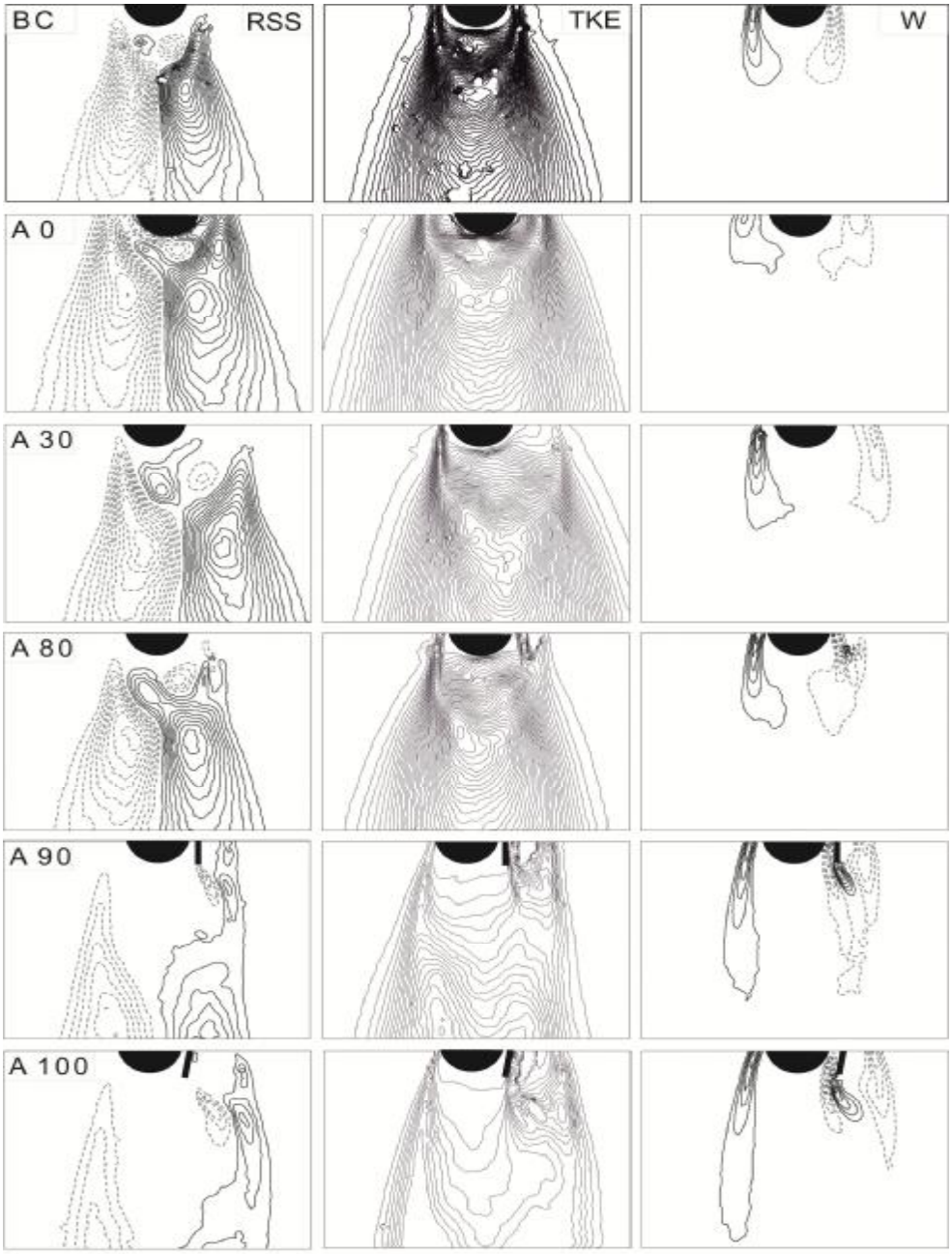


Figure 4.13. The spatial distribution of time-averaged Reynolds shear stress $\langle u'v' \rangle$, turbulent kinetic energy $\langle TKE \rangle$ and vorticity contours, $\langle \omega \rangle$ for gap ratio of 0.1 and bare cylinder case (continue)

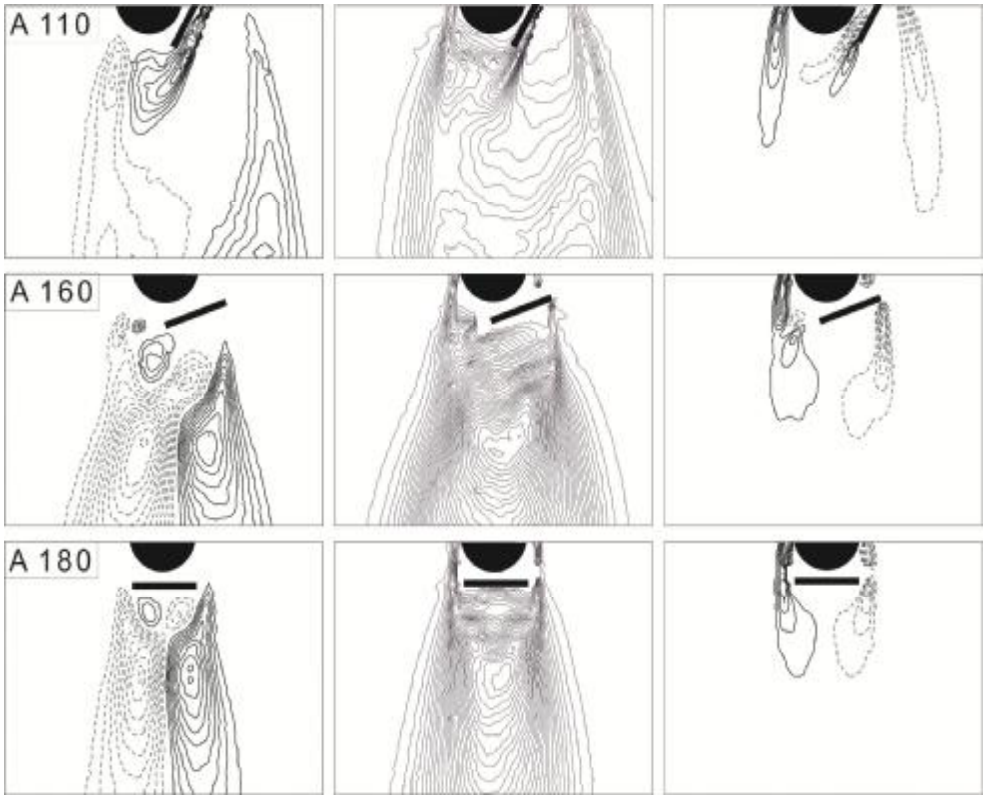


Figure 4.13. The spatial distribution of time-averaged Reynolds shear stress $<u'v'>$, turbulent kinetic energy$<TKE>$ and vorticity contours, $<\omega>$ for gap ratio of 0.1

Due to increasing the clearances between detached plate and the cylinder, the outside shear layers of the system elongates in weak region but the center of the shear layer is behind the cylinder. The situation can be explained as the decreasing the flow intensity. The front of the cylinder is exposed to vortices from the detached plate. The flow characteristics of ***TKE*** for case $\alpha=0^o$ are almost similar for in the gap ratio of 0.1. The effect of the secondary vorticity contours is shown for case $\alpha=90^o$. The center of the shear layer of the cylinder move through the wake region for case $\alpha=90^o$ and the positive vorticity contours of the cylinder is larger in the gap ratio of 0.3. It is said that the controlling of the vortex shedding is occurred in case $\alpha=120^o$ in figure 4.14

With increasing the larger plate angle in Regime II, the shear layers of the cylinder are impinged on the plate and the reattachment of shear layer is occurred in case $\alpha=170^o$ and case $\alpha=180^o$ in figure 4.14. The detached plate behaves like a bluff body in wake region and the secondary shear layer is generated by the detached plate for Regime II.

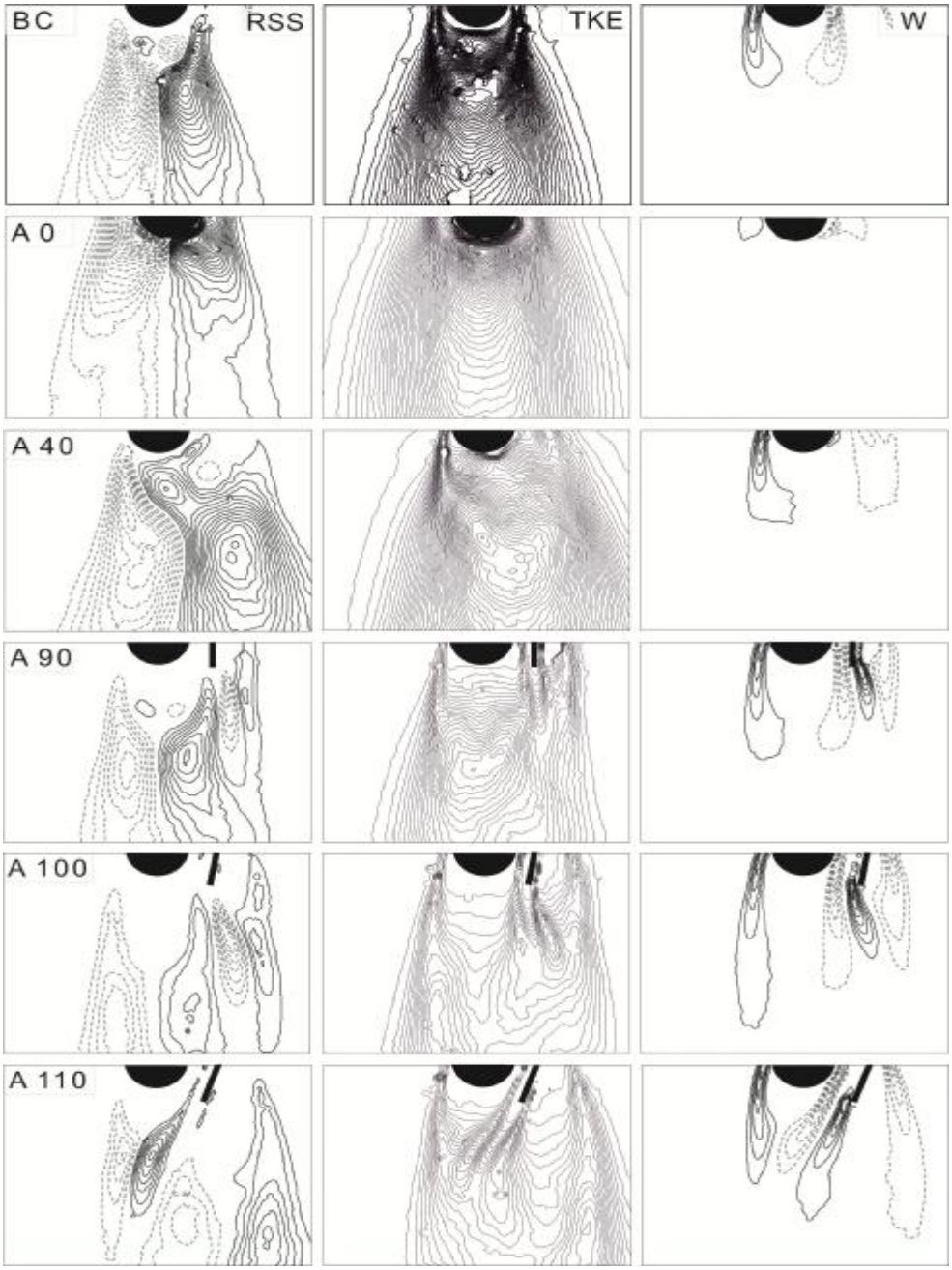


Figure 4.14. The spatial distribution of time-averaged Reynolds shear stress $\langle u'v' \rangle$, turbulent kinetic energy $\langle TKE \rangle$ and vorticity contours, $\langle \omega \rangle$ for gap ratio of 0.3 and bare cylinder case (continue)

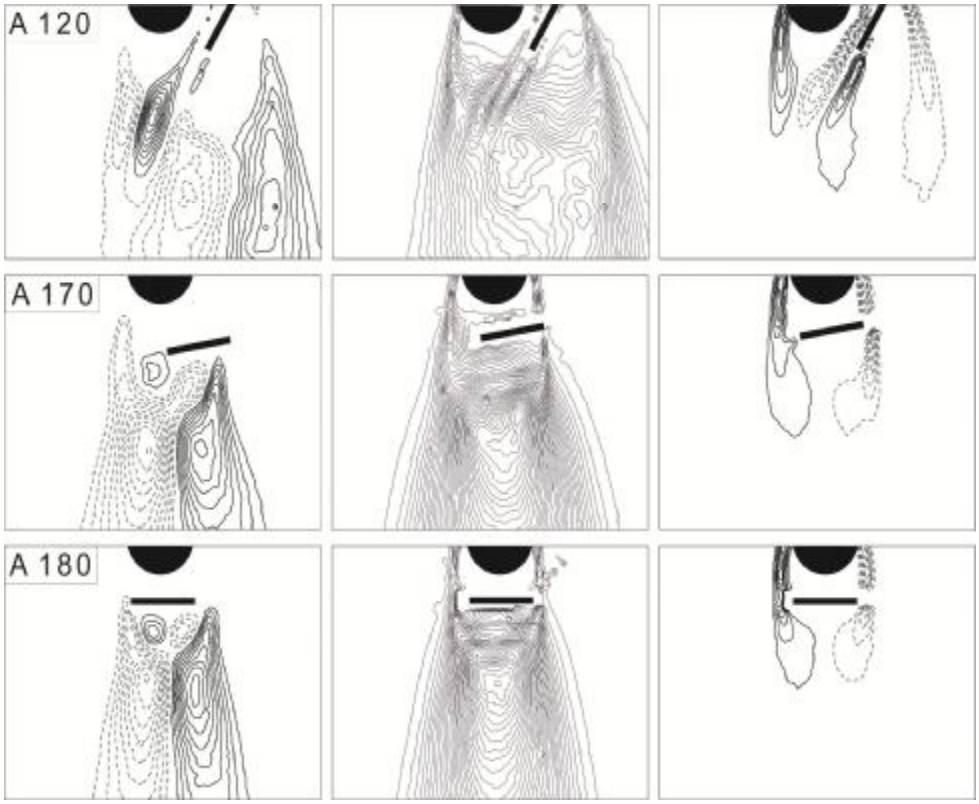


Figure 4.14. The spatial distribution of time-averaged Reynolds shear stress $\langle u'v' \rangle$, turbulent kinetic energy $\langle TKE \rangle$ and vorticity contours, $\langle \omega \rangle$ for gap ratio of 0.3

For Regime I, the width of *TKE* is still larger due to the plate length. The increasing clearness between the plate and the cylinder can permit more flow according to gap ratio of 0.1 and 0.3 for case α=0^o. This trend is observed until gap ratio of 0.9. The detached plate act a shield to incoming flow in Regime I and also the downstream detached plate is obstacle for the shear layers of the cylinder for Regime II.

The vorticity contours of the system for case α=0^o and case α=10^o do not form exactly in the gap ratio of 0.5 in figure 4.15. This situation can be explained that the vorticity contours of cylinder are break downed by the upstream detached plate in Regime I. the positive shear layer of the cylinder is larger due to the detached plate for case α=40^o in figure 4.15. The giving angle to detached plate, the secondary vorticity contours and shear layers of the system in wake region get to extend in Regime II. Up to now, it can be concluded that the detached plate length (L/D) of 1 is not affective for the gap ratio of 0.1, 0.3 and 0.5.

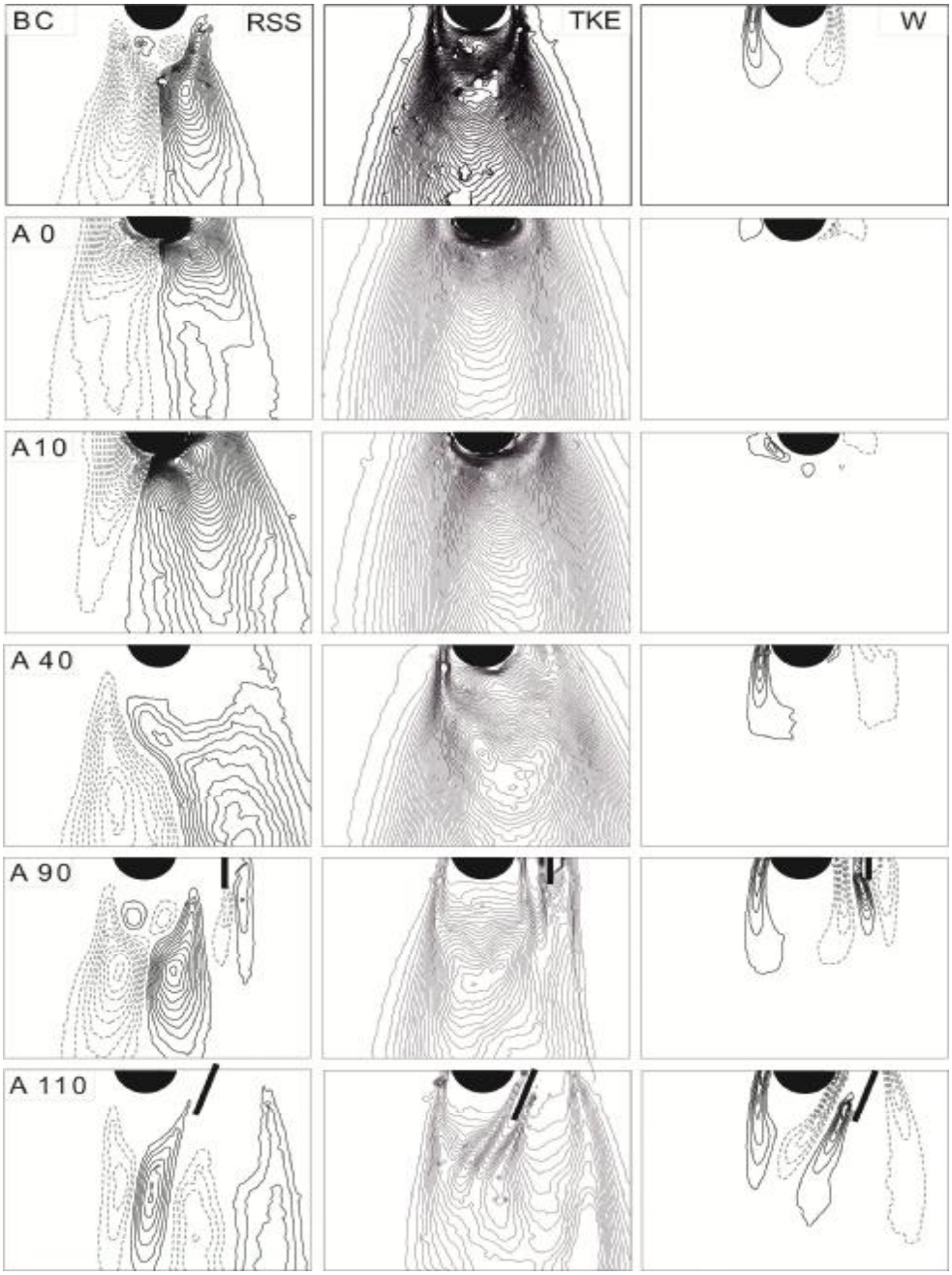


Figure 4.15. The spatial distribution of time-averaged Reynolds shear stress $\langle u'v' \rangle$,turbulent kinetic energy$\langle TKE \rangle$ and vorticity contours, $\langle \omega \rangle$ for gap ratio of 0.5 and bare cylinder case (continue)

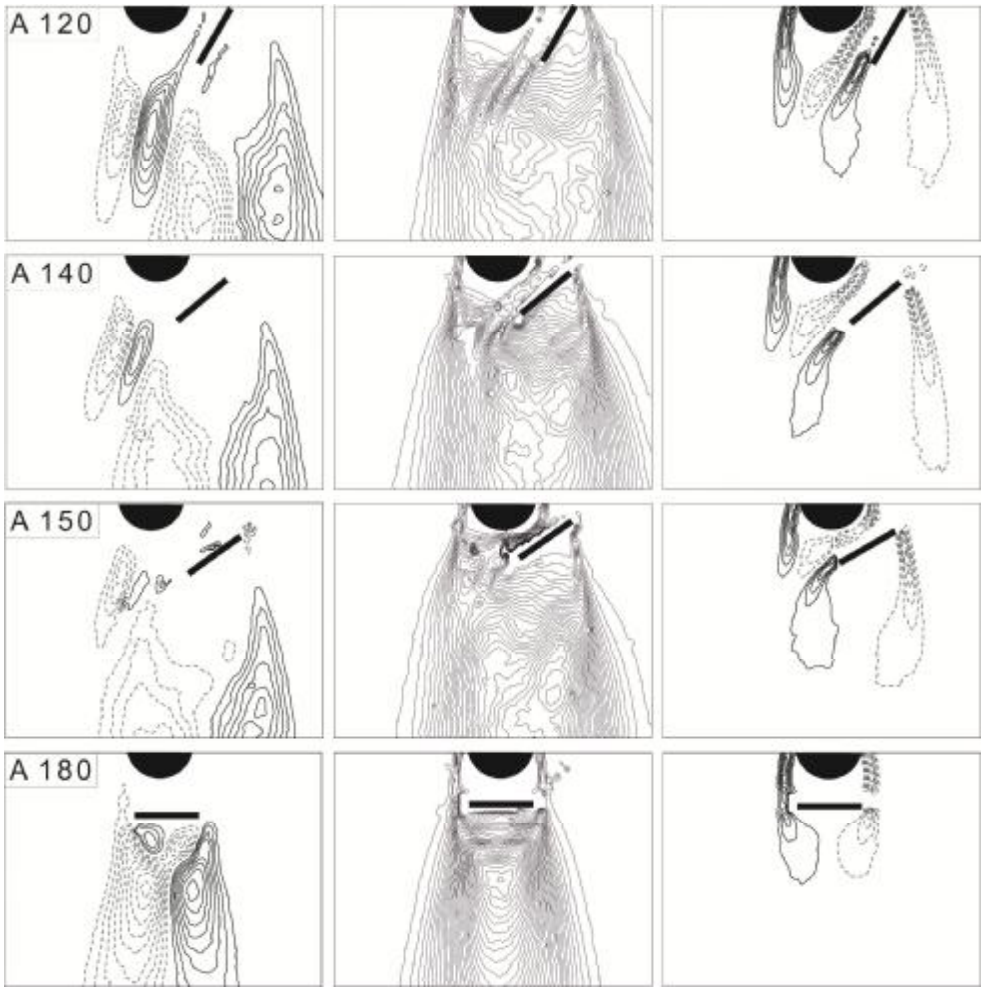


Figure 4.15. The spatial distribution of time-averaged Reynolds shear stress $<u'v'>$,turbulent kinetic energy$<TKE>$ and vorticity contours, $<\omega>$ for gap ratio of 0.5

The flow characteristic of the gap ratio of 0.7 for the detached plate length of 1 is similar for the *L*/*D* of 0.5. The detached plate is obstacle for the incoming flow for case α=0^o so the vorticity contours of the system do not occur in wake region. The front of the cylinder is exposed to vortices from the detached plate. The giving to plate angle, the center of the shear layer of the system elongates in far wake region. The cases from α=20^o to 40^o are satisfied for the control of vortex shedding in figure 4.16. This situation is observed in the *L*/*D* of 0.5 for the gap ratio of 0.7.

For the cases from α=20^o to 40^o, the positive vorticity contour of the cylinder is bigger than the negative vorticity contour of the cylinder in Regime I. Due to increased plate angles, the negative vorticity contour is occurred far from the cylinder until case α=90^o. The intensity of the system's ***TKE*** get to lower until case α=90^o. The case α=90^o has symmetrical flow pattern. Due to the increased distance between the plate and cylinder, the vorticity contours are more affective in other gap ratios. At case α=130, the secondary vorticity contour is larger and does not interact the primary vorticity contours in Regime I. When the plate angle is increased in Regime I, the primary and secondary vorticity contours get to interact with each other. The primary shear layer is rolling up in weak region. And also the vorticity contours impinge on the detached plate in wake region. Especially, case α=160^o, α=170^o and α=180^o in figure 4.16.



Figure 4.16. The spatial distribution of time-averaged Reynolds shear stress $<u'v'>$,turbulent kinetic energy$<TKE>$ and vorticity contours, $<\omega>$ for gap ratio of 0.7 and bare cylinder case (continue)

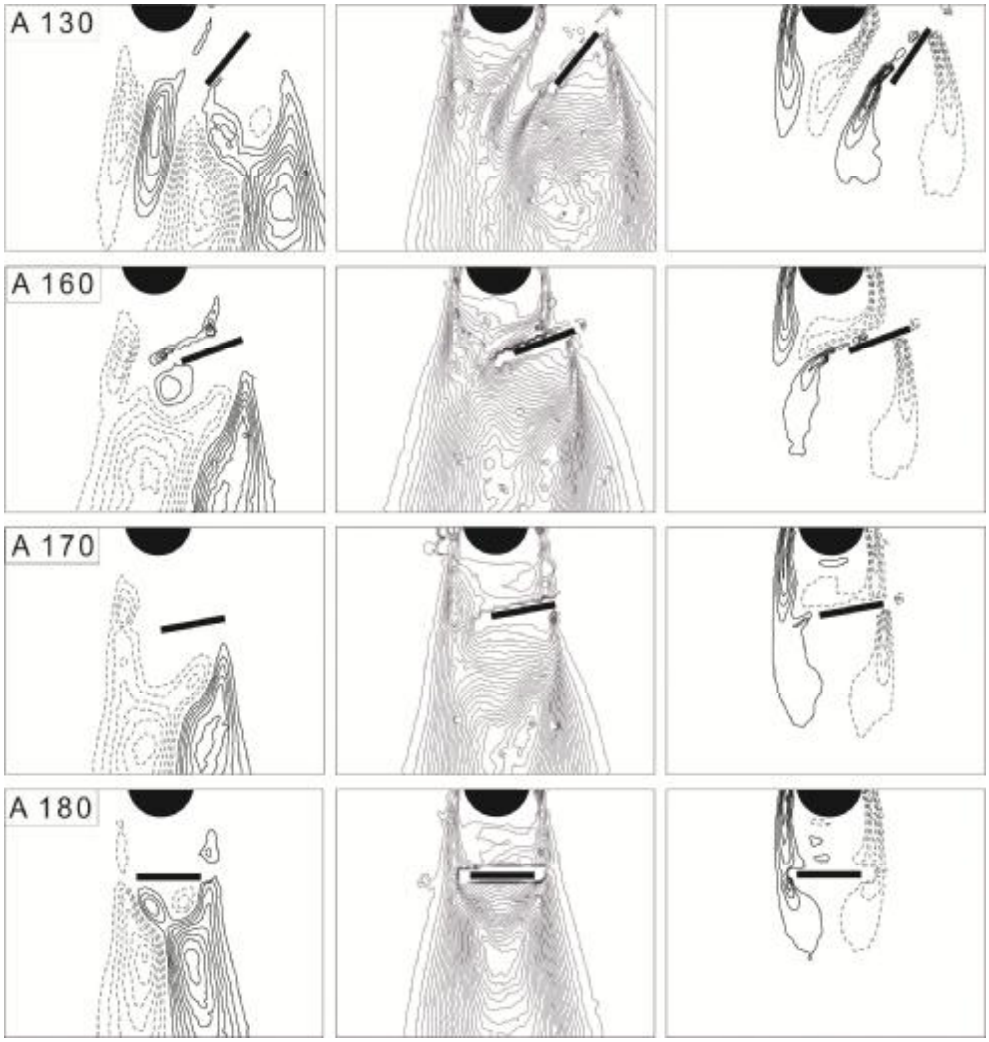


Figure 4.16. The spatial distribution of time-averaged Reynolds shear stress $\langle u'v' \rangle$,turbulent kinetic energy$\langle TKE \rangle$ and vorticity contours, $\langle \omega \rangle$ for gap ratio of 0.7

The free stream flow from the detached plate not only eliminates the flow separation along the rear surface of the cylinder, they also merge toward the wake centerline to create an advancing momentum in the immediate near wake region so that for the lower plate angle, the shear layers of the system elongate far from the weak region and get less intensity for Regime I. It is shown that the cases of the cases from α=20^o to 40^o are satisfied for the suppressing of the vortex shedding in the G/D of 0.9 in figure 4.17.

The trend of flow characteristics of the G/D of 0.7 continue in flow characteristics of the gap ratio of 0.9. The center of shear layer of the system elongates in wake region but differently the primary vorticity contours are far from the cylinder due to plate angle. At case α=170^o, the secondary shear layers and vorticity of the system is not observed at the trailing edge of the detached plate. But especially the detached plate is not effective device for the controlling of vortex shedding in the weak region. It can be concluded that the detached plate for the gap ratio of 0.9 and 0.7 is affective in the L/D of 1.

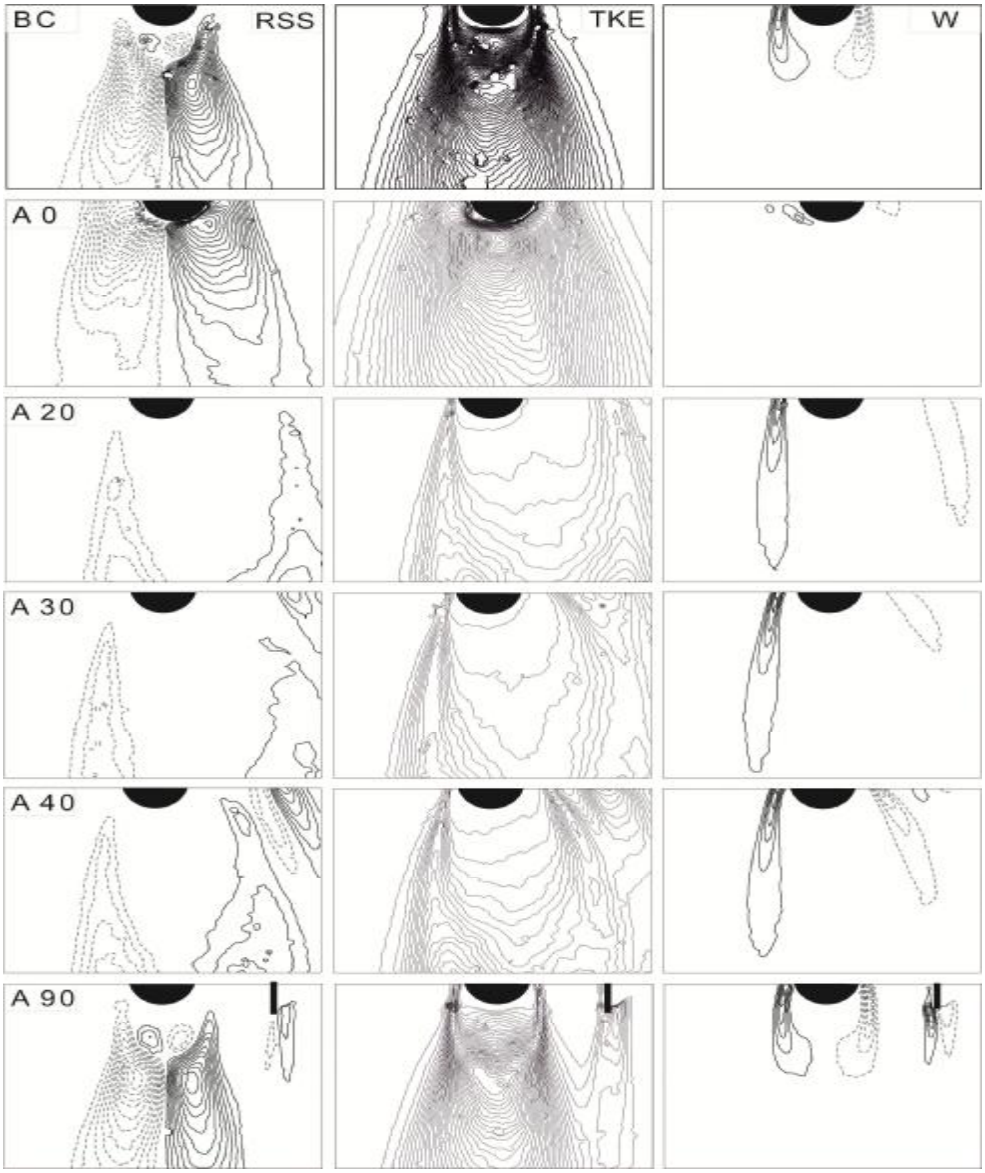


Figure 4.17. The spatial distribution of time-averaged Reynolds shear stress $\langle u'v' \rangle$,turbulent kinetic energy$\langle TKE \rangle$ and vorticity contours, $\langle \omega \rangle$ for gap ratio of 0.9 and bare cylinder case (continue)

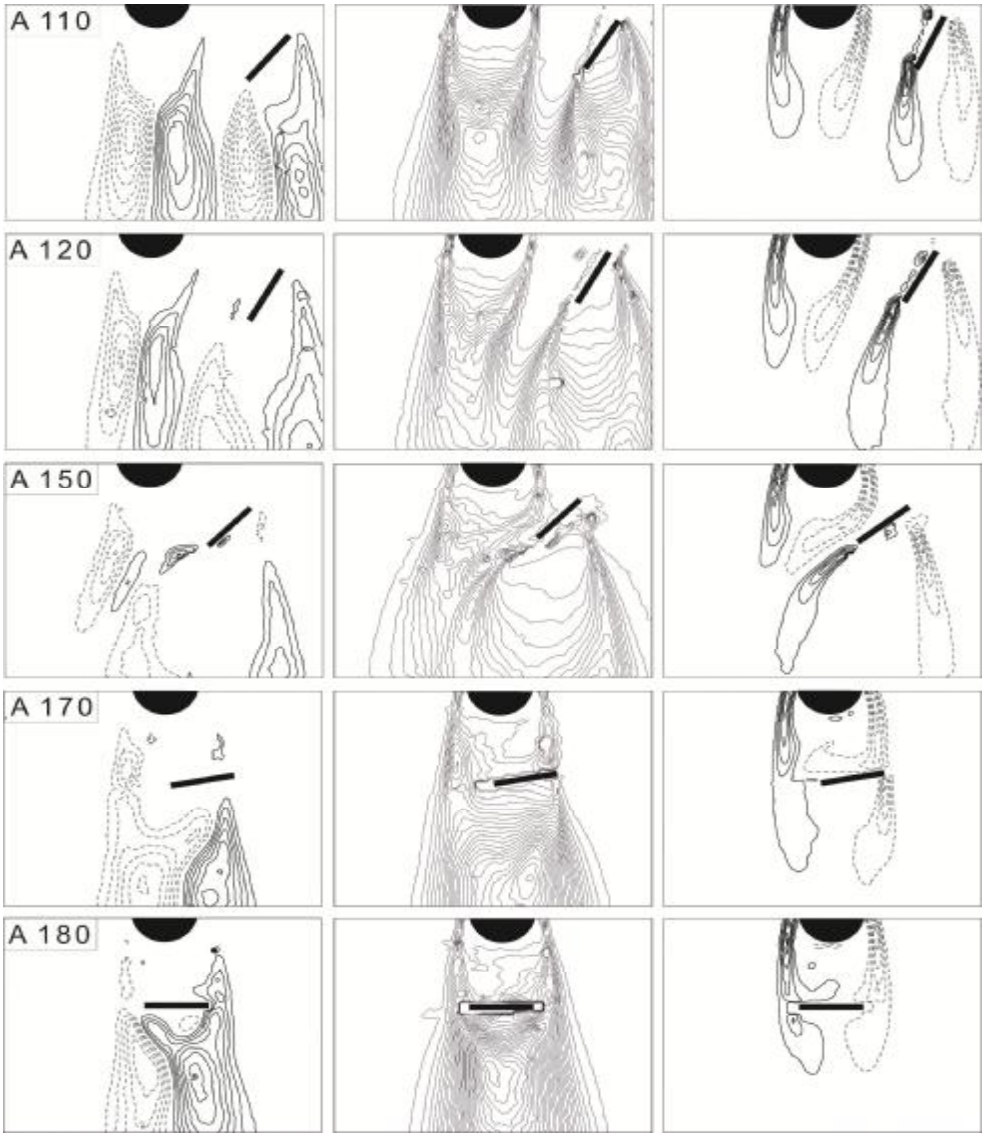


Figure 4.17. The spatial distribution of time-averaged Reynolds shear stress $<u'v'>$,turbulent kinetic energy$<TKE>$ and vorticity contours, $<\omega>$ for gap ratio of 0.9

4.6. Comparison of Flow Control of Single Plate Arrangement for L/D= 1 Case

The experiments of single detached plate arrangement are shown figure 4.18. For the gap ratio of *G*/*D* of 0.1, the maximum decreasing in TKE_{max} is shown in case 100^o at larger angle plate arrangement. The maximum decreasing in TKE_{max} is occurred in case 30^o. The cases 20^o to 40^o are best example for control of vortex shedding in the gap ratio of *G*/*D* of 0.7 and 0.9. For larger angle plate arrangement, case 110^o and case 120^o are satisfied to control of vortex shedding. Generally, to control or suppressing of vortex shedding the single detached plate can be used in downstream detached plate arrangement and the interval of 20^o and 40^o in the gap ratio of *G*/*D* of 0.7 and 0.9.

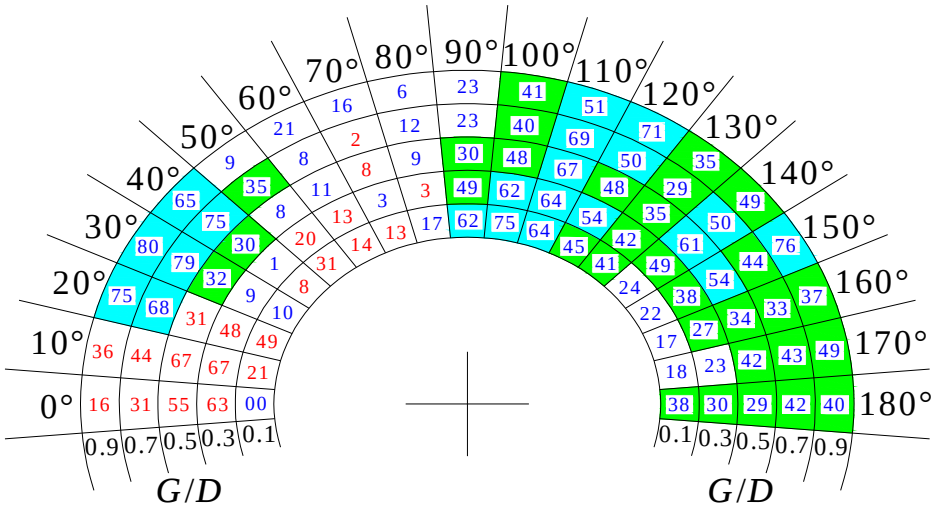


Figure 4.18. All results of experiment at single plate arrangement in the detached plate length of 1 in terms of TKE_{max}

4.7. The Effect of Dual Detached Plate for Plate Length of 1 On The Flow Control

The results demonstrate that the characteristics of the wake are significantly related to the cross-sectional geometries of the detached plate. The relationship between gap ratios and the flow characteristics depends strongly on geometry of the bluff body. The reasons are attributed to differences of flow angle of the separated flow and of steadiness of the separation.

The vortex shedding is suppressed in the gap ratio of 0.1 for the case α=50^o, case α=60^o and case α=90^o in figure 4.19. Obstruction of the dual detached plates to the incoming flow deflects part of the fluid to pass through the cylinder and the vortex shedding is occurred in the far weak region. This trend continue until case α=90^o. The length of vorticity contours of the system is bigger than other gap ratios in the dual detached plates for these cases but in the case α=90^o, the vorticity contours are no longer. The larger vorticity contours is indication of the suppress vortex shedding. As seen in the *TKE* contours, the intensity of *TKE* is lower than the other cases in the gap ratio of 0.1.

For case α=110 and case α=130 in figure 4.19, the primary and secondary shear layer of the system interact with each other behind the cylinder then the mixing of the shear layers are observed. The secondary shear layers of the system are generated by the rear of the trailing edge of plate in Regime II. The clearness of dual detached plates in the downstream acts a vent for the incoming flow.

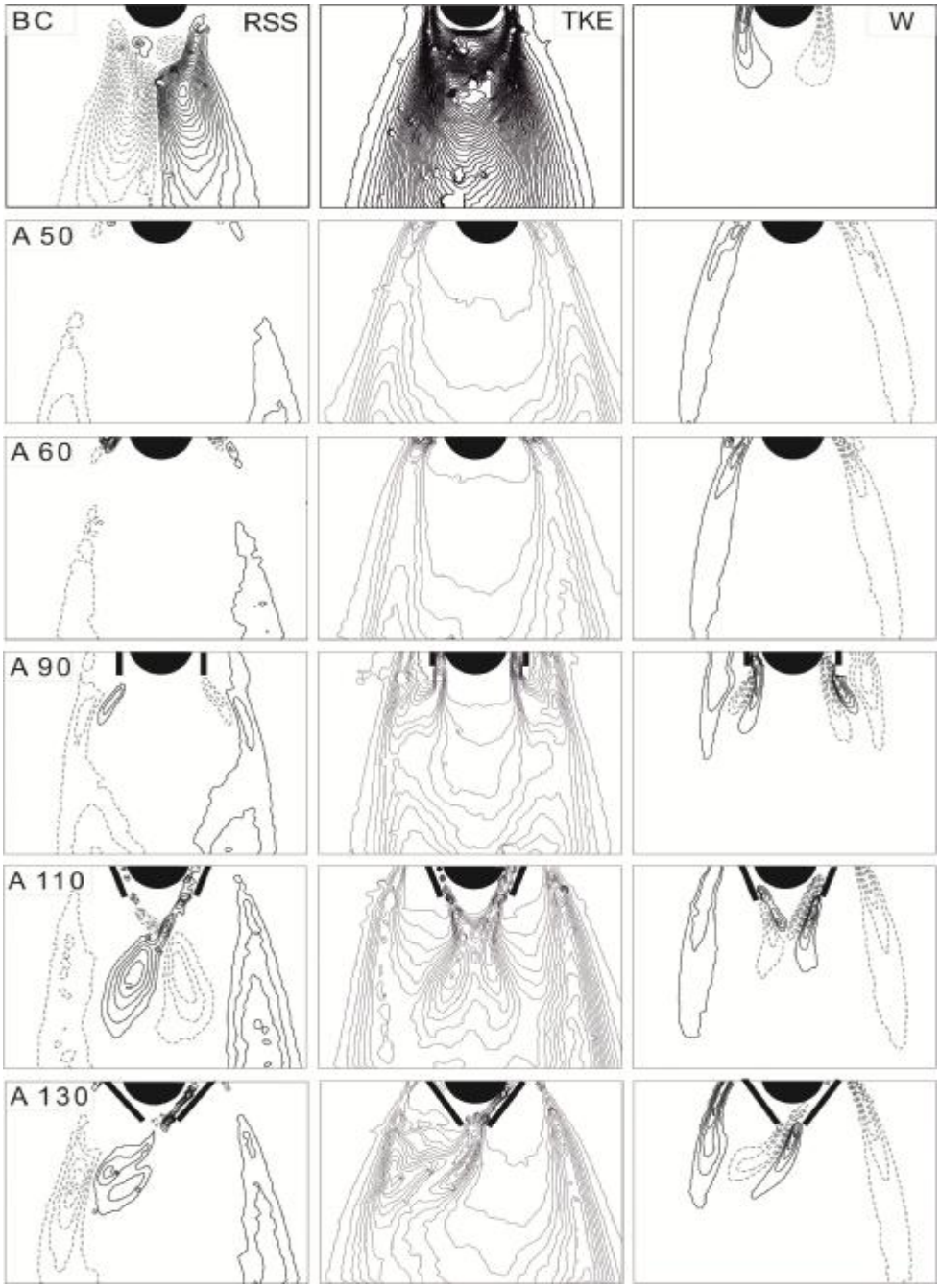


Figure 4.19. The spatial distribution of time-average Reynolds shear stress $<u'v'>$, turbulent kinetic energy$<TKE>$ and vorticity contours, $<\omega>$ for gap ratio of 0.1 and bare cylinder case

Case α=50^o is only case for the suppressing of vortex shedding for the L/D of 1. The center of the shear layers elongates in the far wake. A large amount of the downstream advancing momentum significantly delays the vortex formation farther downstream, leading to a more symmetric flow structure in the far wake region of the cylinder. The center of shear layer of the system is still far from the cylinder in case α=80^o.

After case α=90^o, the secondary shear layer of the system is observed. Two primary shear layers and the primary vorticity contour get to form. For the secondary shear layer and secondary vorticity contour are generated by far and rear of trailing edge of the detached plate. The primary shear layers and vorticity contours in case α=110 and α=130 is generated by the dual detached plate in figure 4.20. The incoming flow from the cylinder through near wake moves in between detached plates. The secondary vortices slowly merge with the growing primary vortices of the same sign of rotation in the gap ratio of 0.1 and 0.3. However further increase in the plate angle results in the larger width with higher concentrations.

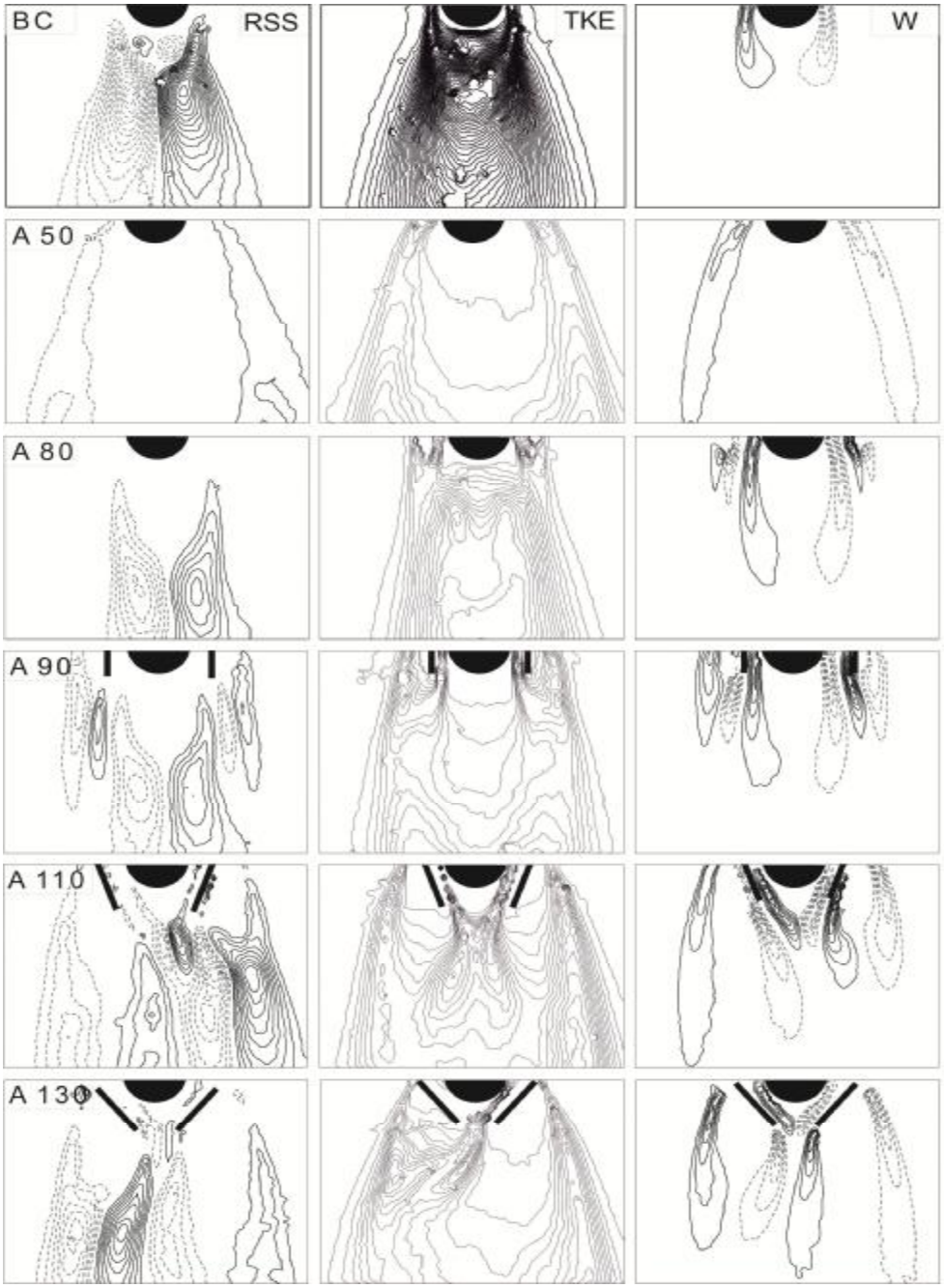


Figure 4.20. The spatial distribution of time-averaged Reynolds shear stress $\langle u'v' \rangle$,turbulent kinetic energy$\langle TKE \rangle$ and vorticity contours, $\langle \omega \rangle$ for gap ratio of 0.3 and bare cylinder case

For case α=50^o to 60^o, the suppressing of vortex shedding is occurred by the dual detached plates in figure 4.21. Differently, the vorticity contours is elongated and also the vorticity pattern is far from the cylinder. The intensity and concentration of ***TKE*** contours behind the cylinder is lower in Regime I. Increasing the plate angle, the width of ***TKE*** get lower until case α=90^o. The case α=90^o has symmetrical flow patterns. The amount of momentum transfer from the shear layer into the wake region is restricted by the detached plate in the gap ratio of 0.5. Increasing the plate angle to larger degrees greatly enlarges the wake width since the detached plate takes a dominant role on formation of the flow structure in Regime I or Regime II.



Figure 4.21. The spatial distribution of time-averaged Reynolds shear stress $\langle u'v' \rangle$,turbulent kinetic energy$\langle TKE \rangle$ and vorticity contours, $\langle \omega \rangle$ for gap ratio of 0.5 and bare cylinder case

Due to the dual detached plate's obstruction, the amount of momentum transfer from the gap into wake region is restricted. A large amount of the downstream advancing momentum significantly delays the vortex formation farther downstream, leading to a more symmetric flow structure in near wake region of the cylinder. The flow characteristics of the case α=40^o show different shape because the secondary shear layer of the system effect on the primary shear layer. The intensity of ***TKE*** contours is less than other cases behind the cylinder. Until case α=60^o, the control of vortex shedding is satisfied in the gap ratio of 0.7 for the dual detached plates.

Case α=90^o has the primary and secondary shear layer and vorticity contours in figure 4.22. The secondary shear layers and vorticity contours are dual because of the far and rear of trailing edge of the plate. The width of the primary shear layer is less than the other cases for the L/D of 1.

It is expected that the use of dual detached plate is significantly effect on downstream flow for larger flow angles since it directly interacts with the shear layer of the cylinder.

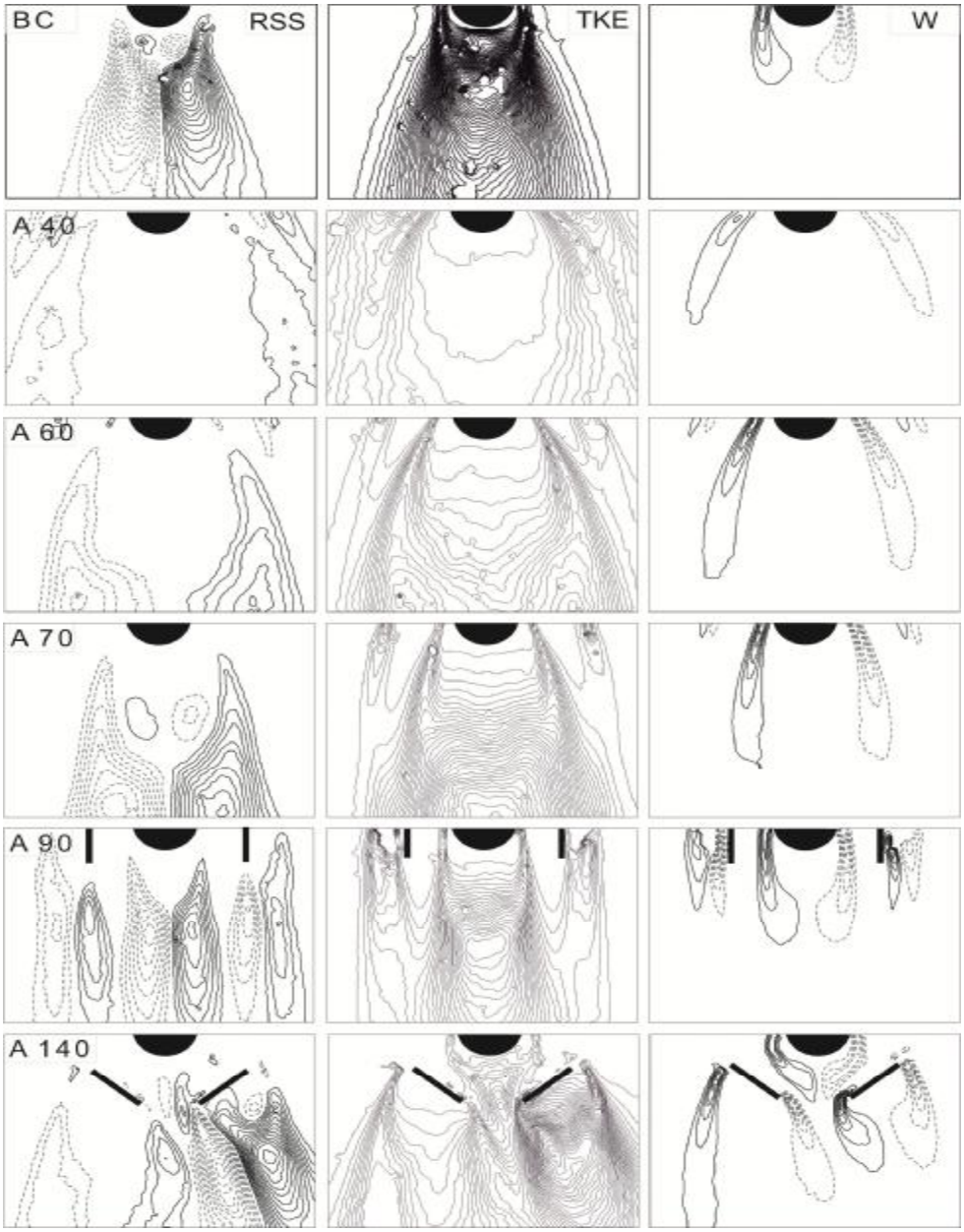


Figure 4.22. The spatial distribution of time-averaged Reynolds shear stress $\langle u'v' \rangle$,turbulent kinetic energy$\langle TKE \rangle$ and vorticity contours, $\langle \omega \rangle$ for gap ratio of 0.7 and bare cylinder case

Due to upstream dual plate arrangement for Regime I, the lower plate angle is effective for the controlling or suppressing of the vortex shedding. The center of the shear layers elongate in far wake region and the analyzed cases in Regime I have different flow characteristics for the gap ratio of 0.9. The intensity of *TKE* contours is weaker for lower plate angle cases for the *G*/*D* of 0.9.

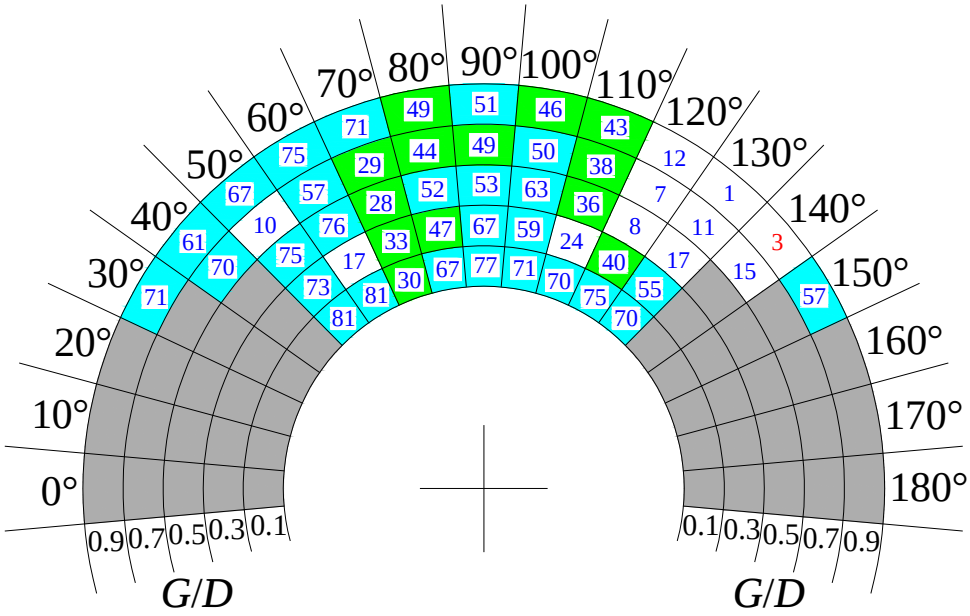
It can be concluded that it is possible to control or suppress of vortex shedding of cylinder in weak region dramatically in the use of *L*/*D* of 1 dual detached plates placed upstream. The optimum case for the controlling or suppressing of the vortex shedding is found to be between $10^o \leq \alpha \leq 60^o$ in the gap ratio of 0.9. For larger plate angles cases, the RSS and *TKE* values of intensity in the shear layer of the cylinder increases to due to the plate's wake disturbance.



Figure 4.23. The spatial distribution of time-averaged Reynolds shear stress $\langle u'v' \rangle$,turbulent kinetic energy$\langle TKE \rangle$ and vorticity contours, $\langle \omega \rangle$ for gap ratio of 0.9 and bare cylinder case

4.8. Comparison of Flow Control of Dual Plate Arrangement for L/D= 1 Case

The experiments of dual detached plate arrangement are shown in figure 4.24. For the gap ratio of *G*/*D* of 0.1, the maximum decreasing in TKE_{max} is shown in case 50^o and case 60^o at lower angle plate arrangement and also maximum decreasing in TKE_{max} is occurred in these cases. The cases 90^o and 100^o are the best case to controlling of the vortex shedding. These cases are the best example for control of vortex shedding all gap ratios. Case 30^o and 150^o is satisfied to control of vortex shedding in the gap ratio *G*/*D* of 0.9. Generally, to control or suppressing of vortex shedding the dual detached plate can be used in upstream detached plate arrangement.



Double plate with a
length of 50 mm

Figure 4.24. All results of experiment at dual plate arrangement in the detached plate length of 1 in terms of TKE_{max}

4.9. The Effect of Arc Shaped Single Detached Plate On The Flow Control

For the Regime I, all cases show similar flow characteristics until case α=90^o. Case α=0^o have symmetrical flow patterns for the shear layers and vorticity contours for the plate length *L/D* of 0.8. The width of the shear layers of the system is still lower than bare cylinder case. Due to detached plate location, the positive vorticity contours of the cylinder is bigger than the other vorticity contours for case α=90^o. The secondary vorticity contours interact with the negative vorticity contours of the cylinder. This trend is shown for case α=100^o and α=110^o in figure 4.25. The center of the shear layer elongates far wake region for the gap ratio of 0.1 in the arc shaped detached plate. The jet flow is observed in case α=110^o so that the flow incoming from the gap is effect on the negative shear layer of the cylinder. Though the positive vorticity contour of the cylinder get bigger in case α=90^o and α=100^o, that of the cylinder has almost same length in case α=110^o. For case α=110^o, the positive vorticity contour is generated by far trailing edge of the detached plate and move with the negative vorticity contour of the cylinder and the positive vorticity contour of the cylinder is affect with these vorticity contours .

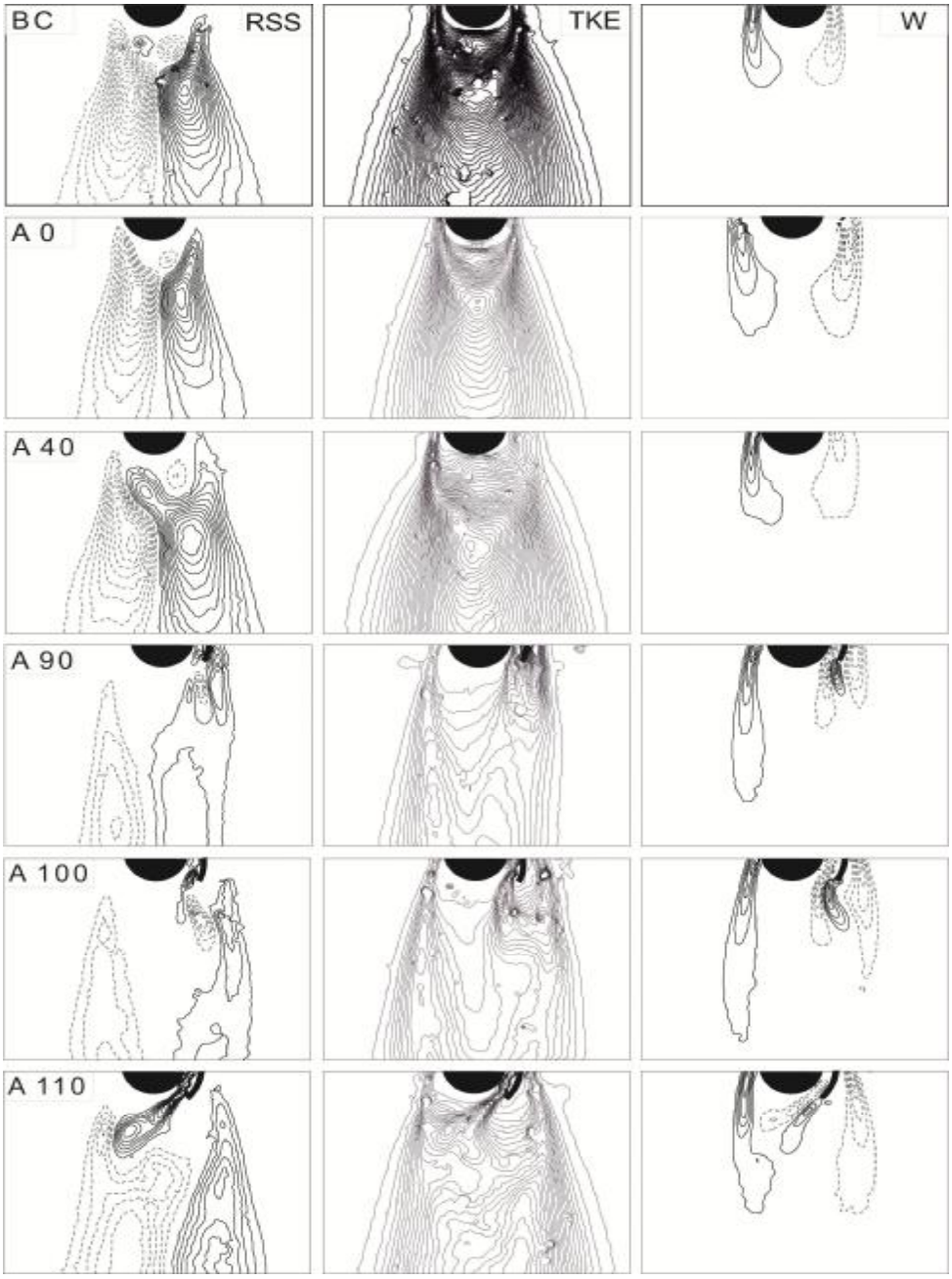


Figure 4.25. The spatial distribution of time-averaged Reynolds shear stress $\langle u'v' \rangle$,turbulent kinetic energy$\langle TKE \rangle$ and vorticity contours,$\langle \omega \rangle$ for gap ratio of 0.1 and bare cylinder case

The width of the shear layer of the system is lower than bare cylinder case for case $\alpha=0^o$ in figure 4.26. The vorticity contours of the system are not elongated because of the upstream detached plate. This trend is observed in the L/D of 1 for gap ratio of 0.3. The vorticity contours generated by the detached plate in Regime I for case $\alpha=0^o$ is impinged on the front of the cylinder so that the vorticity contours do not elongated. In the lower plate angle, we can say that the cases between $10^o \leq \alpha \leq 30^o$ is the best cases for the controlling and suppressing of the vortex shedding in all gap ratios expect gap ratio of 0.1. This situation is similar in the L/D of 1 and 0.5. The case $\alpha=20^o$ and case $\alpha=30^o$ is example of this trend for the L/D of 0.8.

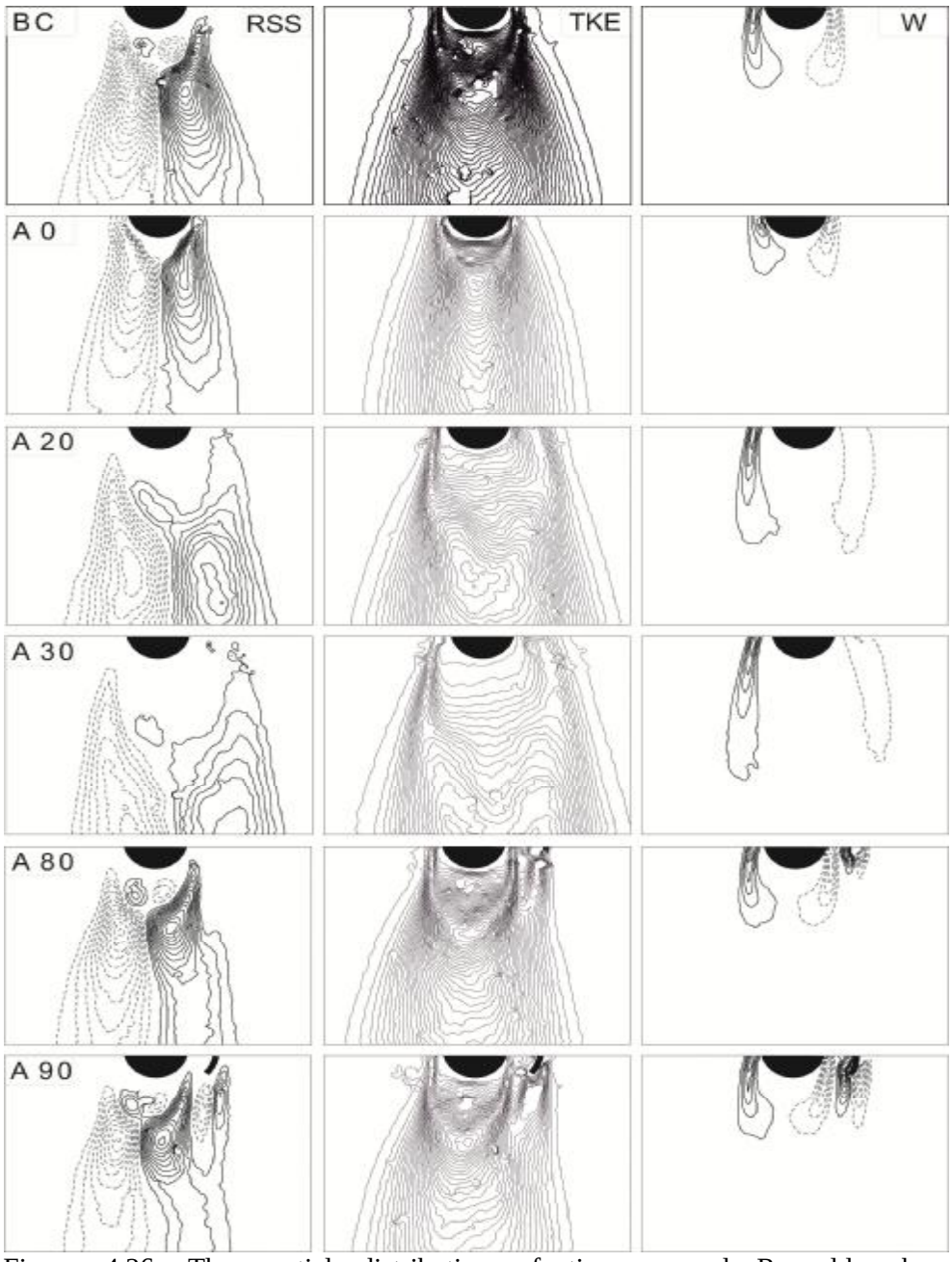


Figure 4.26. The spatial distribution of time-averaged Reynolds shear stress $\langle u'v' \rangle$, turbulent kinetic energy $\langle TKE \rangle$ and vorticity contours, $\langle \omega \rangle$ for gap ratio of 0.3 and bare cylinder case (continue)

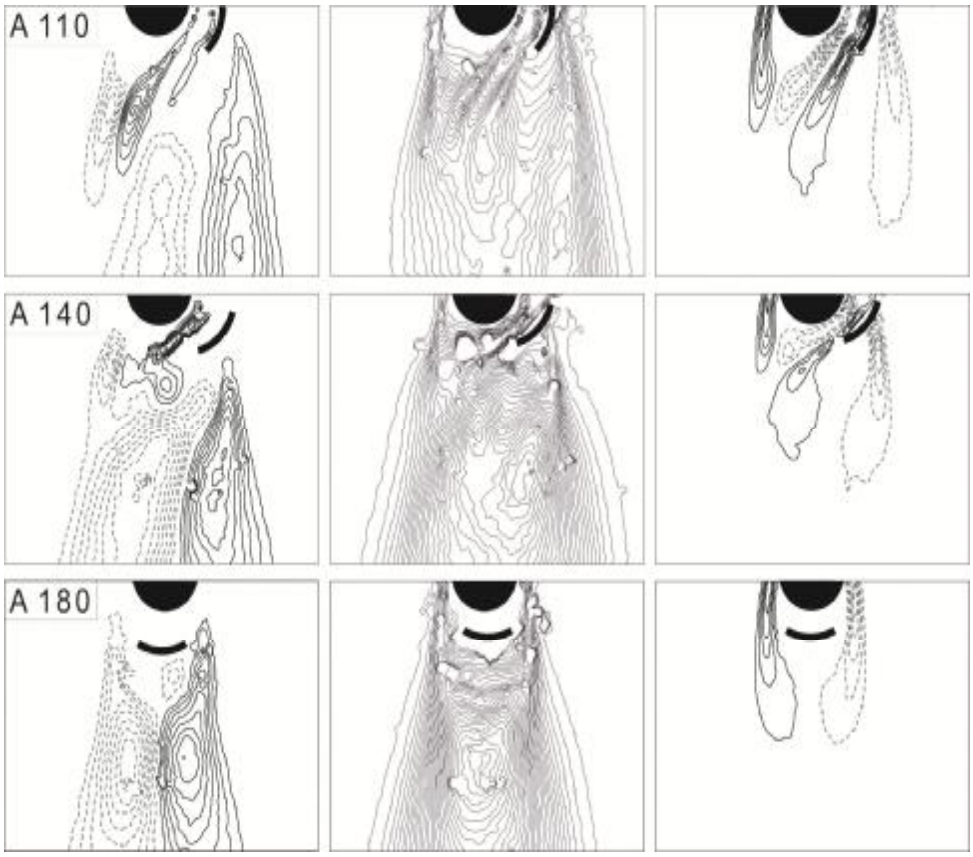


Figure 4.26. The spatial distribution of time-averaged Reynolds shear stress $<u'v'>$,turbulent kinetic energy$<TKE>$ and vorticity contours,$<\omega>$ for gap ratio of 0.3 and bare cylinder case

The flow characteristic trend of gap ratio of 0.3 is valid for the gap ratio of 0.5 in the L/D of 0.8. The secondary shear layer and positive shear layer of the cylinder act single shear layer in case $\alpha=20^{o}$ and case $\alpha=30^{o}$ in figure 4.27. The center of shear layer of system elongates in far wake region. The interaction between the detached plate and the cylinder is less according to the gap ratio of 0.1 and 0.3. It is observed that the secondary vorticity contours is bigger than primary vorticity contours in wake region for Regime II. Although the intensity of primary shear layer of the cylinder is getting loser in Regime II, the secondary shear layer is getting bigger and elongates in far wake region.

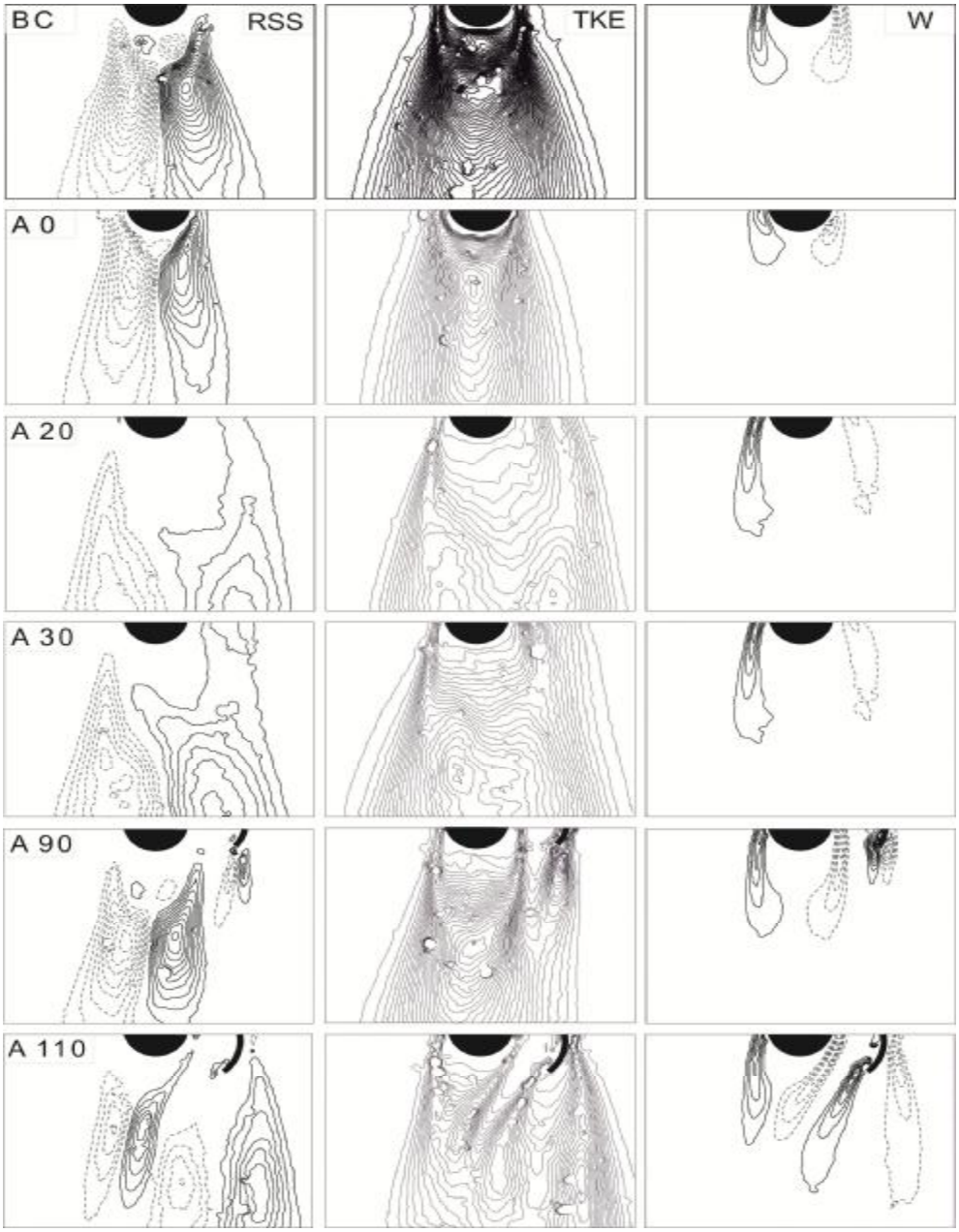


Figure 4.27. The spatial distribution of time-averaged Reynolds shear stress $\langle u'v' \rangle$,turbulent kinetic energy$\langle TKE \rangle$ and vorticity contours,$\langle \omega \rangle$ for gap ratio of 0.5 and bare cylinder case (continue)

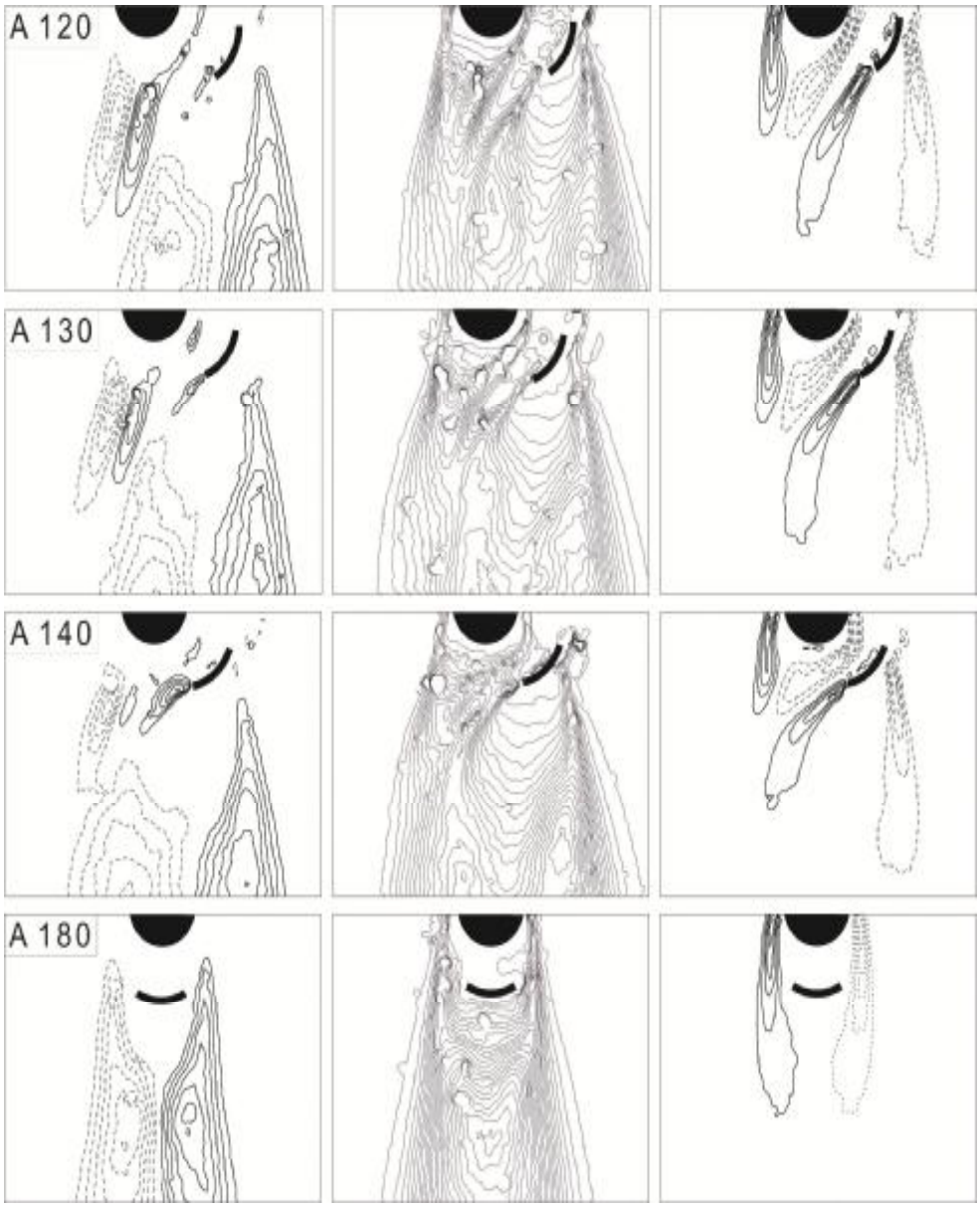


Figure 4.27. The spatial distribution of time-averaged Reynolds shear stress $<u'v'>$,turbulent kinetic energy$<TKE>$ and vorticity contours,$<\omega>$ for gap ratio of 0.1

The flow characteristics trend of G/D of 0.5 is shown for the G/D of 0.7. Case α=10^o and case α=20^o are example of the controlling and suppressing of vortex shedding in figure 4.28. The positive vorticity contours of the cylinder are bigger than the negative vorticity contours of the cylinder. With increasing gap ratio, the interaction of detached plate and the cylinder get weaker for the gap ratio of 0.1 and 0.3. The width of secondary shear layers is bigger than that of primary shear layers in Regime II. With increasing the plate angle in Regime I, the vorticity contour generated by the plate effect on the vorticity contour of the cylinder. The negative of primary and secondary shear layers move together for case α=150^o. The reattachment of the shear layer and vorticity contours is occurred for case α=180^o.

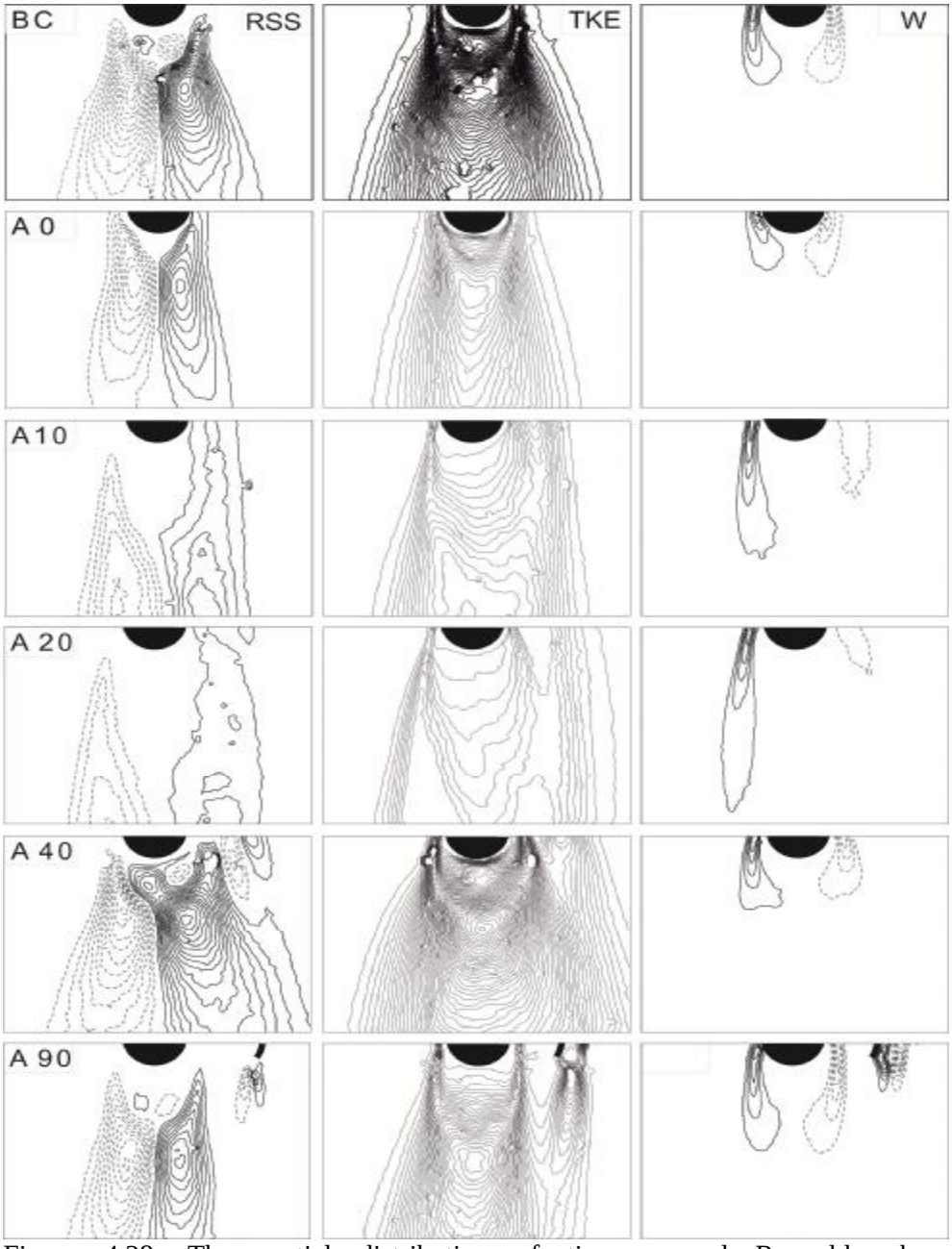


Figure 4.28. The spatial distribution of time-averaged Reynolds shear stress $\langle u'v' \rangle$,turbulent kinetic energy$\langle TKE \rangle$ and vorticity contours,$\langle \omega \rangle$ for gap ratio of 0.7 and bare cylinder case (continue)

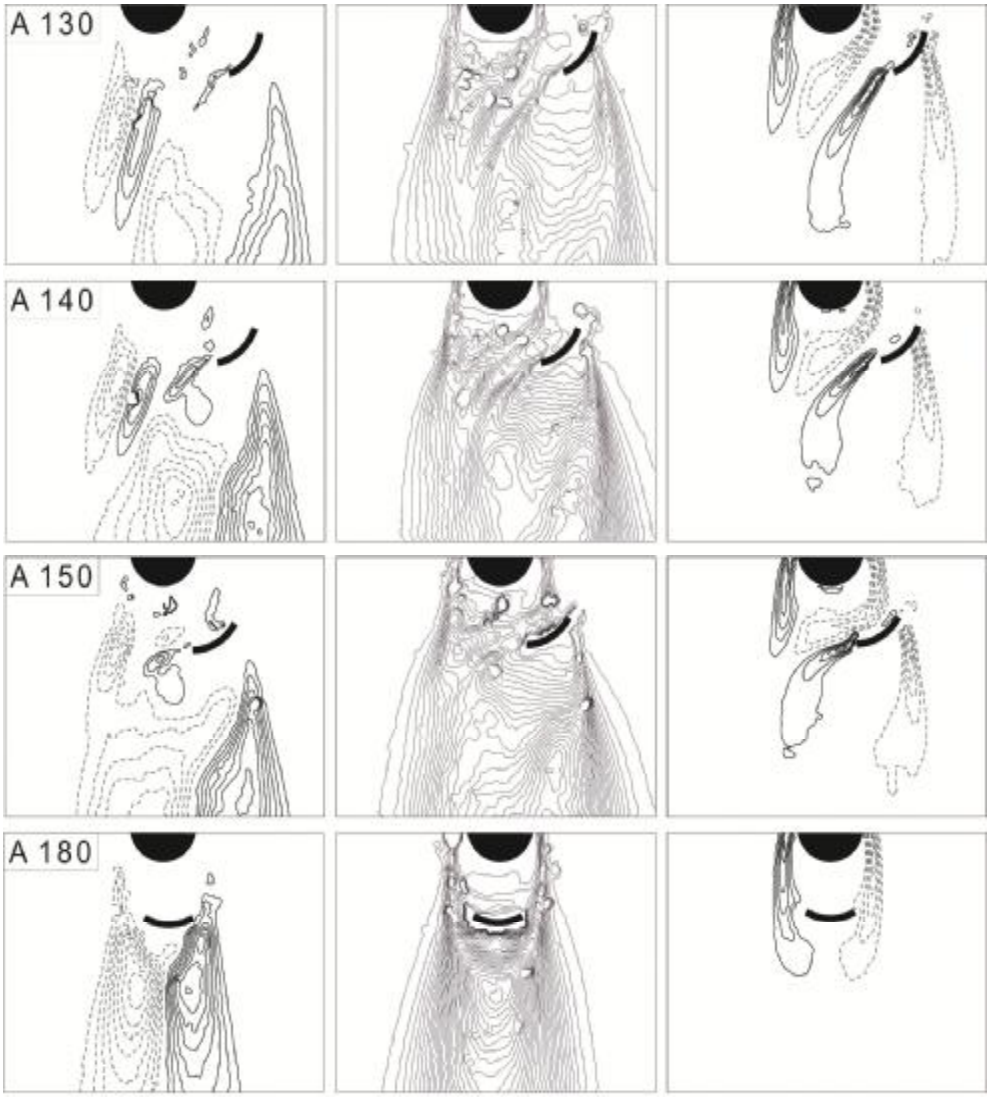


Figure 4.28. The spatial distribution of time-averaged Reynolds shear stress $<u'v'>$,turbulent kinetic energy$<TKE>$ and vorticity contours,$<\omega>$ for gap ratio of 0.7

Due to detached plate location in the L/D of 0.8, for case $\alpha=0^o$, the vorticity contour of the generated by detached plate is impinged on the cylinder so that the vorticity contours of the cylinder elongate in wake region. The positive vorticity contours of the cylinder is getting bigger in case $\alpha=10^o$ and case $\alpha=20^o$ in figure 4.29. Although the center of the shear layer is in far weak region at case $\alpha=30^o$, the positive vorticity contours of the cylinder is not bigger. As the gap distance between the detached plate and the cylinder is increased, it can be expected that the interaction of the plate and the cylinder decreases. With increasing the incoming flow from gap, the primary shear layers move in wake and the center of secondary shear layer elongates towards wake region in case $\alpha=140^o$ and case $\alpha=150^o$. The reattachment of primary vorticity contours is observed in case $\alpha=180^o$ in figure 4.29.

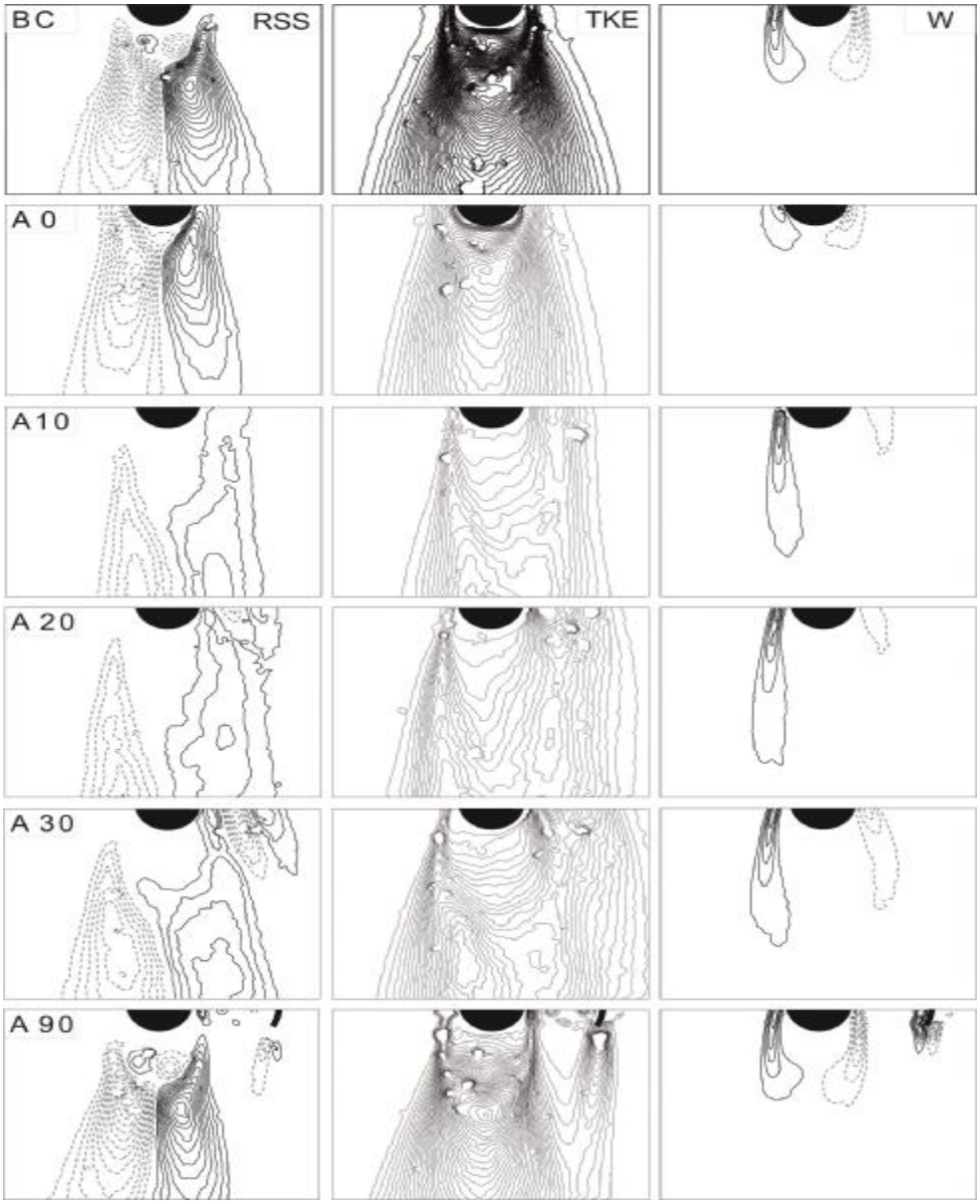


Figure 4.29. The spatial distribution of time-averaged Reynolds shear stress $<u'v'>$,turbulent kinetic energy$<TKE>$ and vorticity contours,$<\omega>$ for gap ratio of 0.9 and bare cylinder case (continue)

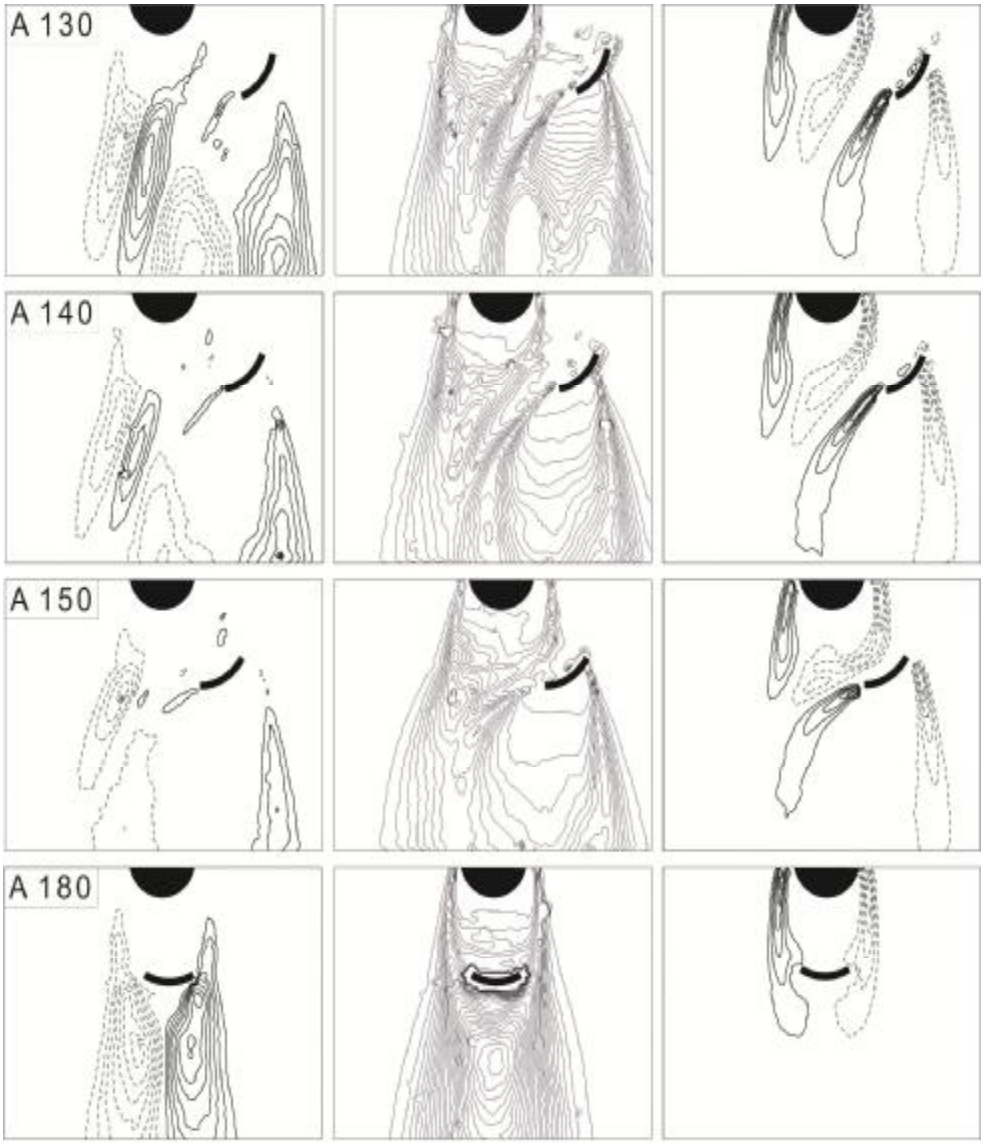
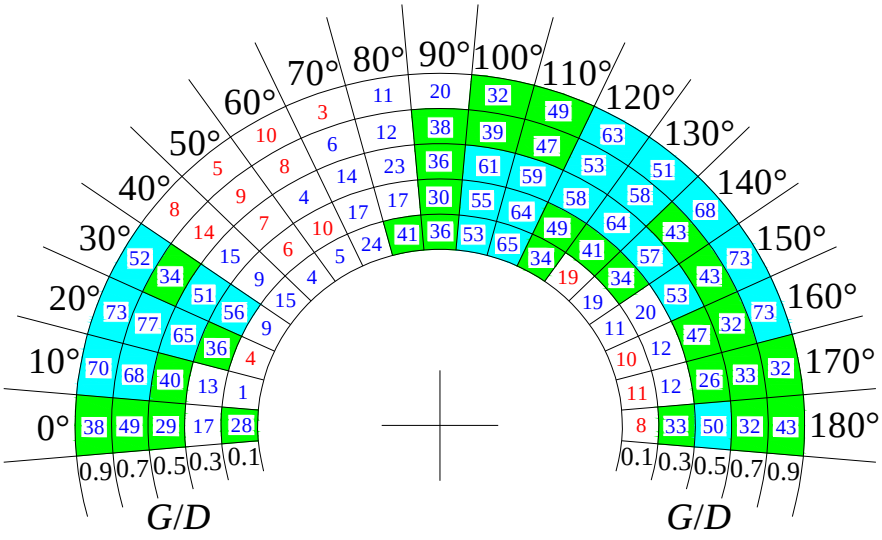


Figure 4.29. The spatial distribution of time-averaged Reynolds shear stress $\langle u'v' \rangle$,turbulent kinetic energy$\langle TKE \rangle$ and vorticity contours,$\langle \omega \rangle$ for gap ratio of 0.9

4.10. Comparison of Flow Control of Single Plate Arrangement for L/D= 0.8 Case

The experiments of single arc shaped detached plate arrangement are shown in figure 4.30. For the gap ratio of *G*/*D* of 0.1, the maximum decreasing in TKE_{max} is shown in case 110^o at larger angle plate arrangement. The maximum decreasing in TKE_{max} is occurred in case 120^o. The cases from 10^o to case 30^o are the best example to controlling of vortex shedding expect gap ratio of *G*/*D* of 0.3 and 0.1. For larger angle plate arrangement, case 120^o, 130^o and 140^o is satisfied to control of vortex shedding and also it can be said that the cases from 100^o to 180^o are satisfied to control of vortex shedding for larger gap ratios. Generally, to control or suppressing of vortex shedding the single detached plate can be used in downstream detached plate arrangement in the *L*/*D* of 0.8.



Single curved plate

Figure 4.30. All results of experiment at single arc shaped plate arrangement in the detached plate length of 0.8 in terms of TKE_{max}

4.11. The Effect of Arc Shaped Dual Detached Plate On The Flow Control

The secondary and primary shear layers of the system interact with each other in case α=90^o. The width of the shear layers of the system is lower than the other case in the gap ratio of 0.1. The primary and secondary vorticity contours interact with each other and the negative vorticity contours of the plate elongate in wake until case α=120^o in figure 4.31. Due to gap ratio, the secondary vorticity contours generated by the far trailing edge of the plate effect on the primary vorticity contours of the cylinder. Especially for Regime II, the flow characteristics are similar for each case in the L/D of 0.8.

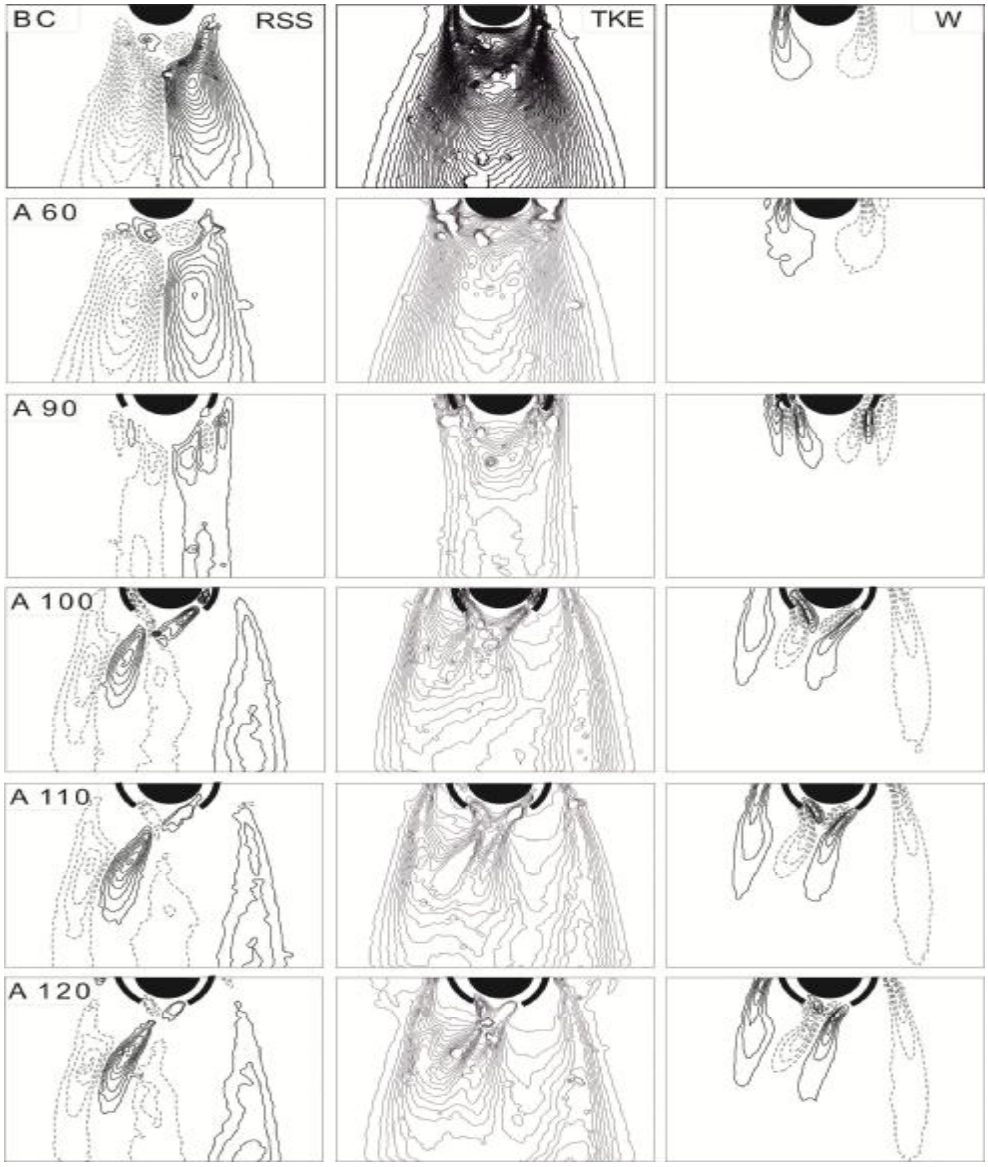


Figure 4.31. The spatial distribution of time-ave.Reynolds shear stress $<u'v'>$, turbulent kinetic energy$<TKE>$ and vorticity contours,$<\omega>$ *for* gap ratio of 0.1 and bare cylinder case

With increasing the gap ratio, for lower plate angle in Regime I, the larger shear layers of the system is observed in case α=40^o. Tough the vorticity contours of the cylinder do not elongate, the vorticity contours of the plate elongate in wake region for case α=40^o in figure 4.32. With case α=80^o, the secondary vorticity contours are appeared and with increasing the plate angle in Regime II. And also the interaction of the shear layers and vorticity contours is observed, clearly.

The trend of *G*/*D* of 0.3 is similar for the *G*/*D* of 0.5 in the *L*/*D* of 0.8. The same flow characteristics are almost observed in all cases for the gap ratio of 0.5. Generally the arc shaped detached plates are affective in the *G*/*D* of 0.1 to 0.5. With increasing plate angle and gap distance, the interaction between the detached plate and the cylinder is getting decrease. The downstream detached arc shaped plate in case α=140^o is obstructed in figure 4.33 for the beginning of the shear layer in wake region.

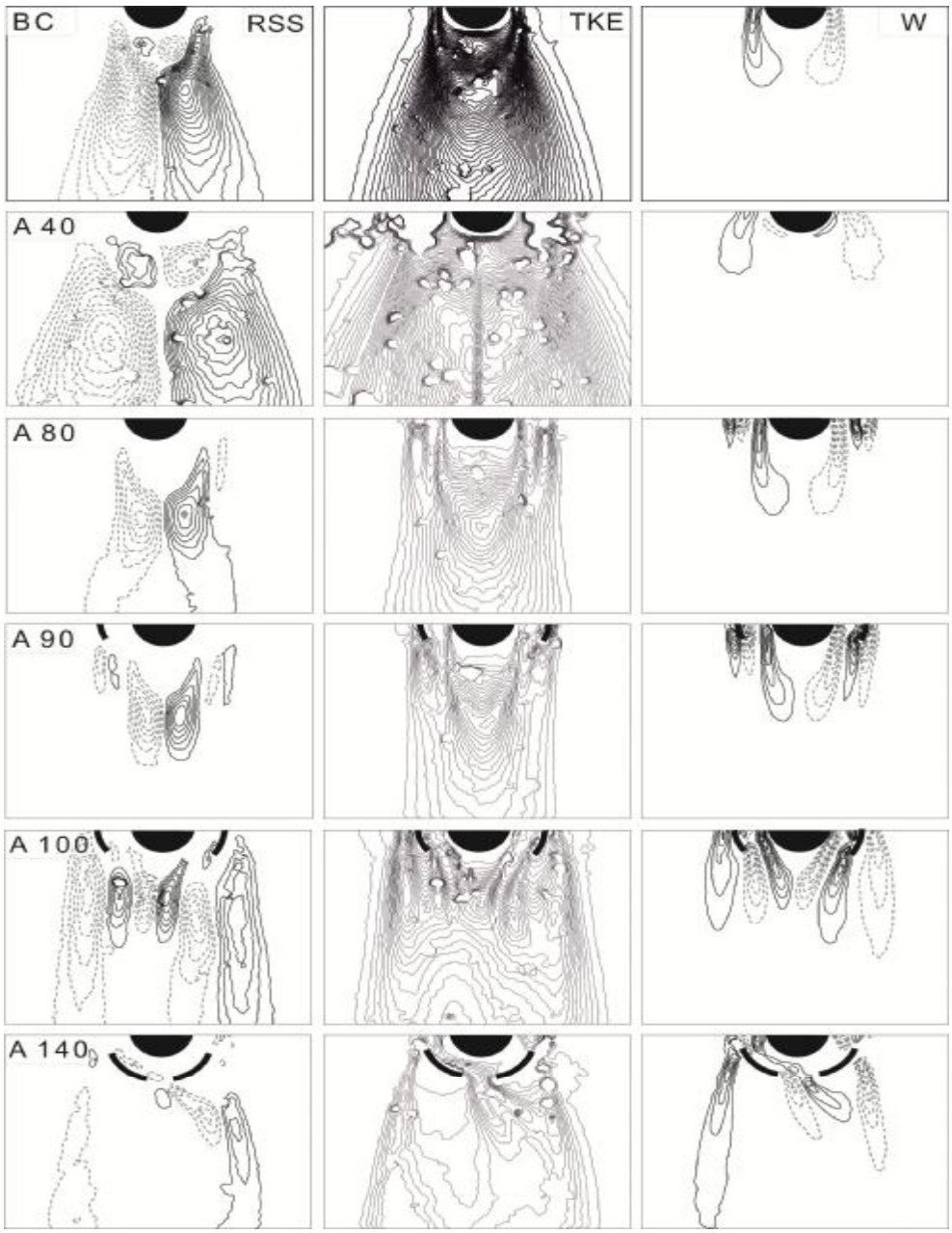


Figure 4.32. The spatial distribution of time-ave.Reynolds shear stress $\langle u'v' \rangle$, turbulent kinetic energy $\langle TKE \rangle$ and vorticity contours, $\langle \omega \rangle$ *for* gap ratio of 0.3 and bare cylinder case

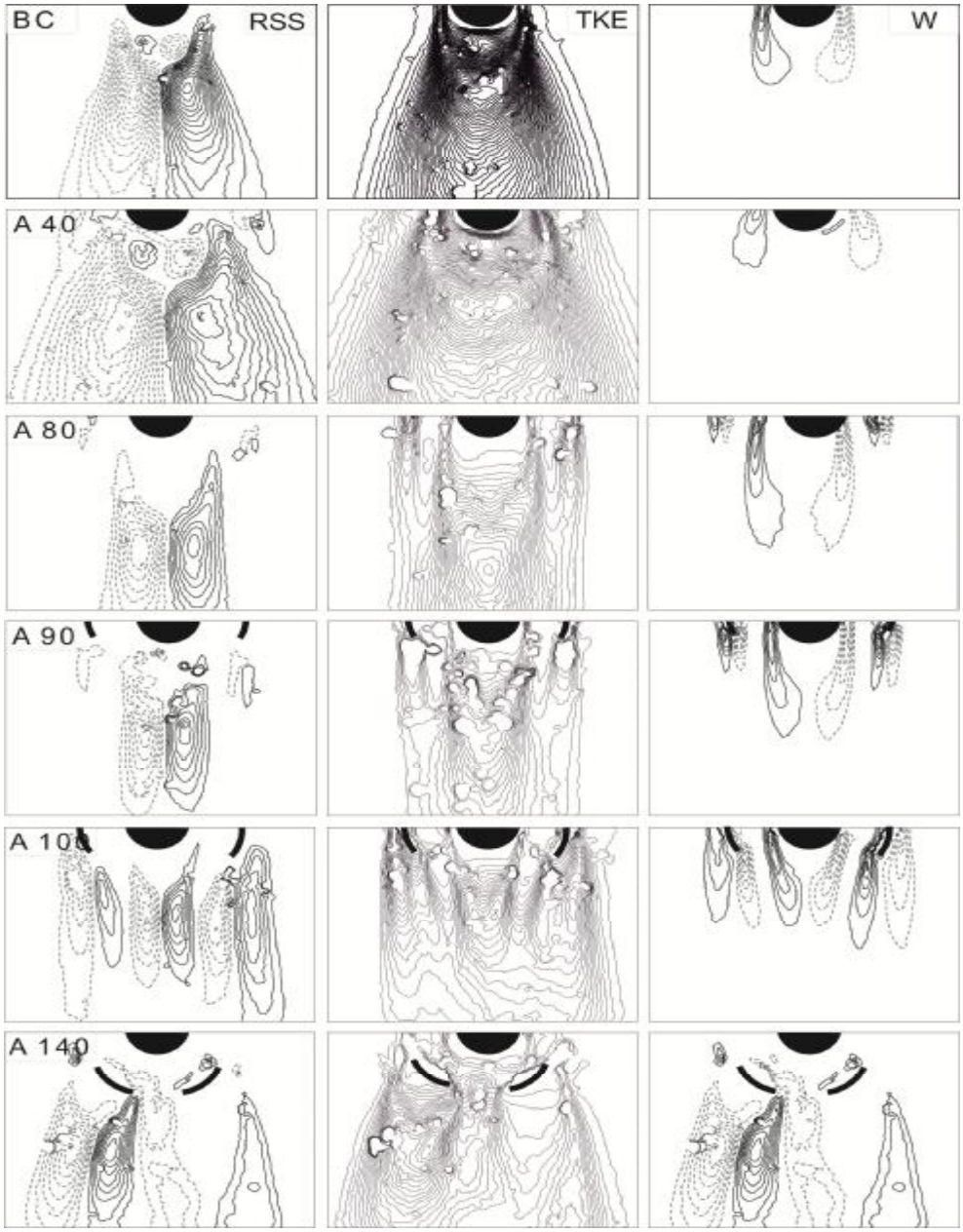


Figure 4.33. The spatial distribution of time-average Reynolds shear stress $\langle u'v' \rangle$, turbulent kinetic energy $\langle TKE \rangle$ and vorticity contours, $\langle \omega \rangle$ *for* gap ratio of 0.5 and bare cylinder case

The center of primary shear layer elongates in far wake region for case α=30^o. But the width of *TKE* is larger than the other cases. The secondary vorticity contours is observed in Regime II. The arc shaped dual detached plates are obstacle for the beginning of the shear layer in near wake region for case α=150^o and α=160^o in figure 4.34.

The flow characteristics of case α=30^o in the *G*/*D* of 0.9 is similar in the *G*/*D* of 0.7. The secondary vorticity contours is observed in Regime II. The arc shaped detached plate is obstacle for the beginning of the shear layer in near wake region for case α=150^o and α=160^o.in figure 4.35.

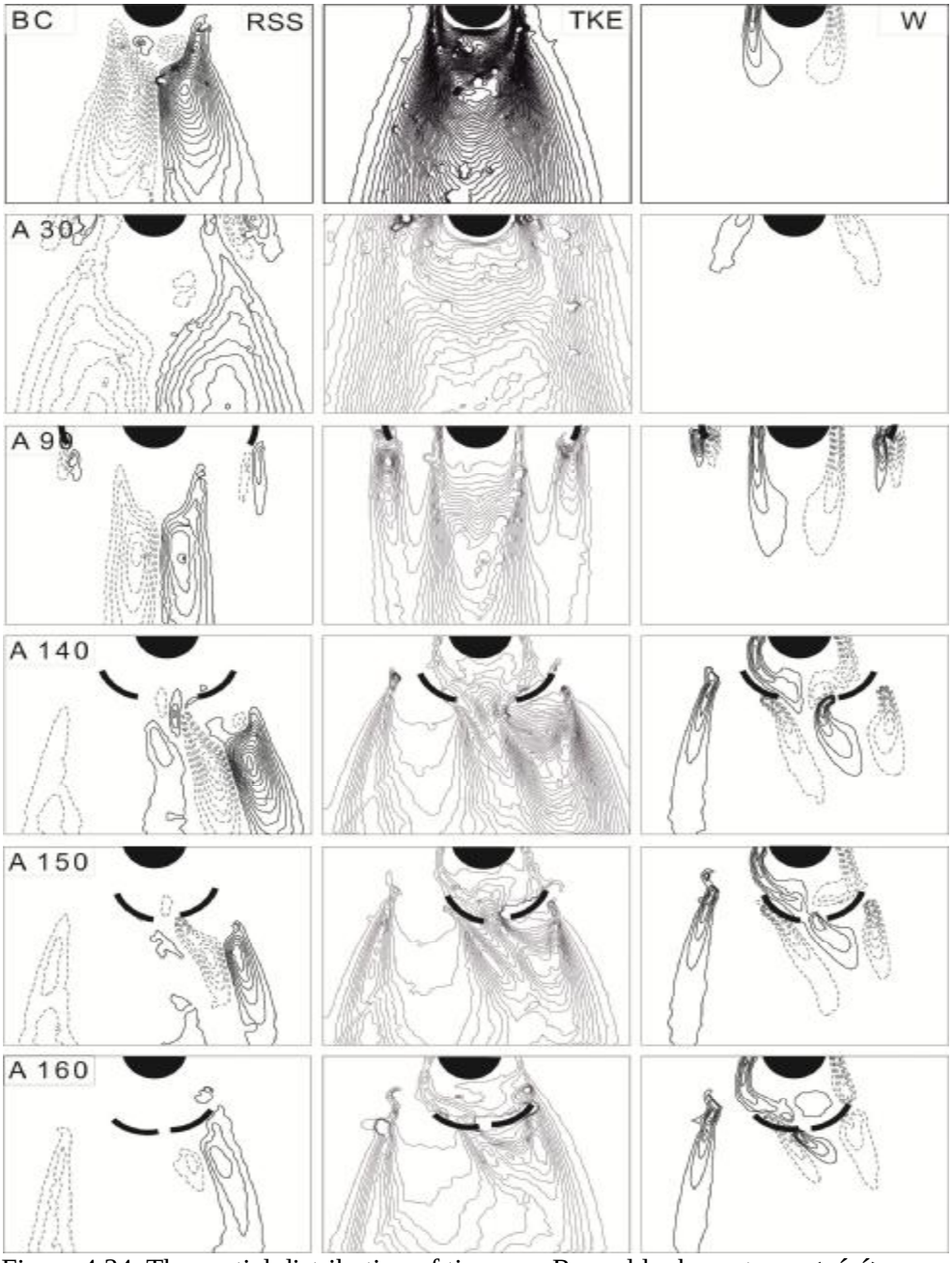


Figure 4.34. The spatial distribution of time-ave.Reynolds shear stress $\langle u'v' \rangle$, turbulent kinetic energy$\langle TKE \rangle$ and vorticity contours,$\langle \omega \rangle$ *for* gap ratio of 0.7 and bare cylinder case

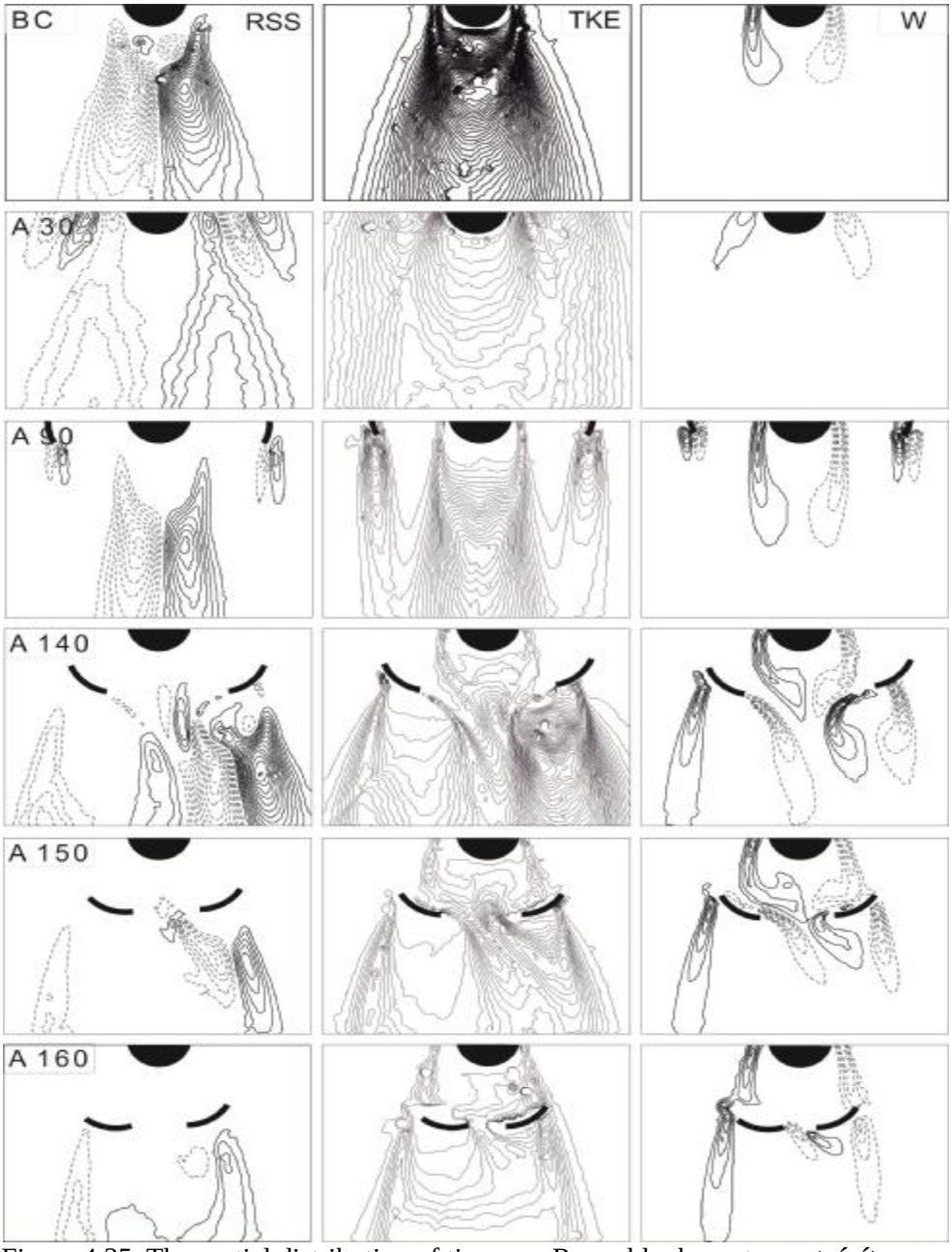
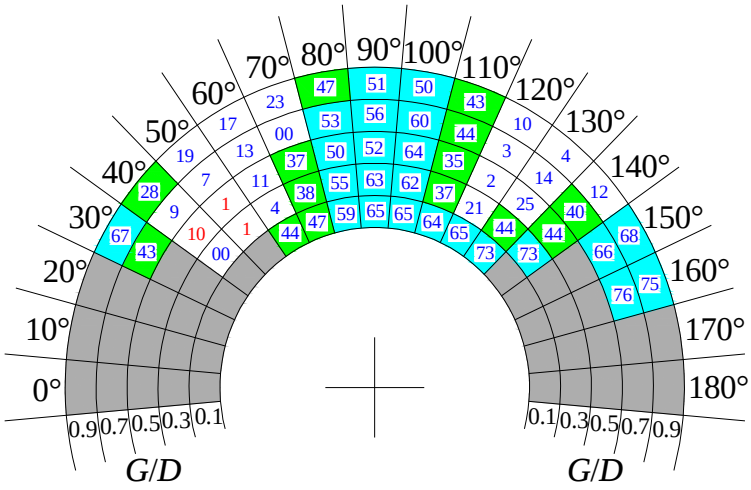


Figure 4.35. The spatial distribution of time-ave.Reynolds shear stress $\langle u'v' \rangle$, turbulent kinetic energy$\langle TKE \rangle$ and vorticity contours,$\langle \omega \rangle$ *for* gap ratio of 0.9 and bare cylinder case

4.12. Comparison of Flow Control of Dual Plate Arrangement for L/D= 0.8 Case

The experiments of dual detached plate arrangement are shown in figure 4.36. For the gap ratio of *G*/*D* of 0.1, the maximum decreasing in TKE_{max} is shown in case 130^o but cases from 80^o to 100^o is the best case to control of vortex shedding all gap ratios also maximum decreasing in TKE_{max} is occurred in these cases. These cases are the best example for control of vortex shedding all gap ratios. For larger angle plate arrangement, case 150^o and case 160 ^{o} are satisfied to control of vortex shedding in the gap ratio *G*/*D* of 0.9 and 0.7. Generally, to control or suppressing of vortex shedding the dual detached plate can be used in upstream detached plate arrangement.



Double curved plates

Figure 4.36. All results of experiment at dual plate arrangement in the detached plate length of 0.8 in terms of TKE_{max}

4.13. Spectral Analysis for Effective Control Cases

In this section, Fast Fourier Transform (FFT) technique was used to evaluate the frequency of vortex shedding for various points. Determination of the vortex shedding frequency gives us the frequency of vibration on the body, thus the intensity of vortex-induced vibrations (VIV). Therefore it is necessary to analyze and find out the effect of detached plates on reducing or eliminating the vortex shedding frequency downstream of the cylinder.

In selected effective cases, the frequency is not observed. For these selected cases, the frequency was investigated to indicate vortex shedding. A clear and distinct peak is an indication of the existence of a dominant vortex structure owing to vortex shedding and consequent vibrations of the vortices. Therefore it is essential to reduce or eliminate a dominant frequency evaluated downstream of the cylinder using flow control techniques.

4.13.1. FFT Analysis for Bare Cylinder

The Strouhal number of a circular cylinder as a function of Reynolds number is shown in Figure 4.37 where the Strouhal number is approximately 0.2 for a wide range of Reynolds number, i.e. $250<Re_D<2\times10^5$.

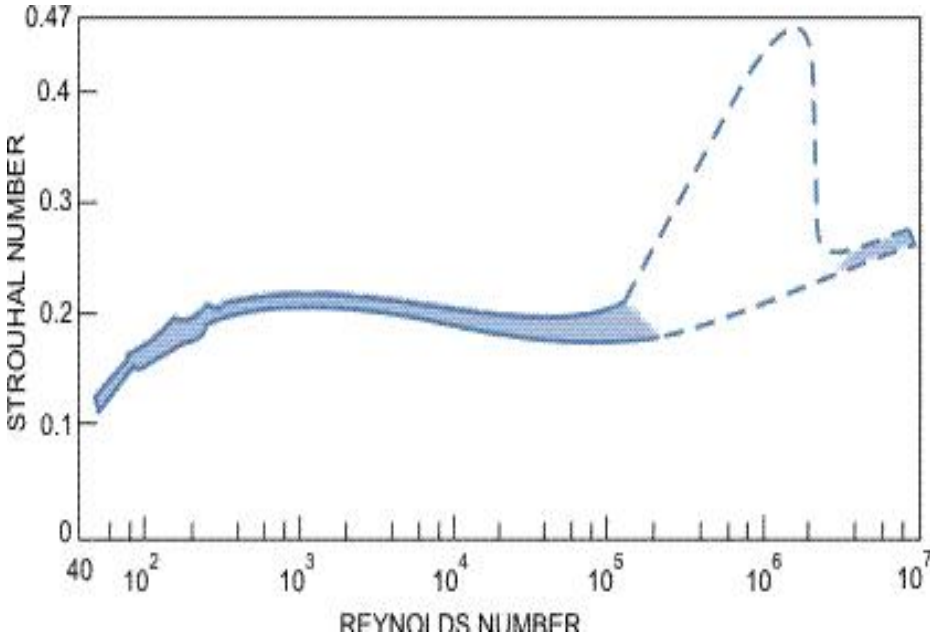


Figure 4.37. The variation of Strouhal number with Reynolds number for a circular cylinder (Blevins, 1990)

Figure 4.38 presents the bare cylinder case having a dominant frequency of f_K =0.53 corresponding to a Strouhal number ($St=f_K\,d/U_\infty$ where d is the diameter of cylinder, U_∞ is the free-stream velocity in the streamwise direction) of St=0.19 which is in agreement with the literature given by Figure 4.37. A clear and distinct peak is an indication of the existence of a dominant vortex structure owing to vortex shedding and consequent vibrations of the vortices. Therefore it is essential to reduce or eliminate a dominant frequency evaluated downstream of the cylinder using flow control techniques.

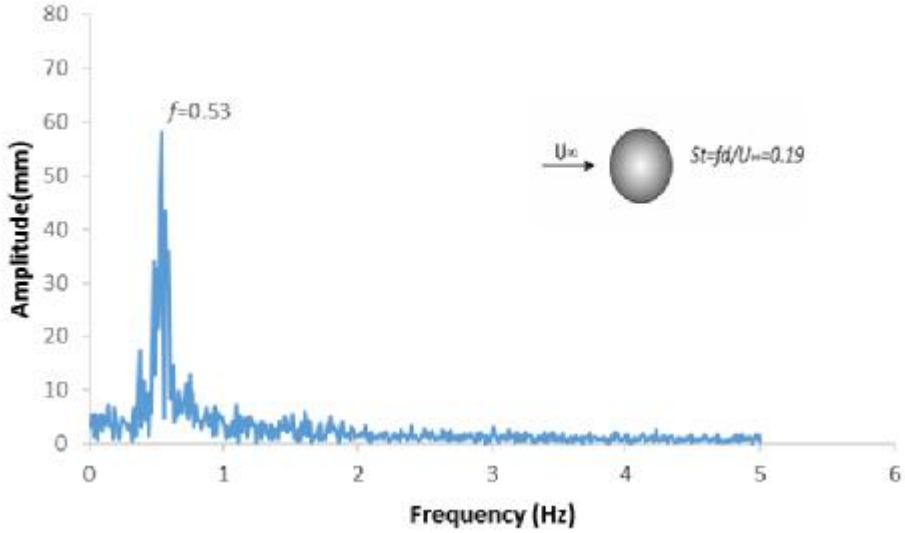


Figure 4.38. Spectral analysis of streamwise velocity fluctuations for bare cylinder

4.13.2. FFT Analysis for Normalized Plate Length (*L*/*D*) of 0.5

The results of selected effective cases at single detached plate for normalized plate (*L*/*D*) of 0.5 are shown in figure 4.39. For all gap ratios, the occurrence of a dominant frequency was searched by FFT analysis behind cylinder. As obviously seen by the figure 4.39, there is no dominant frequency evaluated for all cases. For case 110^o at gap ratio *G*/*D* of 0.1 a dominant frequency having a value of f=0.42 is evaluated. Taking into account the frequency result of natural cylinder as being f_K =0.53, a reduction of almost 20% can be achieved. The decreasing in TKE_{max} is 67% for this case. For all selected cases, there is decreasing in TKE_{max} values. The results of FFT for all gap ratios show that using a single downstream detached plate is satisfied to control of vortex because no frequency is observed behind cylinder. The results of selected effective cases at dual detached plate for normalized plate (*L*/*D*) of 0.5 are shown in figure 4.40. For case 150^o at gap ratio *G*/*D* of 0.5 a dominant frequency having a value of f_K =0.32 is evaluated. Taking into account the frequency result of natural cylinder as being f_K =0.53, a reduction of almost 40% can be achieved. The decreasing in TKE_{max} is 70% for this

case. For all selected cases, there is decreasing in TKE_{max} values. The results of FFT for all gap ratios show that using a single downstream detached plate is satisfied to control of vortex because no frequency is observed behind cylinder.

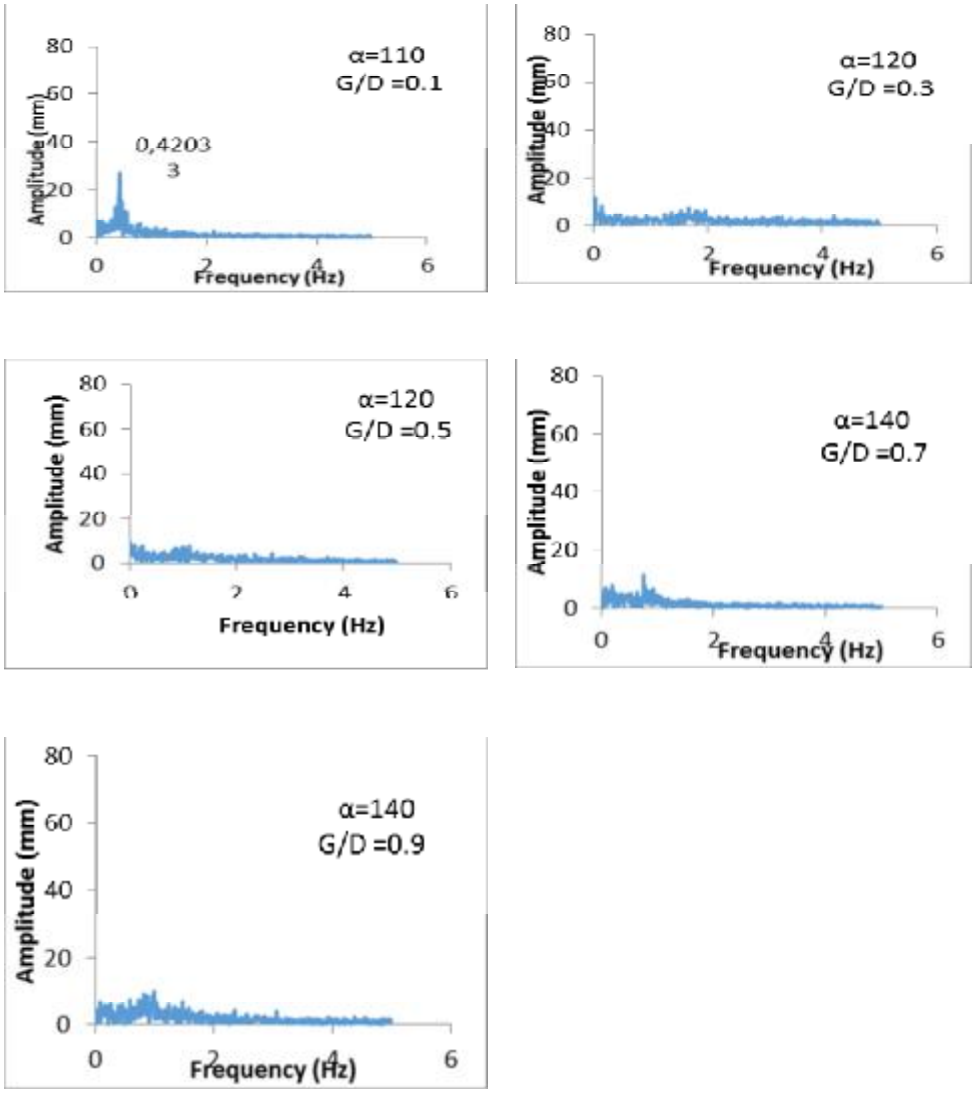


Figure 4.39. Spectral analysis of streamwise velocity fluctuations for effective single detached plate arrangement cases for L/D=0.5

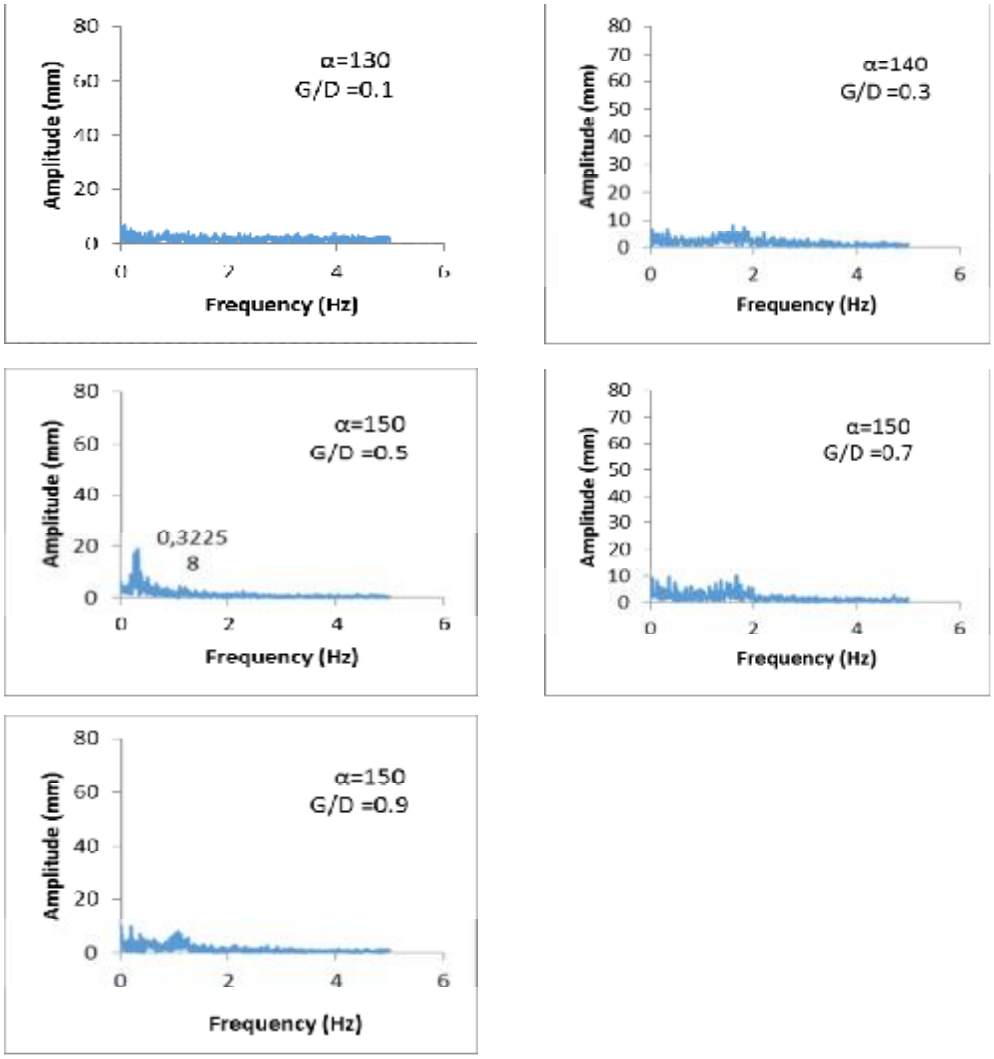


Figure 4.40. Spectral analysis of streamwise velocity fluctuations for dual detached plate arrangement effective cases for *L*/*D*=0.5

4.13.3. FFT Analysis for Normalized Plate Length (*L*/*D*) of 1

The results of selected effective cases at single detached plate for normalized plate (*L*/*D*) of 1 are shown in figure 4.41. For all gap ratios, the occurrence of a dominant frequency was searched by FFT analysis behind cylinder. As obviously seen by the figure, there is no dominant frequency evaluated for all cases. For case 110 at gap ratio *G*/*D* of 0.1 a dominant frequency having a value of f_K =0.32 is evaluated. Taking into account the frequency result of natural cylinder as being f_K =0.53, a reduction of almost 40% can be achieved. The decreasing in TKE_{max} is 64% for this case. For all selected cases, there is decreasing in TKE_{max} values. The results of FFT for all gap ratios show that using a single downstream detached plate is satisfied to control of vortex because no frequency is observed behind cylinder. The results of selected effective cases at dual detached plate for normalized plate (*L*/*D*) of 1 are shown in figure 4.42. The results of FFT for all gap ratios show that using a single upstream detached plate is satisfied to control of vortex because no frequency is observed behind the cylinder.

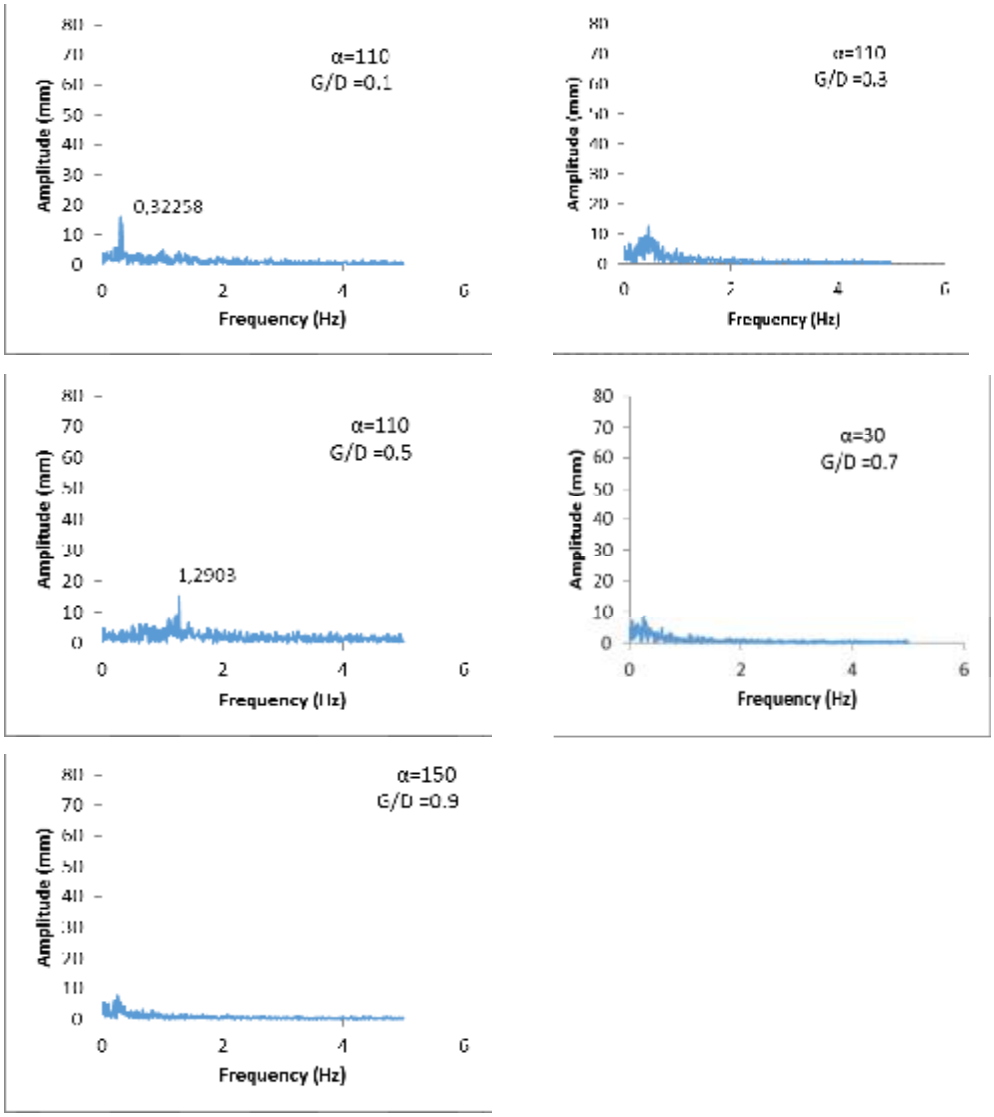


Figure 4.41. Spectral analysis of streamwise velocity fluctuations for effective single detached plate arrangement cases for L/D= 1

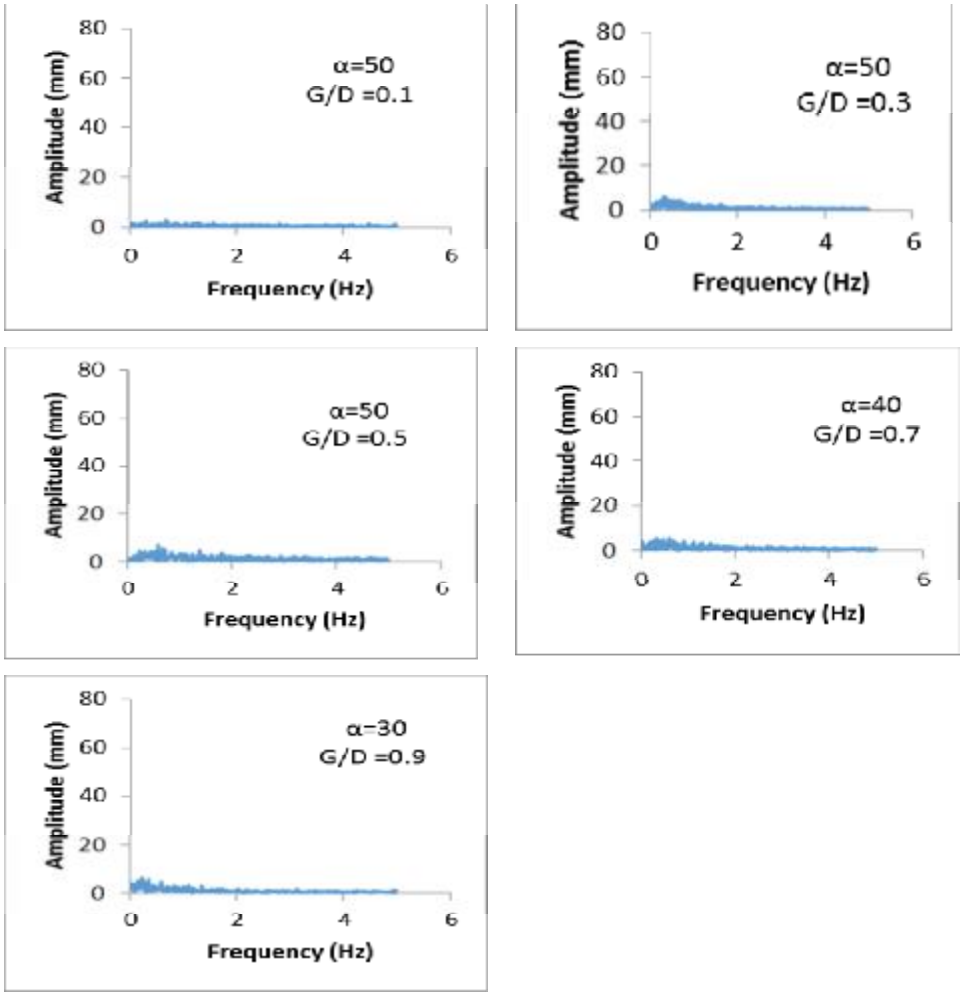


Figure 4.42. Spectral analysis of streamwise velocity fluctuations for effective dual detached plate arrangement cases for L/D =1

4.13.4. FFT Analysis for Normalized Plate Length (L/D) of 0.8

The results of selected effective cases at single detached plate for normalized plate (L/D) of 0.8 are shown in figure 4.43. For all gap ratios, the occurrence of a dominant frequency was searched by FFT analysis behind cylinder. The results of FFT for all gap ratios show that using a single upstream detached

plate is satisfied to control of vortex because no frequency is observed behind cylinder.

The results of selected effective cases at dual detached plate for normalized plate (L/D) of 0.8 are shown in figure 4.44. For case 140^o at gap ratio G/D of 0.7 a dominant frequency having a value of f_K =0.87 is evaluated. Taking into account the frequency result of natural cylinder as being f_K =0.53, an increment of almost 30% can be achieved. The decreasing in TKE_{max} is 40% for this case. For all selected cases, there is decreasing in TKE_{max} values. The results of FFT for all gap ratios show that using a single downstream detached plate is satisfied to control of vortex because no frequency is observed behind cylinder.

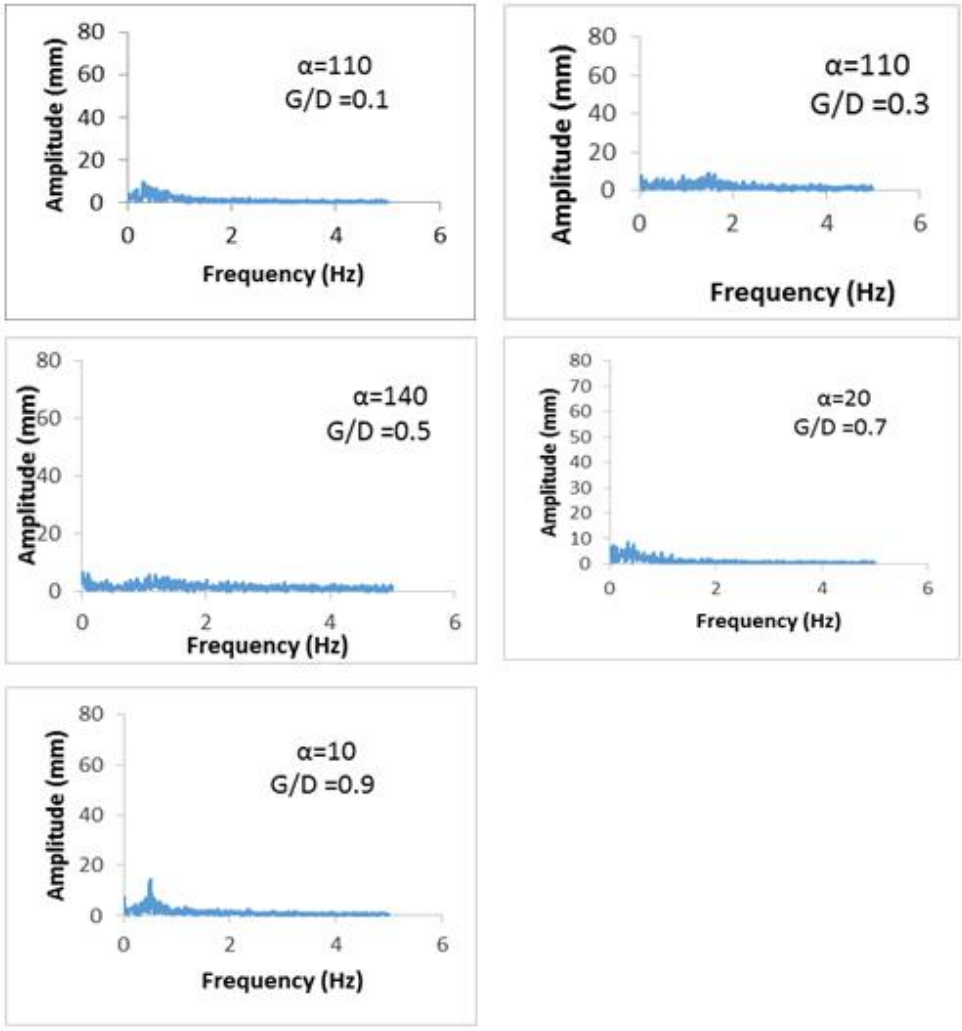


Figure 4.43. Spectral analysis of streamwise velocity fluctuations for effective single detached plate arrangement cases for *L*/*D*=0.8

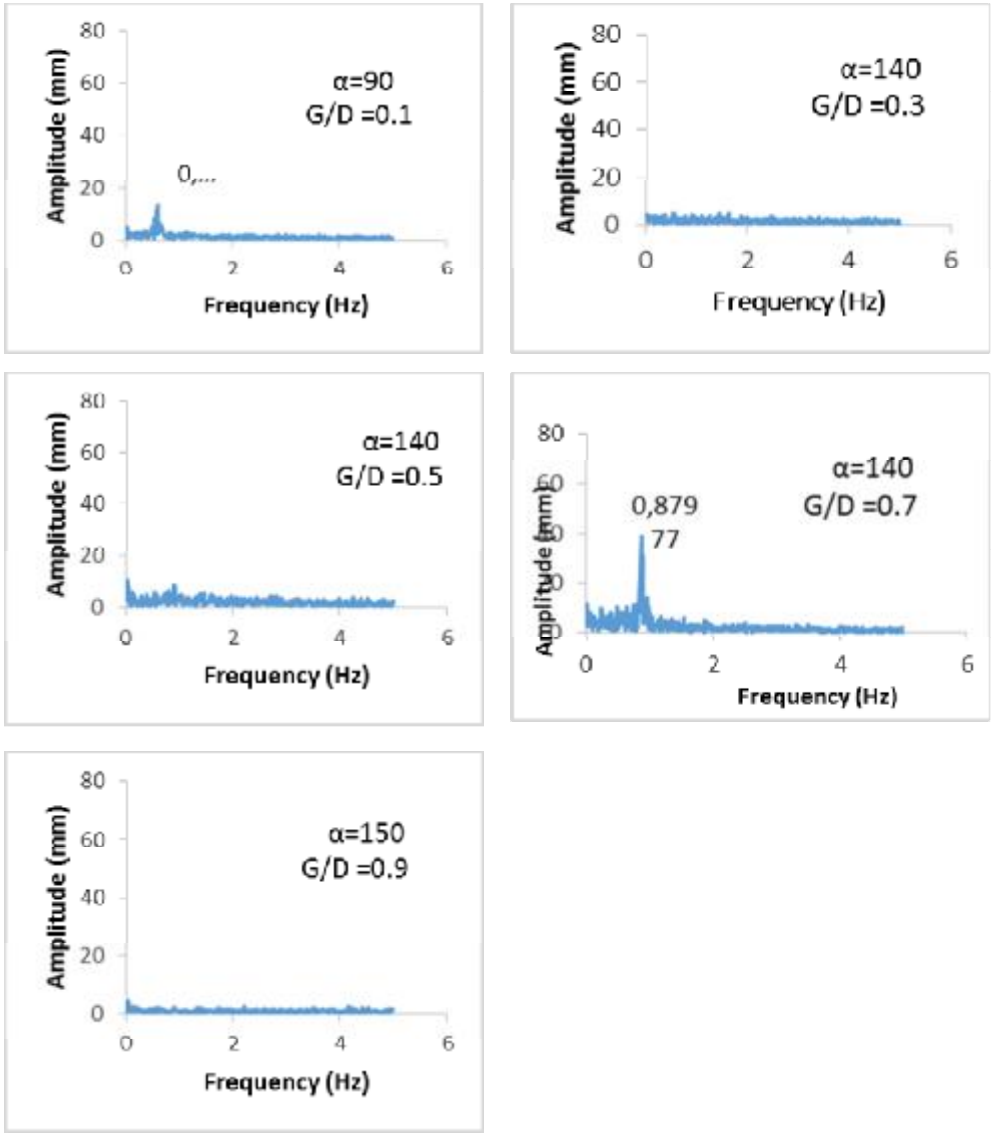


Figure 4.44. Spectral analysis of streamwise velocity fluctuations for effective dual plate arrangement cases for L/D=0.8

5. CONCLUSIONS AND RECOMMENDATIONS

Control of vortex shedding has a great importance since it causes reductions in the time-varying flow-induced forces acting on the bluff bodies. Therefore, many studies have been carried out in the past to establish a method to control the vortex shedding which can be observed easily when fluid flows over a bluff body. The aim of this study is to inspect in detail the variations in the flow structure for a circular cylinder with different plate angles, and to identify the critical gap ratio (*G*/*D*). Experiments were performed for the gap ratios of *G/D*=0.1, 0.3, 0.5, 0.7, 0.9, and the plate angles of α=0^o to α=180^o with an increment of 10^o. Another parameter of the study was the plate length to diameter ratio, *L/D* and taken as *L/D*= 0.5, 0.8 and 1.

The results showed that for the single detached plate arrangement of *L/*D=0.5 with downstream plate arrangements of α=100^o to 150^o are found to be effective on the vortex shedding control. The spectral analysis for *L/D*=0.5 also in consistent with this finding. The maximum reduction in TKE_{max} was obtained for α=10^o. Generally, as the horizontal distance between cylinder and plate increases in the wake region, the interaction between upper and lower shear layers of the cylinder has been decreased. It can be concluded that using single downstream plate arrangement of *L/D*=0.5 is convenient for controlling the vortex shedding. For the dual detached plate arrangements in the plate length of *L/*D=0.5, vortex shedding control was achieved in the interval of α=80^o to 100^o. Increasing with gap ratio in *L/*D=0.5 at dual plate arrangement, it was evaluated that the value of TKE_{max} decreased for the interval α=100^o to 140^o. Distinct observation was obtained for the cases of α=30^o and α=150^o. For the case of upstream dual plate arrangement, flow through the gap was not enough to generate vortical flow structures, hence the vortex shedding was not observed for α=30^o. Similar situation was obtained for α=150^o. The flow patterns of the detached plate length of *L/D*=1 were found to be almost similar with the result of detached plate lengths of

L/D=0.5 for single plate arrangement. It was concluded that using the single detached plate of *L/D*=1 is not effective for the gap ratios of *G/D*=0.1, 0.3 and 0.5 for upstream arrangement of the detached plate. The results demonstrated that the characteristics of the wake are significantly related to the cross-sectional geometries of the detached plate. The relationship between gap ratio and the flow characteristics depends strongly on geometry of the bluff body. The reasons were attributed to differences of flow angle of the separated flow and of steadiness of the separation.

Due to the dual detached plate's obstruction for *L/D*=1, the amount of momentum transfer from the gap into the wake region was restricted. A large amount of the downstream advancing momentum significantly delayed the vortex formation at farther downstream locations, leading to a more symmetrical flow structure in the near wake of the cylinder. It was found that the use of dual detached plate has significant effects on downstream flow for larger plate angles since it directly interacts with the shear layer of the cylinder. Due to upstream dual plate arrangement, the lower plate angle was found to be effective on suppressing the vortex shedding. This situation was assisted by decreasing TKE_{max} for G/D=0.1. It was concluded that it is possible to suppress the vortex shedding in the wake region for *L*/*D*=1 dual detached plates placed upstream. Generally, flow characteristic of the arc shaped single plate arrangement were found to be similar with the plate length of *L/D*=0.5 for single plate arrangement. The angles of $\alpha=40^{o}$ to $\alpha=80^{o}$ for L/D=1 were found to be effective on vortex shedding control which were also valid for *L/D*=0.5, 0.8. The experiments for single and dual plate arrangements of *L/D*=0.5 and 0.8 showed similar results considering the turbulent statistics. Finally, the FFT analysis showed that the vortex shedding frequency was eliminated for the mentioned effective cases and intervals implied above.

According to these findings, for further works the lower plate lengths may be suggested to investigate in order to analyze the elimination of vortex shedding

by using a smaller control element. Furthermore, the drag force measurements should also be studied for the current flow control method.

REFERENCES

Akıllı, H., Akar, A., And Karakaus, C., 2004, "Flow Characteristics Of Circular Cylinders Arranged Side-By-Side İn Shallow Water," Flow Meas. Instrum., 15, Pp. 187–197.

Akıllı, H., And Rockwell, D., 2002. Vortex Formation From A Cylinder İn Shallow Water. Physics Of Fluids, 14 (9): 2957-2967.

Akıllı, H., Karakus, C., Akar, A., Sahın, B. And Tumen, N. F., "Control Of Vortex Shedding Of Circular Cylinder İn Shallow Water Flow Using An Attached Splitter Plate", J. Fluids Eng. 130, 041401, 2008.

Akıllı, H., Sahın, B., And Tumen, N. F., 2005, "Suppression Of Vortex Shedding Of Circular Cylinder İn Shallow Water By A Splitter Plate," Flow Meas. Instrum., 16, Pp. 211–219.

Angrıllı, F., Bergamaschı, S. V., 1982. Cossalter, Investigation Of Wall İnduced Modifications To Vortex Shedding From A Circular Cylinder, J. Fluids Eng. Trans. Asme 104 518-522.

Apelt, B., West, G.S., Szewczyk, A.A., 1973. The Effects Of Wake Splitter Plates On The Flow Past A Circular Cylinder İn The Range 10^4<Re<10^5, J. Fluid Mech. 61 (1) 187–198.

Badr, H., Coutanceau, M., Dennıs, S., Menard C., 1990. Unsteady Flow Past A Rotating Circular Cylinder At Reynolds Numbers 1000 And 10000. Journal Of Fluid Mechanics, 220:459– 484.

Balachandar, R., And Tachıe, T.M., 2001. A Study Of Boundary Layer-Wake İnteraction İn Shallow Open Channel Flows Experiments İn Fluids, 30: 511-521.

Balachandar, R., Chu, V.H., And Zhang, J., 1997. Experimental Study Of Turbulent Concentration Flow Field İn The Wake Of A Bluff Body. Journal Of Fluid Engineering, 199: 263-270.

Balachandar, R., Mıttal, R. And Najjar, F. M., 1997. Properties Of The Mean Wake Recirculation Region İn Two-Dimensional Bluff Body Wakes. J. Fluid Mech. 351, 167–199.

Baz, A. And Ro, J. 1991 Active Control Of Flow-İnduced Vibrations Of A Flexible Cylinder Using Direct Velocity Feedback. Journal Of Sound And Vibration 146, 33-45.

Bearman P. W., 1967. The Effect Of Base Bleed On The Flow Behind A Two-Dimensional Model With A Blunt Trailing-Edge. Aero. Quart. 18, 207–225.

Bearman, P.W. 1984 Vortex Shedding From Oscillating Bluff Bodies. Annual Review Of Fluid Mechanics 16, 195-222.

Bearman, P.W., 1965. Investigation Of Flow Behind A Two-Dimensional Model With Blunt Trailing Edge And Fitted With Splitter Plates, J. Fluid Mech. 21 241–255.

Bearman, P.W., And Wadcock, A.J., 1973. The İnteraction Between A Pair Of Circular Cylinders Normal To A Stream. Journal Of Fluid Mechanics, 61: 499-511.

Bearman, P.W., Trueman, D.M., 1972 An İnvestigation Of The Flow Around Rectangular Cylinders, Aeronaut. Quart. Xxııı 3 229–237.

Bearman, P.W., Zdravkovıch, M.M., 1978. Flow Around A Circular Cylinder Near A Plane Boundary, J. Fluid Mech. 89 (Part 1) 33-47.

Berger, E. 1967 Suppression Of Vortex Shedding And Turbulence Behind

Bıshop, R. E. D. And Hassan, A. Y., 1964. The Lift And Drag Forces On A Circular Cylinder Oscillating İn A Flowing Fluid, Proc. R. Soc. London, Ser. A 277, 51

Blackburn, H. M. And Henderson, R. D., 1999. A Study Of Two-Dimensional Flow Past An Oscillating Cylinder,'' J. Fluid Mech. 385, 255

Bloor, M.S., 1964. The Transition To Turbulence İn The Wake Of A Circular Cylinder. Journal Of Fluid Mechanics, 19: 290-304.

Burestı, G., Lancıottı, A., 1992. Mean And Fluctuating Forces On A Circular Cylinder İn Cross-Flow Near A Plane Surface, J. Wind Eng. Ind. Aerodyn. 41 (1-3) 639-650.

Burns, Ja., Ou Y-R., 1993. Effect Of Rotation Rate On The Forces Of A Rotating Cylinder: Simulation And Control. Icase Report; 93-11.

C.-H. Kuo, L.-C. Chiou, C.-C. Chen, Wake Flow Pattern Modified By Small Control Cylinders, At Low Reynolds Number, At Low Reynolds Number, Journal Of Fluids And Structures 23 (2007) 938–956

Carmer, C.F.V., And Jırka, G.H., 2001. On Turbulence And Transport İn Shallow Wake Flows. Proceedings 29th Iahr Congress, Beijing, China.

Carmer, C.F.V., Weıtbrecht, V., And Jırka, G.H., 2001. On The Genesis And Fate Of Large Coherent Vortical Structures İn Turbulent Shallow Wake Flows. Proc. Iseh/Iahr International Symposium On Environmental Hydraulics.

Chew, Yt., Cheng, M., Luo, Sc., 1995. A Numerical Study Of Flow Past A Rotating Circular Cylinder Using A Hybrid Vortex Scheme. Journal Of Fluid Mechanics 299:35 –71.

Choı, H., Hınze, M., Kunısch, K., 1999. Instantaneous Control Of Backward-Facing Step Flows. Applied Numerical Mathematics, 13:133 –158.

Chong, M. S. And Perry, A. E. 1990. A General Classification Of Three-Dimensional Flow Fields. Phys. Fluids A 2, 765–777.

Cımbala, J. N., Nagıb, H. M., And Roshko, A., 1988. Large Structure İn The Far Wakes Of Two-Dimensional Bluff Bodies, J. Fluid Mech. 190, 265.

Fabrıs, G., 1984. A Conditional-Sampling Study Of The İnteraction Of Two Turbulent Wakes. Journal Of Fluid Mechanics, 140: 355-372.

Ffowcs-Wıllıams, J. E.Andzhao, B. C. 1989 The Active Control Of Vortex Shedding. Journal Of Fluids And Structures 3, 115-122.

Fujısawa, N. And Waruı, H. M. 1994 Active Control Of Vortex Shedding By Cross-Flow Oscillation Of A Circular Cylinder İn A Uniform #Ow. In Proceedings Of The Fourth F¸;Come, Toulouse, France, Pp. 113-118.

Fujısawa, N., Ikemoto, K. And Nagaya, K. 1998 Vortex Shedding Resonance From A Rotationally Oscillating Cylinder. Journal Of Fluids And Structures 12, 1041-1053.

Gad-El-Hak, M., 1996. Modern Developments İn Flow Control. Applied Mechanics Reviews, 49:365–379.

Gad-El-Hak, M., 2000, Flow Control: Passive, Active And Reactive Flow Management. Cambridge University Press, Cambridge, U.K., 421.

Gerrard J.H., 1966. The Mechanics Of Formation Region Of Vortices Behind Bluff Bodies, J. Fluid Mech. 25 401–413.

Gerrard, J.H., 1978. The Wakes Of Cylindrical Bluff Bodies At Low Reynolds Number. Phil. Trnas. R. Soc. London A, 288: 351-382.

Graham, Wr., Peraıre, J., Tang, Ky., 1999. Optimal Control Of Vortex-Shedding Using Low Order Models. Part I: Open-Loop Model Development. International Journal Of Numerical Methods İn Engineering, 7:950 –971.

Graham, Wr., Peraıre, J., Tang, Ky., 1999. Optimal Control Of Vortex-Shedding Using Low Order Models. Part Iı: Model Based Control. International Journal Of Numerical Methods İn Engineering 7:972–990.

Grıffın, M.O., 1978. A Universal Strouhal Number For The ‘Locking-On’ Of Vortex Shedding To The Vibration Of Bluff Cylinders, J. Fluid Mech. 85 591–606.

Grıffın, M.O., Ramberg, E., 1974. The Vortex Street Wakes Of Vibrating Cylinders, J. Fluid Mech. 66 553–576.

Hayashı, M., Sakuraı, A., And Ohya, Y., 1986. Wake İnterference Of A Row Of Normal Flat Plates Arranged Side By Side İn A Uniform Flow. Journal Of Fluid Mechanics, 164: 1-25.

Ho, C.M., And Huerre, P., 1984. Perturbed Free Shear Layers. Annu. Rev. Fluid Mechanics, 16: 365-424.

Hou L., Ravındran, Ss., 1998. Penalty Methods For Numerical Approximations Of Optimal Boundary Flow Control Problems. International Journal Of Computational Fluid Dynamics 11:157–167.

Hou, L., Ravındran, Ss., Yan, Y., 1997. Numerical Solutions Of Optimal Distributed Control Problems For İncompressible Flows. International Journal Of Computational Fluid Dynamics 8:99 –114.

Hou, L., Yan Y., 1997. Dynamics And Approximations Of A Velocity Tracking Problem For The Navier–Stokes Flows With Piecewise Distributed Controls. Sıam Journal On Control And Optimization, 35(6):1847–1885.

Huang, X. Y. 1996 Feedback Control Of Vortex Shedding From A Circular Cylinder. Experiments İn Fluids 20, 218-224.

Igarashı, T., 1984. Characteristics Of The Flow Around Two Circular Cylinders Arranged İn Tandem (2nd Report), Bull. Jsme 27 (233) 2380–2387.

Igarashı, T., Tsutsuı T., 1989. Flow Control Around A Circular Cylinder By A New Method, Trans. Jsme 55 (511) 701–713.

Ingram, G. R. And Chu, V. H., 1987. Flow Around İslands İn Rupert Bay: An İnvestigation Of The Bottom Friction Effect. J. Geophys. Res. 92 (C13), 14521–14533.

Inoue, O., 1985. A New Approach To Flow Problems Past A Porous Plate. Aıaa J. 23, 1916–1921.

Ito, K., Ravındran, Ss., 1998. A Reduced-Order Method For Simulation And Control Of Fluid Flows. Journal Of Computational Physics, 143(2):403–425.

James, D.F., Truong, Q.S., 1972. Wind Load On Cylinder With Span-Wise Protrusion, Proc. Asce J. Eng. Mech. 98 (Em6) 1573–1589.

Jendrzejczk, J.A., Chen, S.S. And Wambganns. M.W., 1979. Dynamic Response Of A Pair Of Circular Tubes Subjected To Liquid Cross Ow. Journal Of Sound And Vibration, 67:263-273

Juarez, H., Scott, R., Metcalfe, R., Bagherı B., 2000. Direct Simulation Of Freely Rotating Cylinders İn Viscous Flows By High-Order Anite Element Methods. Computers And Fluids, 29:547–582.

Kahraman, A., Sahın, B., And Rockwell, D., 2002. Control Of Vortex Formation A Vertical Cylinder İn Shallow Water: Effect Of Localized Roughness Elements. Experiments İn Fluids, 33: 54-65.

Kırgoz, S. And Ardıclıoglue, M., 1997. Velocity Profiles Of Developing And Developed Open Channel Flow. J. Hydraul. Engng 123, 1099–1105.

Kıya, M., Tamura, H., Arıe, M., 1980. Vortex Shedding From A Circular Cylinder İn Moderate-Reynolds Number Shear Flow, J. Fluid Mech. 141 (Part 4) (721-735.

Kumada, M., Hıwada, M., Ito, M., And Mabuchı, I., 1984. Wake İnterference Between Three Circular Cylinders Arranged Side-By-Side Normal To A Flow, Trans, Jpn. Soc. Mech. Eng., Ser. B 50, 1699 (İn Japanese).

Landweber, L., 1942. Flow About A Pair Of Adjacent, Parallel Cylinders Normal To A Stream, D. W. Taylor Model Basin, Department Of Navy, Report 485, Washington, Dc.

Lee, T. And Basu, S. 1997. Nonintrusive Measurements Of The Boundary Layer Developing On A Single And Two Circular Cylinders. Exps. Fluids 23, 187–192.

Lee, T., 1999 Investigation Of Unsteady Boundary Layer Developed On A Rotationally Oscillating Circular Cylinder. Aıaa Journal 37, 328-336.

Legal, P., Chauve, M.P., Lıma, R., And Rezende, J., 1990. Coupled Waked Behind Two Circular Cylinder. Physical Review A, 41: 4566-4569.

Lesage, F., Gartshore, I.S., 1987. A Method Of Reducing Drag And Fluctuating Side Force On Bluff Bodies, J. Wind Eng. Ind. Aerodyn. (25) 229–245.

Lloyd, P.M., And Stansby, P.K., And Chen, D., 2001. Wake Formation Around İslands İn Oscillatory Laminar Shallow-Water Flows. Part1. Experimental İnvestigation. Journal Of Fluid Mechanics, 429: 217-238.

Mahır, N., And Rockwell, D., 1996. Vortex Formation From Forced System Of Two Cylinders. Part Iı: Side By Side Arrangement. Journal Of Fluid Mechanics, 10: 491-500.

Matsumoto, M., Shıraıshı, N. And Shırato H., 1990. Aerodynamic İnstabilities Of Twin Circular Cylinders. In M. Ito, M. Matsumoto, And N. Shiraishi,

Mıttal S., Kumar, V. And Raghuvanshı A., 1997.Unsteady İncompressible Ow Past Two Cylinders İn Tandem And Staggered Arrangements. International Journal For Numerical Methods İn Fluids, 25:1315-1344

Mıttal, S. And Kumar, V., 1999.Finite Element Study Of Vortex-İnduced Cross-Ow And İn-Line Oscillations Of A Circular Cylinder At Low Reynolds Numbers. International Journal For Numerical Methods İn Fluids, 31:1087-1120

Mıttal, S. And Tezduyar T.E.., 1992. A Finite Element Study Of İncompressible Flows Past Oscillating Cylinders And Airfoils. International Journal For Numerical Methods İn Fluids, 15:1073- 1118

Monkewıtz, P. A., 1998. The Absolute And Convective Nature Of İnstability İn Two-Dimensional Wakes At Low Reynolds Numbers. Phys. Fluids 31, 999–1006.

Nakaguchı H., Hashımoto, K., Muto, S., 1968. An Experimental Study Of Aerodynamic Drag On Rectangular Cylinders, J. Japan Soc. Aeronaut. Space Sci. 16 1–5.

Newland, D. Nıemann, H.-J. And Holscher, N. 1990. A Review Of Recent Experiments On The Flow Past Circular Cylinders. J. Wind Engrs Indust. Aerodyn. 33, 197–209.

Ongoren A. And Rockwell, D., 1988. Flow Structure From An Oscillating Cylinder Part 1. Mechanisms Of Phase Shift And Recovery İn The Near Wake. Journal Of Fluid Mechanics, 191:197- 223

Ongoren A. And Rockwell, D., 1988. Flow Structure From An Oscillating Cylinder Part 2. Model Competition İn The Near Wake. Journal Of Fluid Mechanics, 191:225-245

Ozono S., 1999, Flow Control Of Vortex Shedding By A Short Splitter Plate Asymmetrically Arranged Downstream Of A Cylinder. Physics Of Fluids 11(10):2928 –2934.

Park D., Ladd, D., Hendrıcks, E., 1994. Feedback Control Of Von Karman Vortex Shedding Behind Circular Cylinders At Low Reynolds Numbers. Physics Of Fluids 6(7):2390 –2405

Pentek, A., Kadtke., J., 1998. Dynamical Control For Capturing Vortices Near Bluff Bodies, Physical Review E 58(2):1883 –1898.

Perry, A. E. And Steıner, B. D., 1987. Large-Scale Vortex Structures İn Turbulent Wakes Behind Bluff Bodies. Part 1. Vortex Formation. J. Fluid Mech. 174, 233–270.

Prasad, A. And Wıllıamson, C. H. K., 1997. A Method For The Reduction Of Bluff Body Drag. J. Wind Engrs Indust. Aerodyn. 69–71, 155–167.

Prıce, P., 1956. Suppression Of The Fluid-İnduced Vibrations Of Circular Cylinders, Proc. Asce, Eng. Mech. Div.Paper No. 1030 1-22

Rao, S. S. 1995. Mechanical Vibration, Pp. 523–541. Addison-Wesley.

Roshko, A. 1954. On The Development Of Turbulent Wakes From Vortex Streets. Naca Rep. 1191.

Roshko, A. 1961. Experiments On The Flow Past A Circular Cylinder At Very High

Roshko, A., 1954..On The Drag And Shedding Frequency Of Two-Dimensional Bluff Bodies, Naca Tech. Note No. 3169 .

Roussopoulos, K. 1993 Feedback Control Of Vortex Shedding At Low Reynolds Numbers. Journal Of Fluid Mechanics 24, 267-296.

Sarpkaya, T., 1979.Vortex-İnduced Oscillations: A Selective Review. Journal Of Applied Mechanics, 46:241-258

Schar, C., And Smıth R.B., 1993. Shallow Water Flow Past İsolated Topography. Part Iı: Transition To Vortex Shedding. Journal Of The Atmospheric Sciences, 50: 1401-1412.

Seal, C. V. And Smıth, C. R., 1999. Visualization Of A Mechanism For Three-Dimensional İnteraction And Near-Wall Eruption. J. Fluid Mech. 394, 193–203.

Seal, C. V., Smıth, C. R. And Rockwell, D., 1997. Dynamics Of The Vorticity Distribution İn End-Wall Junctions. Aıaa J. 35, 1041–1047.

Shukla S, Govardhan Rn, Arakeri Jh. Flow Past A Cylinder With A Hinged-Splitter Plate. J Fluid Struct 2009;25:713

Shukla, S., Govardhan, R.N., Arakeri, J.H., 2009. Flow Over A Cylinder With A Hinged-Splitter Plate. Journal Of Fluids And Structures 25, 713–720.

Sımpson, A. 1971. On The Flutter Of A Smooth Cylinder İn A Wake. Aeronaut. Q. 22, 25–41.

So, R.M.C., Savkar, S.D., 1981. Buffeting Forces On Rigid Circular Cylinders İn Cross-Flow, J. Fluid Mech. 105 397–425.

Son, J. And Hanratty, T. J. 1961. Velocity Gradients At The Wall For Flow Around A Cylinder At Reynolds Numbers From 5×10^{3} To 10^{5}. J. Fluid Mech. 35, 353–368

Squıre, L. C. 1961. The Motion Of A Thin Oil Sheet Under The Steady Boundary Layer On A Body. J. Fluid Mech. 11, 161–179.

Sumner, D., Wang, S.S.T., Prıce, S. J., And Paıdoussıs, M.P., 1999. Fluid Behavior Of Side-By- Side Circular Cylinders İn Steady Cross-Flow. Journal Of Fluids And Structures 13: 309-338.

Szepessy, S. And Bearman, P. W. 1992 Aspect Ratio And End Plate Effects On Vortex Shedding From A Circular Cylinder. Journal Of Fluid Mechanics 234, 191-217.

Tang, K., Graham, W., Peraıre, J., 1996. Active Flow Control Using A Reduced Order Model And Optimum Control. Aıaa Paper 96-1946.

Tang, S., Aubry, N., 2000. Suppression Of Vortex Shedding İnspired By A Low Dimensional Model. Journal Of Fluids And Structures, 14:443– 468.

Toebes, G. H. 1969 The Unsteady Flow And Wake Near An Oscillating Cylinder. Asme Journal Of Basic Engineering 91, 493-505.

Tokumaru, P. T. And Dımotakıs, P. E. 1991 Rotary Oscillation Control Of A Cylinder Wake. Journal Of Fluid Mechanics 224, 77-90.

Tsuı, Y.T., 1977.On Wake-İndiced Outter Of A Circular Cylinder İn The Wake Of Another. Journal Of Applied Mechanics, Transactions Of The Asme, 99:194-200

Weı, C.Y., And Chang, J.R., 1999. Study Of Base-Bleed Flow And Wake Downstream Of Two Dimensional Bluff Bodies Arranged Side By Side, İn: The Sixth Military Academy Symposium On Fundamental Science, Roc.

Weı, C.Y., And Chang, J.R., 2002. Wake And Base-Bleed Flow Downstream Of Bluff Bodies With Different Geometry. Experimental Thermal And Fluid Science, 26: 39-52.

Weır, A.D., Wood. D.H., And Bradshaw, P., 1981. Interacting Turbulent Shear Layers İn A Plane Jet. Journal Of Fluid Mechanics, 107: 237-260.

Wıllıamson, C.H.K. And Roshko, A., 1988.Vortex Formation İn The Wake Of An Oscillating Cylinder. Journal Of Fluids And Structures, 2:355-381

Wıllıamson, C.H.K., 1985. Evolution Of A Single Wake Behind A Pair Of Bluff Bodies. Journal Of Fluid Mechanics, 159: 1-18.

Wıllıamson, Chk., 1996. Vortex Dynamics İn The Cylinder Wake. Annual Review Of Fluid Mechanics 28:477–539.

Xu G., Zhou, Y., 2004. Strouhal Numbers İn The Wake Of Two İnline Cylinders, Exp. Fluids 37 248–256.

Zdravkovıch M.M., 1988. Review Of İnterference-İnduced Oscillations İn Flow Past Two Parallel Circular Cylinders İn Various Arrangements, J. Wind Ind. Aerodyn. 28 183–200.

Zdravkovıch M.M., 1997. Flow Around Circular Cylinders, Vol. 1: Fundamentals Of Heat And Fluid Flow Oxford Science Publications 21: 125-123. ,

Zdravkovıch, M. M. 1969. Smoke Observation Of The Formation Of A Karman Vortex Street. J. Fluid Mech. 37, 491–496.

Zdravkovıch, M. M. 1981 Review And Classification Of Various Aerodynamic And Hydrodynamic Means For Suppressing Vortex-Shedding. J. Wind Engrs Indust. Aerodyn. 7, 145–189.

Zdravkovıch, M. M., Brand, V. P., Mathew, G. And Weston, A. 1989 Flow Past Short Circular Cylinders With Two Free Ends. J. Fluid Mech. 203, 557–575

Zdravkovıch, M.M., 1968. Smoke Observation Of The Wake Of A Group Of Three-Cylinders At Low Reynolds Number. Journal Of Fluid Mechanics, 32: 339-351.

Zdravkovıch, M.M., 1977. Review Of Flow İnterference Between Two Circular Cylinders İn Various Arrangement, J. Fluids Eng. 199 618–633.

Zdravkovıch, M.M., 1985. Flow İnduced Oscillations Of Two İnterfering Circular Cylinders. Journal Of Sound And Vibration, 101(4):511-521

Zdravkovıch, M.M., 1987.The Effects Of İnterference Between Circular Cylinders İn Cross Flow, J. Fluids Struct. (1) 239–261

Zdravkovıch, M.M., And Stonebanks, K.I., 1990. Intrinsically Nonuniform And Metastable Flow İn And Behind Tube Arrays. International Journal Of Heat And Fluid Flow, 4: 305-319.

Zdravkovıch, M.M., Prıdden, D.L., 1977. Interference Between Two Circular Cylinders; Series Of Unexpected Discontinuities, J. Ind. Aerodyn. 2 255–270.

Zhang, H.J., And Zhou, Y., 2001. Effect Of Unequal Cylinder Spacing On Vortex Streets Behind Three Side-By-Side Cylinders. Physics Of Fluids, 13 (12): 3675-3686.

Zhong, J., Hunag, T. S. And Adrıan, R. J., 1998. Extracting 3d Vortices İn Turbulent Fluid Flow. Ieee Trans. Pattern Anal. Machine Intell. 20, 193–199.

Zhou, Y., And Antonıa, R. A., Critical Points İn A Turbulent Near-Wake, 1994. J. Fluid Mech. 275, 59

Zhou, Y., So, R. M. C., Jın, W., Xu, H. G., And Chan, P. K. C., 1999. Dynamic Strain Measurements Of A Circular Cylinder İn A Cross Flow Using A Fibre Bragg Grating Sensor,'' Exp. Fluids 27, 359.

Zhou, Y., So, R.M.C., Lıu, M.H., And Zhang, H.J., 2000. Complex Turbulent Wakes Generated By Two And Three Side-By-Side Cylinders. International Journal

Zhou, Y., Wang, Z. J., So, R. M. C. S., Xu, J. And Jın, W., 2001. Free Vibrations Of Two Side-By-Side Cylinders İn A Cross Flow,'' J. Fluid Mech. 443, 197

Zhou, Y., Yıu, M.W., 2006. Flow Structure, Momentum And Heat Transport İn A Two-Tandem-Cylinder Wake, J. Fluid Mech. 548 17–48.

Zhou, Y., Zhang, H. J. And Yıu, M. W., (2002). The Turbulent Wake Of Two Side-By- Side Circular Cylinders, J. Fluid Mech. 458, 303.

CIRRICLUM VITAE

Fırat Ekinci was born in 1973 in Adana. He was graduated from Mechanical Engineering Department Of Cukurova University In 1998. After he had completed his Bachelor Degree, he worked as research assistant for 4 years in Mechanical Engineering Department. He had a Master Degree in 2001 at Çukurova University. He has still been working at Ministry Of Science, Industry and Technology. He is married and has got one child.